Subsurface Flow Formation

Inauguraldissertation
der Philosophisch-naturwissenschaftlichen Fakultät
der Universität Bern

vorgelegt von
Matthias Retter
aus Deutschland

Leiter der Arbeit:
Prof. Dr. Peter F. Germann
Geographisches Institut

Subsurface Flow Formation

Inauguraldissertation
der Philosophisch-naturwissenschaftlichen Fakultät
der Universität Bern

vorgelegt von
Matthias Retter
aus Deutschland

Leiter der Arbeit:
Prof. Dr. Peter F. Germann
Geographisches Institut

Von der Philosophisch-naturwissenschaftlichen Fakultät angenommen.

Bern, 29.03.2007   Der Dekan:
                                    Prof. Dr. P. Messerli

Contents

Contents

Abstract

To improve runoff predictions in ungauged basins (PUB), it is essential to better understand runoff formation. Experimental process studies provide key information for implementation in hydrological models. The aim of this thesis was to respond to questions associated with vertical preferential flow and lateral flow in hillslope soil. Major attention is dedicated to the shift from vertical flow (commonly termed "infiltration") to lateral flow, which actually forms the transition from soil hydrology to hillslope hydrology.

To improve the understanding of flow formation at a 100 m² hillslope study site, a longitudinal trench was excavated below the plot to measure subsurface flow components. Further, an innovative instrumentation of a Time Domain Reflectometry (TDR) triplet, containing three wave-guides, was introduced that allowed the determination of in-situ flow vectors during sprinkling experiments. The results revealed that vertical infiltration and its propagating fronts did not move truly vertically. The velocity vectors of the wetting fronts were generally gravity dominated and downslope orientated. Downslope direction (x-axis) dominated in deep soil close to bedrock, whereas no preference between vertical and downslope direction was found in vectors close to the surface. Limitations and uncertainties of the flow vector method are discussed.

The observed orientation of flow vectors indicated apparent anisotropy within the soil. Therefore, the following characteristics were tested as controls on anisotropy: (1) small scale soil structure; (2) layering of the soil profile; (3) boundary conditions of flow; (4) initial conditions. To determine small scale soil characteristics, small scale core samples were analysed for saturated hydraulic conductivity in the vertical and horizontal direction; however, no small scale anisotropy was found. Further, initial condition and layering effects were tested using initial soil moisture content and soil structure characterization. The soil contained no evident layering within the soil profile. It was concluded that apparent anisotropy was caused by boundary conditions of flow, namely increased moisture content at the soil-bedrock interface that caused changes of hydraulic conductivity across the soil layer. Such a change imposed curving of streamlines downslope, as measured by the TDR triplets.

Characteristics of vertical and lateral flows were used to establish a conceptual model of how these flows were initiated and linked with each other to form subsurface flow. Preferential flow does not transfer the water directly and immediately from the soil surface to the investigation trench, because preferential flow is influenced and disrupted by the soil matrix. Thus, during flow formation, patches of localised saturation develop, from where preferential flow is re-initiated. Water is therefore retained at such patches, and their extent determined how quickly flow is responsed at the trench. Once steady-state flow is established, preferential flow paths can be connected directly or indirectly via such patches of localised saturation. This includes a tendency to self-organize into larger preferential flow systems as sites become wetter, which has been noted by other researchers. Correspondingly, individual preferential flow paths can vary substantially with regard to flow velocity (time to concentration) and also to

general flow magnitude. Based on vertical and lateral flow analysis, it was shown, that both, the connectivity and relative flow path length of preferential flow, as well as the ability of the soil matrix to absorb water, determine flow rate and flow response of subsurface storm flow. These findings **help significantly to improve flow predictions for similar ungauged** hillslopes.

Zusammenfassung

Um Abflussvorhersagen in ungemessenen Einzugsgebieten zu verbessern, ist ein tieferes Prozessverständnis der Abflussbildung von Nöten. Experimentelle Studien liefern hierzu wichtige Informationen welche in hydrologische Abflussmodelle implementiert werden können. Den Fokus dieser Arbeit bilden Fragestellungen des vertikalen und lateralen Wasserflusses im Hangboden. Im Speziellen wird das Umknicken von vertikalem Fluss (meist als Infiltration bezeichnet) in einen lateralen Fluss dokumentiert, das zugleich den Skalenübergang der Bodenhydrologie zur Hanghydrologie kennzeichnet.

Um die Abflussbildung eines Untersuchungshanges (100 m²) genauer zu untersucht, wurde an dessen Fuss ein Quergraben ausgehoben, womit unterirdische Abflusskomponenten bestimmt werden konnten. Zudem gestattete eine neuartige Messanordnung von Time Domain Reflectometry (TDR) Messsonden die in-situ Bestimmung von Vektoren des Wasserflusses während den Beregungsexperimenten. Die Ergebnisse zeigten, dass die voranschreitende Feuchtefront der vertikalen Infiltration sich nicht vollständig vertikal bewegte. Generell waren die Geschwindigkeitsvektoren von der Schwerkraft dominiert und hangabwärts gerichtet. In grösserer Bodentiefe, nahe dem anstehenden Gestein, herrschte ein hangabwärts gerichtete Fliessrichtung vor. Oberflächennahe Vektoren hingegen wiesen keine eindeutige Richtungspräferenz auf. Die potentiellen Messfehler und Limitationen der Anwendbarkeit werden zudem diskutiert.

Die beobachtete Orientierung der Fliessvektoren deutet auf eine Anisotropie des Bodens hin. Diese Eigenschaft wurde hinsichtlich ihrer Abhängigkeit von 1.) der kleinskaligen (makroskaligen) Bodensstruktur; 2.) der Schichtung im Bodenprofil; 3.) von den Randbedingungen des Hangsystems; 4.) der Ausgangsfeuchte untersucht. Hierfür wurden kleine Bodenzylinderproben auf gesättigte hydraulische Leitfähigkeit in vertikaler und horizontaler Richtung analysiert. Die erwartete kleinskalige Anisotropie konnte nicht nachgewiesen werden. Sowohl der anfängliche Wassergehalt vor den Beregnungen, als auch die Bodenstruktur am Profil zeigten ferner, dass die Hypothese einer Bodenschichtung verworfen werden muss. Weiterhin schied auch die Variante Systemvorfeuchte aus. Die Ursache für die scheinbare Anisotropie wird mit dem Randeffekt erklärt. In der Grenzschicht vom Boden zum anstehenden Gestein bewirkte der erhöhte Wassergehalt eine Änderung der hydraulischen Leitfähigkeit. Daraus resultierend kommt es zum Umknicken der Flussrichtung hangabwärts, wie bereits durch die TDR Messungen belegt wurde.

Teil dieser Arbeit war des Weiteren die Analyse der Kenngrössen des vertikalen und lateralen Flusses im Hang. Sie ermöglichte die konzeptionelle Erfassung wie diese Flüsse, einmal miteinander verknüpft, zur Entstehung von schnellem unterirdischen Abfluss beitrugen. Präferentielles Fliessen bedingte nicht ausschliesslich einen schnellen und direkten Transfer von der Bodenoberfläche zum Untersuchungsgraben. Vielmehr wurde dieses schnelle Fliessen unterbrochen und von Matrixfliessen beeinflusst. Während der Abflussbildung entstanden somit gesättigte Zonen, die den Ausgangspunkt für erneutes präferentielles

Contents

Fliessen bildeten. Parallel wurde auch in diesen Zonen Wasser zurückgehalten. Massgeblich für die Schnelligkeit der Abflussreaktion im Untersuchungsgraben war die Ausprägung der gesättigten Zonen. Mit Einstellen eines stationären Fliessens konnten sich präferentielle Flieswege direkt oder indirekt über lokal gesättigten Zonen verbinden. Diese Tendenz zur selbstständigen Organisation hin zu grösseren präferenziellen Fliesssystemen mit zunehmendem Sättigungsgrad bestätigen die These anderer Autoren. Damit einhergehend differenzieren sich die individuellen Fliesswege deutlich in der Fliessgeschwindigkeit (Zeit bis zum Einsetzen des Abflusses) und der maximalen Schüttung. Aus den Analyseergebnisse des vertikalen und lateralen Flusses geht folglich hervor, dass die Anschlussfähigkeit und relative Fliesslänge des präferentiellen Flusses sowie die Absorptionsfähigkeit der Bodenmatix entscheidend sind für die zeitliche Abflussentstehung sowie die Abflussmenge von schnellem unterirdischem Abfluss. Die dargestellten Resultate tragen massgeblich zur Verfeinerung von modellbasierten Abflussvorhersagen von ähnlichen nicht bemessenen Hangflächen bei.

Résumé

Pour améliorer la prédiction des ruissellements dans les bassins versants non jaugés, il est important de comprendre leur processus de formation. Les études expérimentales fournissent des informations clé pour tout modèle hydrologique. L'objectif de ce travail est d'apporter des réponses aux questions relatives à l'écoulement/flux préférentiel vertical et latéral dans les sols pentus des bassins versants. Une attention particulière a été portée sur le changement du flux vertical (ou infiltration) en flux latéral, facteur de transition entre l'hydrologie du sol et l'hydrologie du bassin versant.

Afin d'améliorer la compréhension de la formation des écoulements dans un bassin versant expérimental d'une surface de 100 m², une trachée transversale a été tracée en aval du site. De plus, des trios sondes TDR (time domain reflectometry) mesurant in-situ les composantes directionnelles de l'écoulement souterrain et équipées de simulateur de pluie, ont été installées sur le site. Dans cette pente, il a été montré que l'infiltration et son front de propagation ne se déplacent pas véritablement selon la verticale. Les vecteurs vitesse du front d'humectation sont généralement orientés selon la gravité et déviés dans la direction du bas de versant. À proximité du substratum rocheux, la direction d'écoulement privilégiée est sub-horizontale (vers l'aval), alors qu'à proximité de la surface, ne domine aucune direction. Les limites et incertitudes de cette méthodes des vecteurs sont discutés et mis en perspective.

Les orientations des vecteurs d'écoulement mesurés ont mis en évidence une anisotropie dans le comportement du sol vis à vis de l'écoulement. Une analyse a donc été menée afin d'évaluer la pertinence des différentes explications envisageables : (i) la micro structure du sol, (ii) l'organisation pédologique en horizons ou couches, (iii) la nature des conditions aux limites et (iv) les conditions initiales. Dans un premier temps, la caractérisation des conductivités hydrauliques verticales et horizontales sur des échantillons de sol n'a pas montré d'anisotropie à petite échelle. Des études complémentaires ont indiqué que l'anisotropie apparente ne pouvait être expliquée ni par la structure du sol (absence de couches) ni par la distribution des teneurs en eau initiale du sol. Finalement, l'anisotropie apparente est attribuée aux conditions aux limites de l'écoulement. Celles-ci augmentent la teneur en eau du sol à l'interface sol-substratum rocheux et créent alors des changements de conductivité à travers la couche de sol. Ces changements provoquent le changement de direction des lignes de courant/flux vers l'aval du bassin versant, mises en évidence par les trios sondes TDR.

La caractérisation des écoulements verticaux et horizontaux ont permis d'établir un schéma conceptuel expliquant la naissance, la formation et l'interaction entre les écoulements souterrains aboutissant à l'écoulement de surface. Le flux préférentiel ne permet pas le transfert de l'eau directement et immédiatement de la tranchée, du fait que ce type de flux est interrompu par la matrice du sol. Durant la formation du flux, se développent des zones de saturation engendrant le flux préférentiel. Une fois le régime permanent établi, les écoulements préférentiels se connectent directement ou indirectement via les zones de haute saturation. Ce processus s'organise de lui-même dans tout le réseau des cheminements préférentiels au

Contents

fur et à mesure que le site devient humide, comme reporté dans la littérature. Par conséquent, les écoulements préférentiels peuvent varier substantiellement selon vitesse de réponse du flux et l'amplitude maximale du flux. Basé sur l'analyse de l'écoulement vertical et latéral, les paramètres déterminants l'intensité du flux et la réponse de la surface du sol à une averse sont: les connexions des écoulements préférentiels entre eux, leur longueur relative et enfin l'aptitude de la matrice à absorber l'eau. Ces résultats permettent d'améliorer la qualité de prédiction des écoulements dans des cas similaires de bassins versants non jaugés.

Chapter 01

Introduction

1.1 Motivation

"Hydrology is many things to different people. In many areas of the world it is the difference between life and death, flood or drought, plenty or famine" (Beven, 2006a). For Bernese people living in the floodplains of the river Aare, hydrology may make the difference between timely precaution and flooded assetss (Bundesamt für Geologie, 2005).

River flood flows and water levels are a direct result of precipitation and catchment characteristics. Hydrologists have a wide range of tools based on the analysis of existing data, expressed as empirical relationships or calibrated hydrological models. Prediction of flow is a major challenge as it is subject to uncertainties (Beven, 2006a). For most catchments, the parameters of rainfall-runoff models cannot be obtained by calibration, as no runoff data exists (e.g. due to continual decline in hydrological gauging networks over recent decades, remoteness or inaccessibility). The general decline in gauging world wide causes a trend of currently increasing uncertainty associated with the prediction of water quantity (Sivapalan et al., 2005). The present thesis was initiated by these uncertainties in hydrological prediction.

Experimental investigations into subsurface flow, which is an important contributor to stream flow in most upland catchments (review in Weiler et al., 2006), help to better understand runoff formation processes. Knowledge of hillslopes is an essential component required to estimate the rainfall-runoff response of an entire catchment to provide predictions. Using science to reduce uncertainty in the predictions of flows is therefore the motivation for the present work.

1.2 Approaches towards greater process understanding and integration

In 2003, right before the start of the present dissertation, the International Association of Hydrological Sciences (IAHS) launched a new initiative that emerged out of meetings in Maastricht (18-27 July, 2001), Kofu (28-29 March, 2002) and Brasilia (20-22 November, 2002). It is the IAHS Decade on Predictions in Ungauged Basins (PUB) (2003–2012), aimed at

> "formulating and implementing appropriate science programmes to engage and energize the scientific community, in a coordinated manner, towards achieving major advances in the capacity to make predictions in ungauged basins" (PUB, 2006; Sivapalan et al., 2003).

Ungauged catchments have long been considered as significant problem par excellence in hydrological prediction, but PUB also recognizes that it may not be possible to make entirely accurate predictions of the response to rainfall of ungauged catchment areas, since we will never be able to know the characteristics of those catchments in sufficient detail to allow a full description of the hydrology.

Recognizing the great diversity of interests and expertise of hydrologists, and the diverse

aims of prediction, PUB has adopted a philosophy of variety in terms of applications and prediction methods. The PUB science plan emphasizes a paradigm shift away from methods based on calibration towards methods based on increased understanding (Figure 1-2). There are many avenues towards gaining the required understanding (seven cohesive science themes mentioned in PUB, 2006). Amongst them, science theme 1 contains basin inter-comparison and classification. Its objective is experimental process studies at many scales (see below) and the use of new types of observations and data that give deeper insights into hydrological processes. McDonnell et al. (2005) argued that new data sources and process concepts may form new measures of model acceptability, as the community moves away from traditional calibration-reliant model schemes to more process-based descriptions. McDonnell et al. (2005) concluded that measures of water flow path, source and age of water may help to constrain conceptualizations of runoff generation and thus help to reduce predictive uncertainty. Thus, innovation and the development and application of innovative instrumentation are crucial (Hopmans and Pasternack, 2006).
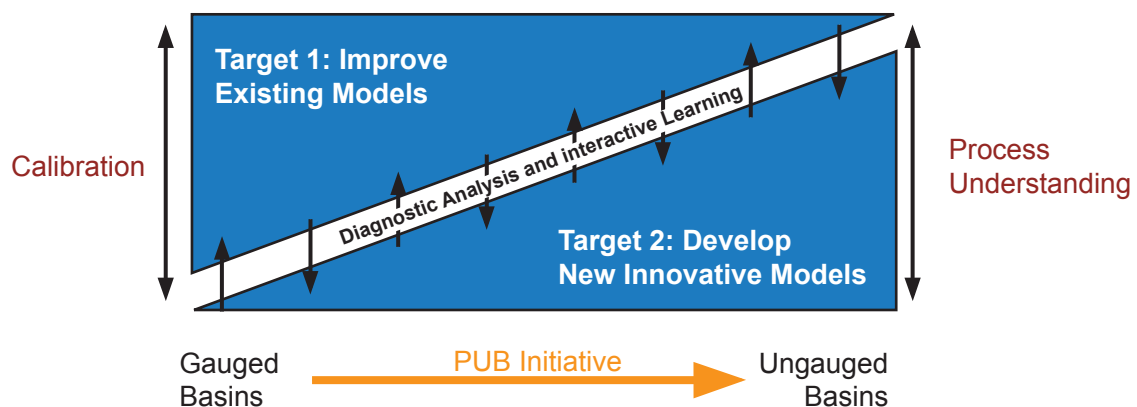
Figure 1.2. Towards a paradigm change- from calibration to understanding. Adopted from PUB (2006).

Within science theme 1, the main engines of the research activities and progress are PUB working groups. These working groups are formed in a self-organizing manner, and overcome traditional boundaries of specialization (Sivapalan et al., 2005; Franks et al., 2005). A PUB Working Group on Slope InterComparison Experiment (SLICE) was founded within science theme 1 "basin inter-comparison and classification" in September 2005 (Retter, 2005). SLICE was built upon the growing interest in intercomparsion of hillslopes. A first workshop was held at H.J. Andrews Experimental Forest in Oregon, USA between September 26-28, 2005. It was convened and organized by Jeff McDonnell (Oregon State University), Jim Freer (Lancaster University), Peter Troch (University of Arizona), Kevin McGuire (Plymouth State University), and the author (University of Bern). Many of the 40 hydrologist, who attended the meeting, had published experimental process studies of high scientific impact. The workshop allowed to exchange and compare data and therefore stimulated intense discussion on site similarities and differences. These discussions also

included the use of new types of observations. While the focus of the meeting was on trenched hillslopes (equipped with a trench at the bottom end of the hillslope to record subsurface stormflow), findings from hillslope where trenching was not possible were also discussed (e.g. steep mountainous regions). The workshop also allowed to give a presentation on the innovative measurement technique for vectors of subsurface flow used in the present dissertation. Finally, the participants developed a preliminary hillslope classification system (hillslope typology) and markedly enhanced process understanding which is essential to reduce predictive uncertainty of water flow in streams.

1.3 Experimental process studies at the plot and hillslope scale

Experimentation is defined by the adjustment of system variable(s) or parameter(s) of an experimental system with controlled boundary and initial conditions, to test a conceptual model. Because complete control is difficult in most natural hydrological systems, there are innovative surrogate settings to answer fundamental questions on infiltration, runoff generation, and water storage (Hopmans and Pasternack, 2006). Sprinkling experiments are a common experimentation. Here, a square pulse of well defined water input is applied to a system whose initial conditions are well monitored.

Studies of runoff processes are generally conducted at three scales (Figure 1-3):

■ Plot scale: the smallest scale, which is a soil compartment or soil profile,

■ Hillslope scale: which concerned the mechanisms by which precipitation is delivered to the stream channel, and

■ Catchment scale, whose integration captures the processes of the entire drainage basin.
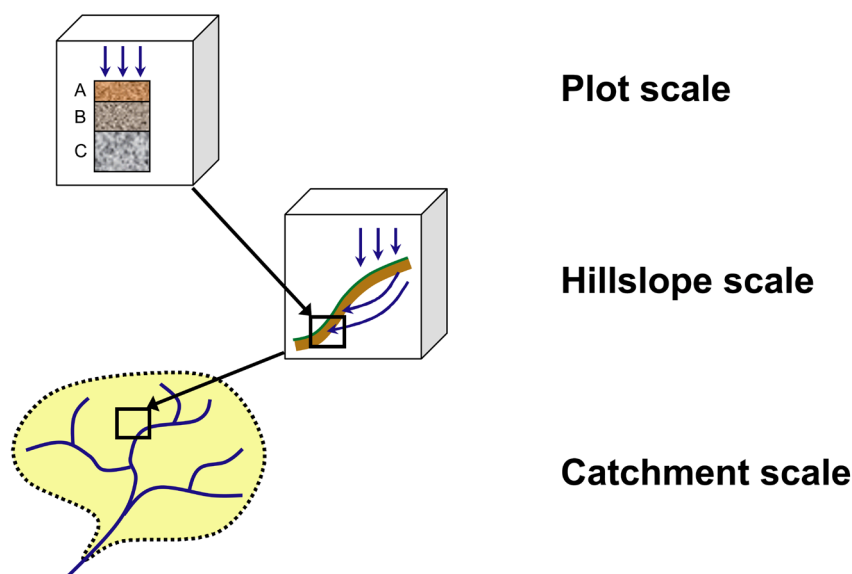

Figure 1.3. *Spatial scales where runoff processes take place (adopted from Uhlenbrook and Leibundgut, 1997).*

Some important case studies associated with plot and hillslope scale are briefly summarized below.

Experimental process studies at the plot scale on infiltration identify the effect of preferential flows of water in soils. An early literature review highlighted features like the flow of water through a system of large pores that allows for fast flow (Beven and Germann, 1982). Later, various types of fluid mechanics approaches to preferential flow (Germann, 2001; Germann et al. 2002) were used, but the definition and classification of preferential flow is still under investigation (Gerke, 2006; Germann et al., 2007). Tracing of flow paths also helped to conceptualize the phenomena (Flury et al., 1994; Weiler and Naef, 2003).

Many experiments at the hillslope scale have previously been performed (Anderson and Burt, 1990; Smakhtin, 2002; Beven, 2006b). Germann (1990) described a sprinkling-drainage experiment of a hillslope that included tracer application and Time-Domain-Reflectometry (TDR, see below). A few studies have investigated soil lateral conductivity (Wood, 1999; Leibundgut et al., 1999; Lin et al., 2006). Flow above bedrock layers was e.g. described by Mosley (1979) and Gutknecht (1996). Later, others focused on lateral macropore/pipe flow processes, and thresholds and nonlinearities that are associated with flow-impeding layers (McGlynn et al., 2002; Tromp-van Meerveld et al., 2007; review in Weiler et al., 2006). The author also investigated the connection of vertical and lateral flow pathways at the hillslope scale (Retter, 2003). This revealed a fast response of lateral pipe flow during rainfall events. Water table levels were an important trigger for pipe flow. Unfortunately, unexpected small amounts of rainfall during the study hampered a proper investigation of the relationship between vertical and lateral flow pathways at the field site (Retter, 2003).

A more comprehensive literature review is provided for the specific research topics (chapters 2 to 4).

1.4 Basics on measurement technique used and principles of investigation

The vector approach to subsurface flow of the present dissertation uses the Time-Domain-Reflectometry (TDR) technique. An overview of the basics is given below. TDR transmits a quickly rising time pulse along the wave-guide. If the wave-guide is of a uniform impedance and properly terminated, the entire transmitted pulse will be absorbed in the far-end termination and no signal will be reflected back to the TDR. But where impedance discontinuities exist, each discontinuity will create an echo that is reflected back to the reflectometer (hence the name). Increases in the impedance create an echo that reinforces the original pulse while decreases in the impedance create an echo that opposes the original pulse. The resulting reflected pulse that is measured at the output/input to the TDR is displayed or plotted as a function of time for a given transmission medium (Dirksen, 1999;Evett, 2003).

TDR is a standard (indirect) method used to determine soil moisture water content in porous media. Over the last two decades substantial advances have been made in TDR technique. The key to TDR's success is its ability to accurately determine the permittivity (dielectric number) of a material from wave propagation, and the fact that there is a strong relationship between the permittivity of a material and its water content, as demonstrated in the pioneering works of Hoekstra and Delaney (1974) and Topp et al. (1980). Recent reviews and reference work on the subject include Roth et al. (1990), Topp and Ferre (2002), Robinson et al. (2003), and Topp, (2003). The TDR method is a transmission line technique that determines an apparent TDR permittivity from the travel time of an electromagnetic wave that propagates along a transmission line. Usually this involves two or more parallel metal rods being embedded in a soil or sediment. TDR probes are usually between 10 and 30 cm in length and connected to the TDR via a coaxial cable (Dirksen, 1999; Evett, 2003).

TDR together with infiltration experiments have been intensively used as a principle investigation tool within the Soil Science Section at the Department of Geography. Methods were refined during more than a decade of active research on infiltration experiments. Previous results on infiltration into undisturbed soils, rapid transient flows in soil, and preferential flow were based on soil moisture time series of high temporal resolution (e.g. Bürgi, 1994; Germann et al., 1997; Germann et al., 2002). Recently, a manual was developed at the section to facilitate the use of TDR along with infiltration experiments in research, and teaching (Alaoui, 2005).

1.5 Objectives and research questions

This contribution deals with the plot scale and the hillslope scale. It was chosen because of previous experimentations respectively unsolved questions of the author (Retter, 2003) and most importantly because of updated recent objectives as stated in a research proposal (SNF, 2004).

Soil hydrologists deal typically with vertical preferential flow at the plot scale, whereas hydrologists dealing with flow processes at hillslope to catchment scales strongly consider rapid lateral flows. The rational of prioritizing lateral flow in hillslopes over vertical infiltration is based on the much longer lateral flow paths and residence times of the water when compared with its vertical soil passage. But indeed, the shift from vertical flow (commonly termed "infiltration") to lateral flow may thus form the transition from soil hydrology to hillslope hydrology. With regard to the two principle directions in hillslope hydrology, vertical and lateral, the overall research question asks: What is the spatial orientation of subsurface flow within a hillslope soil? (SNF, 2004).

The objectives supersede a previous study on the connection of vertical and lateral flow pathways at the hillslope scale (Retter, 2003). In examining the spatial orientation of flow in a hillslope soil, a new approach consisting of three TDR wave-guides was chosen. As often, measurements and results are restricted to a praticular scale. In this thesis measures

of velocity are used because of their ability to easily upscale information. Velocities are used to characterize and compare flow in vertical and lateral directions. Such relationships and premises may help to upscale hydrological response in different environments and at different scales as outlined by Blöschl (2001, 2006). Lastly, the objective of the study was to evaluate suitable direct measurement techniques for the downslope subsurface fluxes. Beven (2006b) claimed this objective in a recent review on streamflow generation, that contained the heading "What is there still to learn about streamflow generation?"

1.6 Outline of the thesis

The present thesis contains three manuscripts (chapters 2, 3, and 4), followed by a synthesis (chapter 5). The specific objectives of the individual contributions are:

Chapter 2: Vectors of subsurface stormflow in a layered hillslope during runoff initiation

by M. Retter, P. Kienzler, P.F. Germann

Introduces the measurement setup and provides answers to

- How "vertical" is vertical infiltration?
- Can we find evidence for "bending of flow" from the vertical to lateral?
- How does the velocity vector of the wetting front relate to runoff concentration time?
- What is the potential of the used setup to improve understanding of hillslope runoff?

Chapter 3: The causes for anisotropy measured on a uniform hillslope layer

by M. Retter, A. Rimmer, P.F. Germann

Analyses the results of chapter 2 and provides answers to

- How to explain the field observation of downslope flow initiation?
- What are the causes for apparent anisotropy that was indicated by the direction of wetting front propagation?
- Does a quantitative analysis of a simple 2D steady state model provide explanation of the field observations on anisotropy?

Chapter 4: Use of vertical and lateral flow velocities to characterise subsurface flow formation on a grassland hillslope

by M. Retter

Provides hillslope scale results on flow velocities and provides answers to

- What are the characteristics of vertical and lateral flow?
- How are vertical and lateral flows linked together to trigger the formation and intensity of subsurface stormflow?

Chapter 5 (Synthesis).

01
02
03
04
05

References

Alaoui, A. (2005): Evaluation der Bodenverdichtung mittels TDR-Methode. Évaluation de la compaction des sols par la méthode TDR. Benutzerhandbuch. Bundesamt für Umwelt, Wald und Landschaft, Bern. 74p. download http://www.buwalshop.ch; code: VU-4816-D

Anderson, M.G. and P. Burt (1990): Process Studies in Hillslope Hydrology. John Wiley & Sons Ltd., Chichester. UK. 539p.

Beven, K. (2006a): Searching for the Holy Grail of Scientific Hydrology: Qt=H(S, R, Δt)A as closure. Hydrol. Earth Syst. Sci. 10, 609-618.

Beven, K.J. (2006b): Streamflow Generation Processes. Benchmark Papers in Hydrology, No. 1, IAHS Press, Wallingford, UK, 431p.

Beven K. and P. Germann (1982): Macropores and water flow in soils. Water Resources Research 18(5), 1311-1325.

Blöschl, G. (2006): Hydrologic synthesis – across processes, places and scales. Special section on the vision of the CUAHSI National Centre for Hydrologic Synthesis (NCHS), Water Resources Research, invited paper, in press.

Blöschl, G. (2001): Scaling in hydrology. Hydrological Processes 15, 709-711.

Bundeamt für Geologie (2005): Bericht an den Bundesrat über die Hochwasserereignisse 2005. checked January, 28, 2007.
http://www.bafu.admin.ch/naturgefahren/01921/01948/index.html?lang=de

Bürgi, T. (1994): Bestimmung des Dynamik des Bodenwassers mittels Tensiometern und TDR-Sonden unter Feldbedingungen. Diploma thesis. supervised by Prof. P.F. Germann, geographisches Institut der Universität Bern, 90p.

Dirksen, C. (1999): Soil physics measurements. GeoEcology, Catena, Reiskirchen, 154p.

Evett, S.R. (2003): Soil Water Measurement by Time Domain Reflectometry. In: Stewart, B.A. and T.A. Howell (ed.): Encyclopedia of Water Science. Marcel Dekker, Inc. New York. Pp. 894-898.

Flury, M., Flühler, H., Jury, W.A., and J. Leuenberger (1994): Susceptibility of soils to preferential flow of water: A field study. Water Resources Research 30(7), 1945-1954.

Franks, S., Sivapalan, M., Takeuchi, K., and Y. Tachikawa (Eds)(2005): Predictions in Ungauged Basins: International Perspectives on the State of the Art and Pathways Forward. IAHS Publ. 301, 348 + xii pp.

Gerke, H.H. (2006): Review Article-Preferential flow descriptions for structured soils. J. Plant Nutr. Soil Sci. 169, 382–400. doi: 10.1002/jpln.200521955.

Germann, P.F., Helbling, A., and T. Vadilonga (2007) Rivulet approach to the in-situ characterisation of flow in a highly saturated soil. Vadose Zone Journal, in press.

Germann, P.F., Jäggi, E., and T. Niggli (2002): Rate, kinetic energy and momentum of preferential flow estimated from in-situ water content measurements. Europ. J. Soil Sci. 53, 607-618.

Germann, P.F. (2001): A hydromechanical approach to Preferential Flow. In: Anderson, M.G. and P.D. Bates (eds): Model Validation – Perspectives in Hydrological Sciences, 233-260. John Wiley 6 Sons, Ltd., Chichester.

Germann, P.F., Di Pietro, L., and V.P. Singh (1997): Momentum of flow in soils assessed with TDR-moisture readings. Geoderma 80, 153-168.

Germann, P.F. (1990): Macropores and hydrologic hillslope processes. In: Anderson, M.G. and P. Burt (1990): Process Studies in Hillslope Hydrology. John Wiley & Sons Ltd., Chichester. UK, 327-364.

Gutknecht, D. (1996): Abflußentstehung an Hängen – Beobachtungen und Konzeptionen (transl. Runoff Gerneration on Hillslopes –Observations and Concepts). Österreichische Wasser- und Abfallwirtschaft. 48 (5/6),134-144.

Hoekstra, P. and A. Delaney (1974): Dielectric properties of soils at UHF and microwave frequencies. Journal of Geophysical Research 79, 1699-1708.

Hopmans, J.W. and G. Pasternack (2006): Experimental hydrology: A bright future. Preface to special issue. Advances in Water Resources 29, 117-120.

Leibundgut, C., J.J. McDonnell, and G. Schultz. (1999): Preface. In: Leibundgut, C. et al. (ed.):

Integrated methods in catchment hydrology—Tracer, remote sensing, and new hydrometric techniques. IAHS Publ. 258. Int. Ass. of Hydrological Sciences Press, Wallingford, UK.

Lin, H.S., W. Kogelmann, C. Walker, and M.A. Bruns. (2006): Soil moisture patterns in a forested catchment: A hydropedological perspective. Geoderma 131(3-4), 345-368.

McDonnell, J.J., McGlynn, B., Vache, K., and I. Tromp-van Meerveld (2005): A Perspective on Hillslope Hydrology in the Context of PUB. in: Predictions in Ungauged Basins: International Perspectives on the State of the Art and Pathways Forward (ed. by Franks, S., Sivapalan, M., Takeuchi, K., and Y. Tachikawa), 204-212. IAHS Publ. 301. IAHS Press, Wallingford, UK.

McGlynn, B.L., McDonnell, J.J., and D.D. Brammer (2002): A review of the evolving perceptual model of hillslope flowpaths at the Maimai catchments, New Zealand. J. of Hydrology, 257, 1-26.

Mosley, M.P. (1979): Subsurface flow velocities through selected forest soils, south island, New Zealand. J. of Hydrology, 55, 65-92.

Retter, M. (2007): Use of vertical and lateral flow velocities to characterise subsurface storm flow formation on a grassland hillslope. Manuscript in preparation.

Retter, M., Rimmer, A., and P.F. Germann (2007): The causes for anisotropy measured on a uniform hillslope layer. Vadose Zone Journal, Manuscript under review.

Retter, M., Kienzler, P., and P.F. Germann (2006): Vectors of subsurface stormflow in a layered hillslope during runoff initiation. Hydrology and Earth Sci. Systems, 10, 209-220.

Retter, M. (2005): Bericht zum SLICE-Workshop. Hydrobrief Nr. 30. Fachgemein-schaft Hydrologische Wissenschaften, Deutschland.
http://www.fghw.de/chapvero/docs/hydrobrief30.pdf

Retter, M. (2003): Exploring subsurface flow paths at the Low Pass field site, Oregon, USA. Diploma thesis, Universität Freiburg. Principal supervisor M. Weiler. Unpuplished. 96p.

Robinson, D.A., Jones, S.B., Wraith, J.M., Or, D., and S.P. Friedman (2003): A review of advances in dielectric and electrical conductivity measurements in soils using time domain reflectometry. Vadose Zone Journal 2, 444-475.

Roth, K., Schulin, R., Flühler, H., and W. Attinger (1990): Calibration of time domain reflectometry for water content measurements using a composite dielectric approach. Water Resour. Res., 26, 1990.

PUB (2006): Predictions in Ungaged Basins. Homepage of the initiative. http://www.pub.iwmi.org/ (checked January, 28, 2007).

Sivapalan, M., Wagener, T. , Uhlenbrook, S., Zehe, E., Lakshmi, V., Liang, X., Tachikawa, Y., and P. Kumar (eds)(2005): Predictions in Ungauged Basins: Promises and Progress. PUB : Promises and Progress. Proceedings of IAHS Assembly held at Foz do Iguaçu, Brazil, April 2005. IAHS Publ. 303.

Sivapalan, M., Takeuchi, K., Franks, S.W., Gupta, V.K., Karambiri, H. , Lakshmi, V., Liang, X., McDonnell, J.J., Mendiodo, E.M., O'Connell, P.E., Oki, T. , Pomery, J.W., Schertzer, D. , Uhlenbrook, S., and E. Zehe (2003): IAHS Decade on Prediction in Ungauged Basins (PUB), 2003–2012: Shaping an exciting future for the hydrological sciences. Hydrological Sciences Journal 48 (6), 857-881.

Smakhtin, V.U. (2002): Some early Russian studies of subsurface storm-flow processes. Hydrol. Process. 16, 2613–2620 .

SNF (2004): Swiss National Science Foundation. Proposal of Prof. Germann #200020-101562. www.snf.ch

Topp, G.C. (2003): State of the art of measuring soil water content. Hydrological Processes 17, 2993–2996.

Topp, G.C. and T.P.A. Ferré (2002): Water content. In: Methods of Soil Analysis. Part 4. (ed. by Dane, J.H. and G.C. Topp), SSSA Book Series No. 5, Soil Science Society of America, Madison WI.

Topp, G.C., Davis, J.L., and A.P. Annan (1980): Electromagnetic determination of soil water content: measurements in coaxial transmission lines. Water Resources Research 16, 574-582.

Tromp-van Meerveld, H.J., Peters, N.E., and J.J. McDonnell (2007): Effect of bedrock permeability on subsurface stormflow and the water balance of a trenched hillslope at the Panola Mountain

Research Watershed, Georgia, USA. Hydrological Processes, in press.

Uhlenbrook, S. and C. Leibundgut (1997): Abflussbildung bei Hochwasser. Wasser und Boden 9, 13-22.

Weiler M., McDonnell J.J., Tromp-van Meerveld I., and T. Uchida (2006): Subsurface Stormflow. in: Anderson, M.G. and J.J. McDonnell (eds.): Encyclopedia of Hydrological Sciences 3 (10), Wiley and Sons Ltd., Chichester, UK.

Weiler, M. and F. Naef (2003): An experimental tracer study of the role of macropores in infiltration in grassland soils. Hydrological Processes 17, 477–493.

Wood, E.F. (1999): The role of lateral flow: Over- or underrated. in: Tenhunen, J.D. and P. Kabat (eds.): Integrating hydrology, ecosystem dynamics, and biogeochemistry in complex landscapes. p. 197–215. John Wiley & Sons Ltd., Chichester, UK.

01

02

03

04

05

Chapter 02

Vectors of subsurface stormflow in a layered hillslope during runoff initiation

Matthias Retter[1], Peter Kienzler[2], Peter F. Germann[1]

[1]   Department of Geography, University of Bern, Hallerstr. 12, 3012 Bern, Switzerland
[2]   Institute of Environmental Engineering, ETH Zürich, Schafmattstrasse 8, 8093 Zürich, Switzerland

01

02

03

04

05

Abstract

The focus is the experimental assessment of in-situ flow vectors in a hillslope soil. We selected a 100 m² trenched hillslope study site. During prescribed sprinkling an obliquely installed TDR wave-guide provides for the velocity of the wetting front in its direction. A triplet of wave-guides mounted along the sides of an hypothetical tetrahedron, with its peak pointing down, produces a three-dimensional vector of the wetting front. The method is based on the passing of wetting fronts. We analyzed 34 vectors along the hillslope at distributed locations and at soil depths from 11 cm (representing top soil) to 40 cm (close to bedrock interface). The mean values resulted as follows v_x= 16.1 mm min^{-1}, v_y= -0.2 mm min^{-1}, and v_z= 11.9 mm min^{-1}. The velocity vectors of the wetting fronts were generally gravity dominated and downslope orientated. Downslope direction (x-axis) dominated close to bedrock, whereas no preference between vertical and downslope direction was found in vectors close to the surface. The velocities along the contours (y-axis) varied widely. The Kruskal-Wallis tests indicated that the different upslope sprinkling areas had no influence on the orientation of the vectors. Vectors of volume flux density were also calculated for each triplet. The lateral velocities of the vector approach are compared with subsurface stormflow collected at the downhill end of the slope. Velocities were 25-140 times slower than lateral saturated tracer movements on top of the bedrock. Beside other points, we conclude that this method is restricted to non-complex substrate (skeleton or portion of big stones).

2.1 Introduction

For a wide range of hillslopes subsurface stormflow (SSF) is considered a major runoff generating process. For instance, Weyman et al. (1973) studied the direction and occurrence of the subsurface runoff component and found the following: Infiltration is driven by gravity and thus flow in slopes is dominated by vertical unsaturated movements towards the profile base, where lateral subsurface flow originates due to breaks in vertical permeability (distinct soil horizons or impermeable bedrock). They further argued that, once saturated conditions have been generated, lateral flow should occur, because the equipotential lines within the saturated soil will be nearly orthogonal to the gradient of the slope. The authors mentioned also that runoff response will be considerably delayed if water has to move first to the base of the soil profile, but lateral flow controls the magnitude of hillslope response.

Harr (1977) used tensiometer plots to closer look at the magnitude and direction of water fluxes in a hillslope. Between storms the vertical flux component at the 10 cm-depth was less than the downslope (lateral) components, but similar during storms. Conversely, vertical flux components at the 70- and 130 cm-depths were inferior to the downslope components during storms but similar to downslope components between storms. Greminger (1984) calculated two-dimensional and Wheater et al. (1987) calculated three-dimensional soil water fluxes

from tensiometer data. They monitored lateral components during dry conditions and after high intensity rainfall. They also determined the triggering factors such as slope angle, degree of saturation, hydraulic conductivity of soil horizons, and rainfall intensity. Anderson and Burt (1978) illustrated the influence of contour curvature (three-dimensional) on moisture movement.

Preferential flow in soil pipes occurs laterally above and within soil layers of lower permeability such as solid rocks and glacial tills or perched water tables (Sidle et al., 2000; Koyama and Okumura, 2002; Uchida et al., 2005). Beven and Germann (1982) considered infiltration, with its possible preferential flow, as driven by gravity. Buttle and McDonald (2002) investigated preferential flow systems in a thin soil at a slope by a combined approach consisting of TDR wave-guides and water/solute studies. The former measurement indicated vertical infiltration whereas the latter focused on lateral flow towards a trench. Both, matrix flow and preferential flow have to bend from mainly vertical to the predominant lateral direction. However, the processes leading to the pattern are poorly understood. Sherlock et al. (2000) discussed the necessity to include the general uncertainty associated with hydrometric techniques in the subsurface (e.g. calculation of hillslope flow paths).

We present the results of an investigation on the direction of flow at the hillslope scale. We focus on the direction of the infiltration fronts that are associated with sprinkling and that lead to runoff. The objectives of this paper are:

i)   How "vertical" is vertical infiltration?

ii)   Can we find evidence for "bending of flow" from the vertical to lateral?

iii)   How does the velocity vector of the wetting front relate to runoff concentration time?

iv)   What is the potential of the setup, to improve understanding of hillslope runoff?

2.2 Study site

The hillslope site was located at Lutertal, community of Reiden, northern Switzerland. We consciously selected a site where lateral SSF is likely to occur. An illustration of the study site is provided in Figure 2.1. Average annual precipitation at the site is 1056 mm. During the past 30 years the site has been under grassland. Prior to all experiments on the meadow we mowed the gras down to 5 cm. The slope angle α was 13.5°. On it we randomly chose a 12x16 m² plot. We marked the sidewise and top borders on the surface to determine the sprinkling area of 100 m². At the bottom end of the plot we excavated a trench down to the bedrock. The soil consisted of a top Ah-horizon (0-8 cm) and a sandy loam B-horizon with an average depth down to 45 cm. The particle size distribution in the B-horizon was 20% sand, 53.1% silt, and 22.9% clay by weight. Packing density within the 25 cm of soil depth amounted to 2 g cm^{-3} and increased to 3 g cm^{-3} for the layer down to 40 cm. Rooting depth of the grass was down to about 10 cm soil depth.

We observed vertical macropores within B-horizon at the trench face, mostly created by earthworms (Lumbricidae). Macropore density in the B-horizon was 248 per m^2. Further, small lateral soil pipes (diameter 3-8 mm) occurred at the transition between the B-horizon and bedrock.

The underlying bedrock is composed of siltstone (Molasse) with reduced hydraulic conductivity. We detached a siltstone cube by a saw and performed laboratory experiments. During sprinkling experiments (intensity =12 mm h^{-1}) onto the top surface the propagating wetting front was measured by TDR wave-guides. The velocity amounted to 1.4 mm min^{-1} (surface to depth of 3.5 cm) and 0.16 mm min^{-1} (surface to depth of 9.3 cm). No wetting arrived at 13 cm depth during 1 hour of sprinkling. (I. Willen-Hincapié, University of Bern, pers. comm.).

Figure 2.1. *The Lutertal study site on a grassland slope in northern Switzerland. Note the brownish trench face which was excavated at the bottom end of the instrumented 100 m² plot.*

2.3 Methods

Germann and Zimmermann (2005a) applied a novel approach to two sprinkling experiments at the 1-m^2-plot scale. This is now extended to the hillslope scale.

2.3.1 Basics on TDR application

Obliquely installed TDR wave-guides record the temporal increase of volumetric soil moisture θ [m^3 m^{-3}] when the wetting front moves across. This increase between the initial volumetric soil moisture θ_{ini} and the maximum volumetric soil moisture θ_{max} is outlined for a single TDR wave-guide in Figure 2.2. In a further step, the direction of the vector component is set equal to the one of the wave-guides. The steady advancement of the wetting front during the interval t_U to t_L yields:

$$\vec{v}_i = \frac{\vec{l}_i}{t_{L,i} - t_{U,i}} = \frac{\Delta q_i}{\Delta t_i} \cdot \frac{\vec{l}_i}{w_{max_i}} \qquad (1)$$

where $w_{max} = \theta_{max} - \theta_{ini}$ [$m^3\,m^{-3}$], l is the length of wave-guides positioned between U_i (x,y,z) and L_i (x,y,z), t_U and t_L are the arrival times of the wetting front at U and L, and $\Delta\theta/\Delta t$ is the slope of $\theta(t)$ between t_U and t_L. Likewise, according to Germann et al. (2002) and Germann and Zimmermann (2005b), the vector of the average volume flux density, q [$m\,s^{-1}$], during t_U < t < t_L in the direction of the wave guides is:

$$\vec{q}_i = v_i \cdot w_{max_i} = \vec{l}_i \cdot \frac{\Delta q_i}{\Delta t_i} \qquad (2)$$
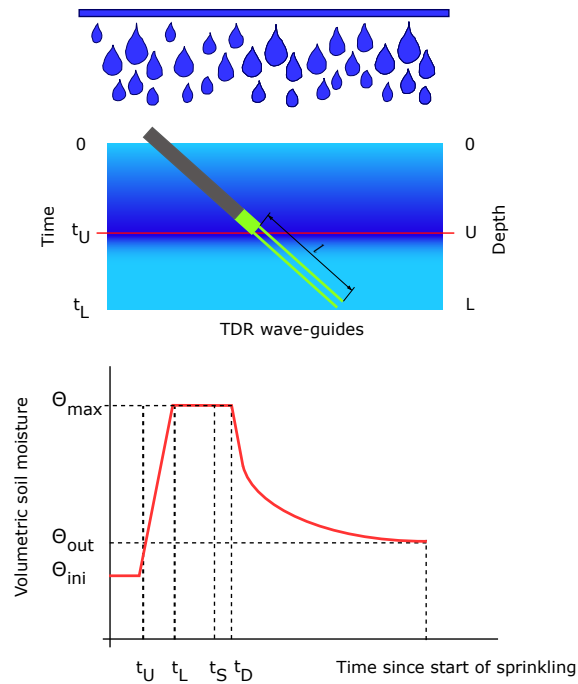
Figure 2.2. *Schematic representation of an obliquely installed wave-guide, a downwards travelling wetting front (up) and the linear increase of θ as the wetting front moves steadily (below). t_S indicates end of sprinkling.*

The index i ∈ (e, t, s) refers to the wave-guides, Figure 2.3. The procedure is repeated for the two other wave-guides. Figure 2.3 shows the installation of one triplet, containing three TDR wave-guides, which are orthogonally aligned to each other. Figures 2.3 and 2.4 show the arrangement of the wave-guides in the coordinate system. The vector sum (norm vector) is:

$$v_{tot} = \sqrt{\vec{v}_x{}^2 + \vec{v}_y{}^2 + \vec{v}_z{}^2} \qquad (3)$$

$$q_{tot} = \sqrt{\vec{q}_x{}^2 + \vec{q}_y{}^2 + \vec{q}_z{}^2} \qquad (4)$$
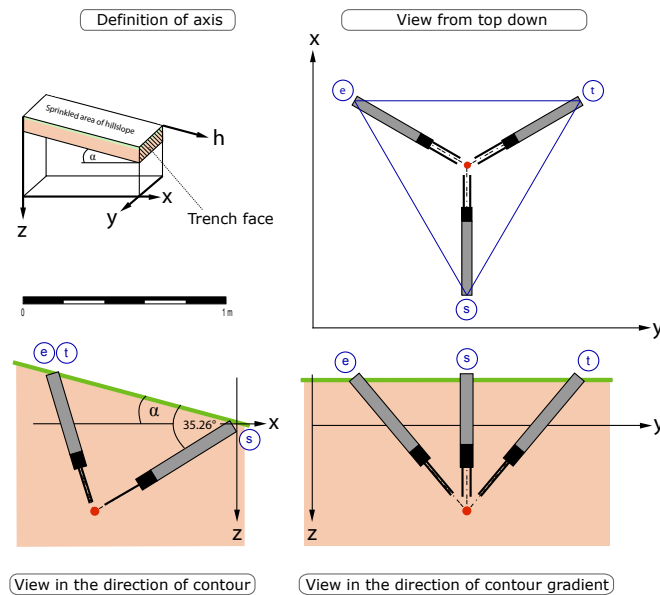
Figure 2.3. Definition of axis (top left) and scheme of mounting a triplet of TDR wave-guides in a hillslope soil by its different views. Probes (black) are attached to aluminum pipes (dark grey). Note that y-axis becomes positive towards right and negative towards left. And z-axis becomes more positive with increasing depth.

The representative sampling volume of a TDR wave-guide depends on the geometry of the probe, essentially the geometric factor. Decreasing the length of rods decreases geometric factor, making them less susceptible to electrical conductivity interference. Thus, for technical reasons, there is an optima between the accuracy of travel time measurement and conductivity losses. It is suggested for field measurement that wave-guides have a length between 0.15 m and 0.30 m (Robinson et al., 2003). Besides, for the vector method in particular the following applies: The longer the wave-guides, the less sensitive the measurements will get. On the other hand, the longer the wave guides the larger the control volume for assessing the vectors. In the end ease of installation, guaranteeing correct position of the rods, was found to be decisive.

2.3.2 Instrumentation

TDR wave-guides

One TDR wave-guide consisted of two $l = 0.15$ m long, parallel stainless steel rods, 30 mm apart and each 5 mm in diameter. The TDR wave-guides were electrically connected with a 50 Ω coax cable to a SDMX 50 coaxial multiplexer and further to a Campbell TDR 100 device, which generated the electrical pulses and received the signals. Both units were controlled by a Campbell CR 10x micro logger and the measurement interval was set to 90 s to more closely record the breakthrough of the wetting. The time resolution was the highest possible for the setup used.

We distributed ten triplets of TDR wave-guides across the hillslope, Figure 2.4. The rotation symmetric head of a wave-guide was attached to an aluminum pipe, whose outer diameter was smaller than the one of the probe (Figure 2.3). To install wave-guides we drilled holes using a soil auger and a supporting precision tripod. We put the wave-guides into the drill holes and then pushed them into the last 15 cm of soil. For that we also used the tripod with its guide rail. We carefully paid attention to avoid gaps between steel rods and soil (Gregory et al., 1995) and to avoid changes in soil structure (Rothe et al., 1997). Finally, the remaining drill hole space was sealed with bentonite. The depth, L, of triplets (see Figure 2.2) ranged between 11 cm (close to soil surface) and 35 cm (towards the boundary of soil-bedrock). A further deep installation of triplets was not possible, because there was a gradual transition from B- to C-horizon. This did not allow an installation between 35 and 40 cm soil depth. We located triplets in the way that sprinkled upslope contributing areas varied. Supplementary, a few oblique TDR wave-guides, called L1 – L6, were installed 2-4 cm above the bedrock interface right into the trench face. We aligned those wave-guides within the plane formed by the h- and y-axis and situated them with an angle of 45° to the x-axis. Sheet metal canopies (20 x 35 x 0.4 cm) were pushed into the soil above L1 – L6, but still parallel, with a space of 10 cm between L and the canopies. Thus, they protected each of the six wave-guides against flow in z-direction. This setup allowed a direct measurement of the established lateral wetting front along the h-axis and on the bedrock interface, where SSF is likely to occur.
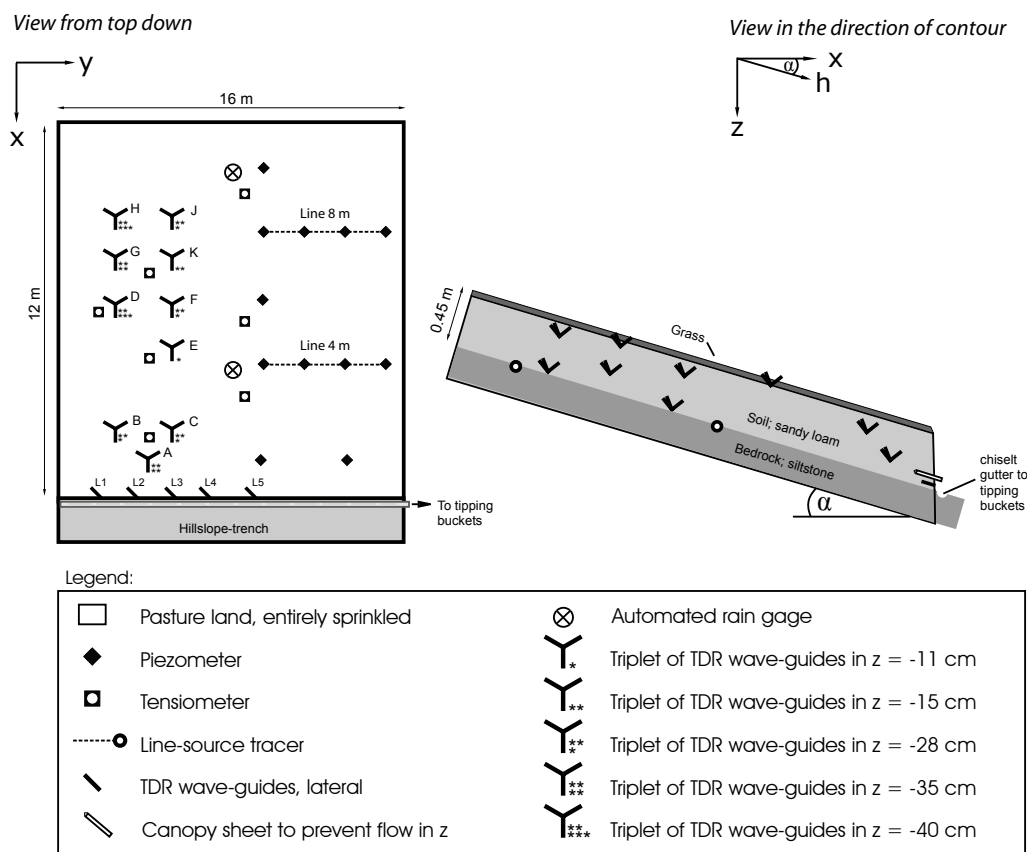

Figure 2.4. Instrumentation and setup of TDR triplets on the hillslope. Left: top down view; right: view in the direction of contour (profile).

To calculate volumetric water content, we used the transfer function by Roth et al. (1990), who separated the impacts on the dielectric number of the wave geometry from the soil properties such as bulk density and the content of clay in organic matter. For calibration prior to the installation in the field, each wave-guide was totally submerged and the corresponding dielectric number was set equal to the volumetric water content of 1 m^3 m^{-3}.

Sprinkling

The entire 100 m^2 hillslope segment was artificially sprinkled until SSF reached steady state. In order to account for different runoff concentration times we applied varying intensities and durations of sprinkling. We performed the following experiments: 11.5 mm h^{-1} for 13.08 h, 19 mm h^{-1} for 5 h, 35 mm h^{-1} for 3.08 h, and 56 mm h^{-1} for 3.5 h respectively. This range was achieved by different pumping pressures and two kind of systems: a sprinkler (design: Gardena) and a nozzle system by Rain Bird. Two automatic rainfall gauges, seven distributed rainfall samplers (manually checked every hour) and a water meter (sum normalized by measured sprinkling area) allowed the input to be calculated precisely. Prior to experiments we installed a vestibule around the site and also optimized the homogeneity of intensity distribution by several tests-runs. For details on the spatial distribution within the hillslope see appendix (page 38).

We also conducted sprinkling experiments on 1-m^2 subplots. These concerned triplets A-E. The rain simulator here consisted of 100 nylon tubes with inner diameters of 2 mm, which were mounted in a 0.1 x 0.1 m square pattern through a square of sheet metal of 1 m x 1 m. A gear moved the suspended sheet metal backwards and forwards ±50 mm in both horizontal dimensions such that it took approximately 1800 s for one tube outlet to return to the same spot. Distance between releases of drops down to the soil surface was 0.5 m. Controlled water supply was from a pump via a manifold to the tubes.

In addition, data of three natural storms were included in the analyses. The small storm on 30/05/2005 lasted 50 min with a total sum of 9.6 mm. The rainfall on 26/10/2004 was characterized by a widely distributed amount of 12.8 mm during daylight hours. We classified two events with a mean intensity of 3 mm h^{-1}. The maximum observed intensity on that day was 2.8 mm per 10 min.

Tracer experiments

We carried out two kinds of tracer experiments to track SSF. First, during sprinkling application to the entire slope, Dirac delta spikes using the flourescence dyes Pyranin, Naphtionat and Uranin were fed into the sprinkler at early, mean, and late times. Flow in the hose towards the sprinkler was turbulent, ensuring that the tracer was well mixed by the time it reached the sprinkler or the nozzles. Tracers moved through the soil system and we took samples directly at the trench face to get tracer travel times.

Second, piezometer holes were used as two line sources of salt tracer (bromide, chloride) directly above the soil-bedrock interface at 4 and 8 m upslope of the trench (see Figure 2.4). The tracer was quickly injected. We collected separate series of samples at the trench face (diffuse matrix flow), directly at the outlet of individual soil pipes and in summary at the tipping buckets. This allowed tracer front velocity to be calculated. It was determined by distance divided by time of first arrival minus the time of injection. Thus, it is a direct measure of presumed lateral flow along the bedrock.

Generally, the time interval of sampling was 60 s at the trench face and for total SSF, until flow stopped. We averaged the calculated tracer front velocities from different soil pipes in order to get mean travel times through the hillslope system.

Piezometers and monitoring of flow

The site had twelve piezometers, which reached to the bedrock at the bottom end. The inner diameter of the tube was 3 cm. At five piezometers a pressure transducer allowed automatic readings of water levels, and eight served as the tracer source (Figure 2.4). Additionally, we collected SSF in the trench by a led chamfer in the sandstone. Tipping buckets measured the SSF right next to the end of the trench. Metal sheet flow gutters allowed us to collect overland flow on the surface of the grassland hillslope. We also measured it by 100 ml tipping buckets.

2.4 Results

A total of 123 passages of wetting fronts were recorded by TDR wave-guides. They were generated either by 1-m^2 subplot irrigation, entire sprinkling of the hillslope or natural rain events. Figure 2.5 shows a breakthrough of wetting at the TDR wave-guides of one triplet. For all data the increase in soil moisture averaged to 6.2%vol. We analysed the rise of $\theta(t)$ between θ_{ini} and θ_{max} by linear regressions. The coefficients of determination, R^2, exceeded 0.9 for 66 wetting fronts and we approximate constant wetting front velocities for the progressing wetting front. We ignored 21 wetting fronts, as they were not a complete set of the three components. Thus, we used the increasing wetting phase for the assessment of v and q (according to Equation 1 and 2). From the total number of velocities at the TDR wave-guides, 34 datasets on triplets (equal to 102 single velocities) were finally derived. To enhance eadability velocities are reported in mm min^{-1}. Table 2.1 lists the components of the vectors that are described by the means v_x= 16.1 mm min^{-1}, v_y=for -0.2 mm min^{-1}, and v_z= 11.9 mm min^{-1}.
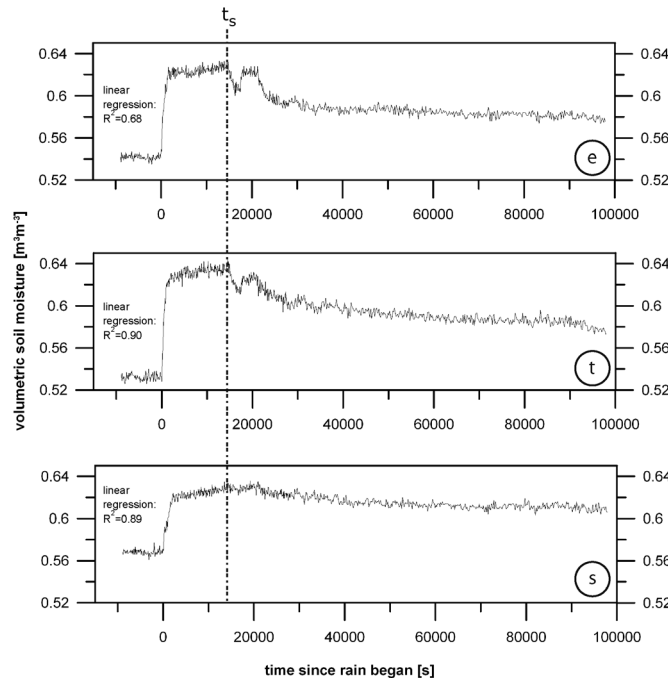
Figure 2.5. *Time-series of volumetric soil moisture for the three TDR wave-guides e, t, and s of triplet E in 11 cm depth on 27/05/2005 (ID #15). A continual, linear increase of soil moisture between θ_{ini} and θ_{max} is assumed. The analysed coefficients of determination for these slopes are mentioned next to the graphs.*

Table 2.1. *Components of velocities and volume flux densities in spatial xyz-space for triplets during different sprinkling events.*

ID #	Date	Type of sprinkling	Intensity $[mm\,h^{-1}]$	Triplet	Depth of TDR triplet [cm]	Velocity of wetting front $[mm\,min^{-1}]$				Volume flux density $[mm\,min^{-1}]$			
						V_x	V_y	V_z	V_{tot}	q_x	q_y	q_z	Q_{tot}
1	03/11/2004	hillslope	11.5	A	35	1.5	−0.2	0.4	1.6	0.8	−0.1	0.2	0.9
2	03/11/2004	hillslope	11.5	B	28	6.8	0.3	1.8	7.0	3.8	0.1	1.0	3.9
3	03/11/2004	hillslope	11.5	C	28	2.9	−0.6	1.2	3.2	1.7	−0.3	0.7	1.9
4	03/11/2004	hillslope	11.5	D	40	3.3	−0.2	1.5	3.7	1.9	−0.1	0.8	2.1
5	03/11/2004	hillslope	11.5	E	11	8.9	4.2	1.7	10.0	2.0	−0.5	1.6	−
6	03/11/2004	hillslope	11.5	F	28	3.4	−0.8	2.5	4.3	5.8	−1.3	2.8	2.6
7	03/11/2004	hillslope	11.5	K	15	10.1	−2.1	5.2	11.5	1.2	−0.3	0.2	6.5
8	03/11/2004	hillslope	11.5	J	28	1.0	0	0.5	1.0	6.7	1.1	0.5	−
9	12/11/2004	hillslope	19	A	35	2.1	−0.5	0.5	2.2	14.3	−7.8	24.9	1.2
10	12/11/2004	hillslope	19	B	28	12.0	2.0	1.0	12.2	17.3	−1.6	14.8	6.8
11	12/11/2004	hillslope	19	E	11	24.0	−13.4	42.9	51.0	18.4	1.8	3.0	29.8
12	27/05/2005	hillslope	56	A	35	31.0	−2.9	26.5	40.9	11.6	−1.8	9.1	22.8
13	27/05/2005	hillslope	56	B	28	32.6	3.2	5.6	33.3	24.0	−15.9	54.4	18.8
14	27/05/2005	hillslope	56	C	28	20.1	−3.1	15.2	25.4	50.1	21.7	23.2	14.8
15	27/05/2005	hillslope	56	E	11	38.4	−25.6	86.8	98.3	3.4	−0.9	1.5	61.6
16	27/05/2005	hillslope	56	K	15	89.2	34.8	38.6	103.2	4.4	0.4	2.6	59.3
17	20/05/2005	1 m²	35	A	35	6.2	−1.6	2.8	7.0	3.8	0.5	0.8	3.8
18	13/05/2005	1 m²	35	A	35	8.1	0.8	4.7	9.4	5.2	−1.6	1.4	5.1
19	13/05/2005	1 m²	35	B	28	6.7	0.9	1.5	7.0	2.4	−1.3	2.8	3.9
20	20/05/2005	1 m²	35	C	28	8.8	−2.9	2.4	9.5	11.5	0.1	12.8	5.6
21	07/06/2005	1 m²	55	A	35	4.4	−2.3	5.2	7.2	3.7	−0.3	2.1	3.9
22	07/06/2005	1 m²	55	C	28	20.8	0.2	21.8	30.2	12.3	−1.6	3.4	17.2
23	16/07/2005	1 m²	80	A	35	7.0	-0.5	4.0	8.1	6.6	0.4	2.7	4.3
24	16/07/2005	1 m²	35	B	38	22.2	−3.1	6.8	23.4	21.6	4.2	13.5	12.8
25	16/07/2005	1 m²	56	C	28	11.8	0.8	5.3	12.9	0.8	−0.1	0.2	7.1
26	16/07/2005	1 m²	80	E	11	35.9	7.1	23.6	43.6	3.8	0.1	1.0	25.8
27	30/05/2005	Natural rain event	11.5	E	11	14.5	−2.5	13.1	19.7	8.6	−1.4	7.7	11.6
28	24/05/2005	Natural rain event	7	B	28	5.9	−1.5	1.9	6.3	3.2	−0.8	1.0	3.5
29	26/10/2004	Natural rain event	see text	A	35	0.9	−0.1	0.6	1.1	0.5	0.03	0.3	0.6
30	26/10/2004	Natural rain event	see text	B	28	2.3	−0.2	0.7	2.5	1.3	−0.1	0.4	1.3
31	26/10/2004	Natural rain event	see text	C	28	77.0	−25.2	29.5	86.2	43.1	−13.7	16.3	48.0
32	26/10/2004	Natural rain event	see text	E	11	1.5	−0.4	1.0	1.8	0.9	−0.2	0.6	1.1
33	26/10/2004	Natural rain event	see text	B	28	3.0	−0.1	2.8	4.1	1.7	0.05	1.4	2.2
34	26/10/2004	Natural rain event	see text	C	28	23.0	−1.5	2.9	23.2	13.3	−0.8	1.7	13.4

The velocity of wetting within the soil are six orders of magnitude faster than in the underlying bedrock. This shift of velocities caused water to accumulate at the soil bedrock interface. Water generated lateral flowpaths on the sloping bedrock interface within the hillslope.

Vectors of the triplets A, B, and C from repeated 1-m^2 subplot sprinkling events on equal intensities were analyzed by paired sample t-tests. Since the significant value for all three cases is around 0.29, we conclude that the results are reproducible for the same sprinkling intensities and thus no change in xz-direction occurred.

Correlations between the different depths of the triplets and vector sum v_{tot} were not detectable (R^2=0.42, n=33). No significant relation was found between sprinkling intensity and either v_{tot} for all data (R^2=0.25, n=33) and neither one found for sprinkling intensity or the spatial orientation of the velocity vector.

Initial soil moisture conditions varied over 11%vol for all data and 5%vol for all data generated by hillslope sprinkling experiments. The higher θ_{ini}, the less data are available up to "wet" conditions for a precise determination of slope of $\theta(t)$ between t_U and t_L. Thus, we got best fitting results for the slope between t_U and t_L when the initial hillslope system was driest (ID # 12-16). We tested correlations of θ_{ini} conditions with v_{tot} and also with the amount of soil moisture increase during infiltration. For both cases no significant correlations were found.

The time series of θ after sprinkling showed an extended tailing of up to 4 days until initial soil moisture conditions were reached again. This pattern was more dominant for deep triplets and for the experiments in November (ID # 1-11), when transpiration was negligible. The long-tailed pattern is shown in Figure 2.5.

An overview of all vectors is given by 2D hillslope slices (Figure 2.6). The results are plotted in a linear scale, although dimensions differ over two orders of magnitude.

(a)
View in direction of contour
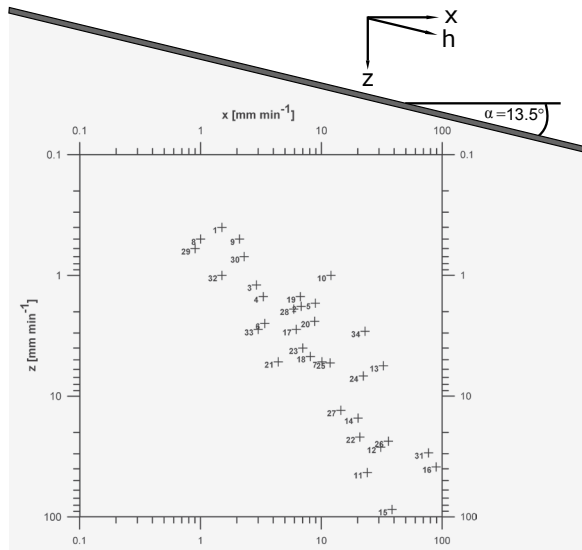
(b)
View from top down onto soil surface
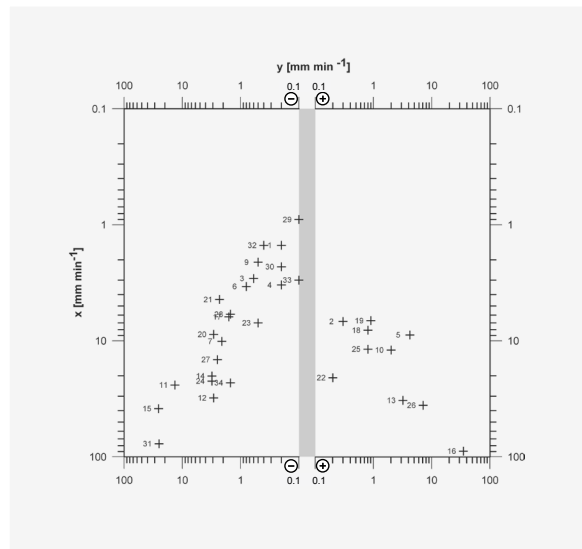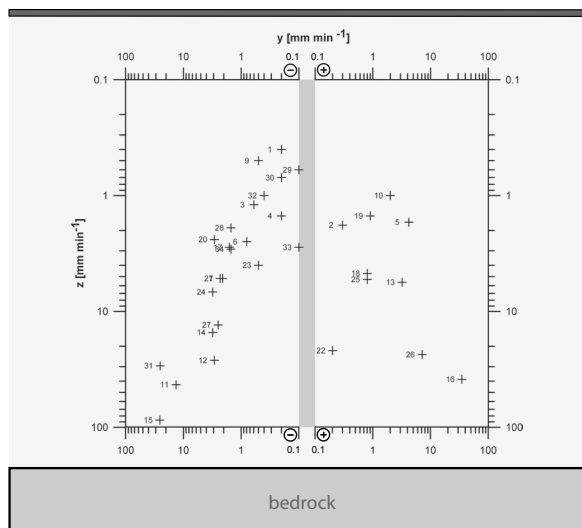
(c)
View in the direction of contour gradient

Figure 2.6. Resulting velocity vectors of the wetting front at various triplets on the hillslope. Vectors are not shown in arrow format but point format. Given ID numbers refer to information provided in Table 2.1. The graphs are embedded in "physical" descriptions to support orientation on the different views.

2.4.1 Analysis of x- y- z- velocity components during infiltration towards the spatially dominant direction

Of main interest is the view in the y-direction of contours i.e., looking at the x-z plane in our notation, Figure 2.6a. The ID numbers and corresponding alphabetic code refer to the location of triplets on the hillslope. All vectors show a downhill component. The dominance of the z- against the x-components was checked with a t-test for all data (see Table 2.2). A significance value of the test of 0.1 was selected because the pattern should trace clearly. Presuming this significance value, we could not find z- or x-components dominating except for the vectors at depth ≤ -28 cm and ≤ -35 cm where the x-components exceeded the z-components (see bold numbers). Even so, the mean angle of the resulting two vectors is 11° and 18° steeper than the h-axis. Thus, we do not consider the orientation of the wetting front as to be fully lateral.

Table 2.2. *Values of t-test to analyse x- and z-components for the dominating direction of the resulting vector.*

Selected triplets	Total number of vectors	t-test		
		Test value, T	Degrees of freedom, df	Sig. (2-tailed)
All (Natural events, sprinkling of hillslope, and 1 m^2 plots)	34	1.184	66	0.241
Sprinkling of hillslope	15	0.046	28	0.964
Sprinkling of all 1 m^2 plots	10	1.324	18	0.202
Sprinkling of deep 1 m^2 plots A, B, C	9	1.551	16	0.140
All data of shallow triplets E, K	8	0.116	14	0.909
All data of deep triplets A, B, C, D, F; where $z \geq 28$ cm	25	1.870	48	**0.068**
Sprinkling of deepest triplets A, D; where $z \geq 35$ cm	8	2.66	14	**0.019**

The observed direction in the xy-plane (Figure 2.6b) is widely aligned around y=0. By means of the t-test, a dominating x-direction (a downhill force rather than a spreading along the contours) is proposed. This is confirmed by a strong significance value of 0.05. The fast velocities (ID # 11, 15, 16) concerned the shallow triplets K and E, where the upper end of TDR rods is situated merely in 5-10 cm soil depth. Thus they are are within easy reach for the wetting. Amongst fast velocities ID 12, 22 and 31 correspond to deep triplets A and C.

The yz-view (Figure 2.6c) reveals the dominance in the z-direction, which is supported by a significant value < 0.05 (t-test). The above mentioned fast velocities at the shallow triplets also trace in this view. In summary, the wide spreading distribution along the y-axis is characterised by a mean velocity of -1.1 mm min^{-1} and showed a coefficient of variation of -8.4. We use the latter descriptor to characterise the heterogeneity in the soil.

As triplets B, C, F, and J are located at the same depth, we also addressed the question of the effects of differing upslope sprinkling area on orientation. Using data from 11 mm h^{-1} sprinkling, we analysed the resulting vector of the infiltration front for xz-components. The Kruskal-Wallis test (Kruskal and Wallis, 1952) indicated that the ratings of the resulting vector (its orientation towards a lateral component) did not differ with the upslope sprinkling area (chi-square= 3, asymp. sig. = 0.392).

The question of scale: do vector components for the same triplets differ between 1-m^2 subplot sprinkling and hillslope sprinkling? This could merely be investigated for given intensities of 55 mm h^{-1} and given equal antecedent soil moisture for triplets A and C, where we emphasised the xz-components. Here, we refrained from applying a test, as the sample size was too small. But from a visual check of Figure 2.6 the direction of the wetting front changed moderately between the two types of sprinkling.

The lateral vectors of SSF at the trench face were analysed on the basis of the mean average of L1 to L5. For the 1-m^2 subplot sprinkling events ID # 21, 22 it amounted to 2.5 mm min^{-1}. And for the entire hillslope event on 14/06/2005 the front velocity was calculated to 4.6 mm min^{-1}.

2.4.2 Time to concentration of runoff and tracer travel times

SSF, initiated by sprinkling, flowed into the trench through up to nine soil pipes. Except two (where L2 and L3 were installed) all flow pathways where not visible until the first runoff indicated an active pipe. These horizontal preferential pathways contributed almost the total SSF. As proved by visual observations very little percolation out of the matrix occurred. Pipe outlets were located close to the soil-bedrock interface showing the existence of microchannels according to Sidle et al. (2001). The same soil pipes were repeatedly active. The characteristics of the SSF as time to concentration and mean tracer velocity are shown in Table 2.3. Time to concentration of SSF, calculated as lag time between start of sprinkling to start of SSF, varied between 43 and 120 min. It depended on sprinkling intensity (R^2=0.98). Table 2.3 also shows the accumulated charge of sprinkling (initial loss) until SSF occurred. We detected a weak proportionality with sprinkling intensity.

During sprinkling five Dirac delta pulses of tracer allowed travel times to be measured from the first tracer arrival at the trench face. For saturated conditions, as indicated by the piezometers, it amounted to around 7 min (Table 2.3). Thus, tracer travel times during wet conditions and active runoff at the trench were 5 to 10 times faster than initial time to concentration of flow. During almost initial conditions on 14/06/2005 when one tracer was fed into sprinkling 20 min past start of sprinkling, the tracer travel time was 80 min, which was similar to the time to concentration (74 min).

Table 2.3. *Characteristics on the generation of subsurface stormflow (SSF) and results of tracer applications.*

	03/11/2004	12/11/2004	27/05/2005	14/06/2005	14/06/2005	14/06/2005
Sprinkling intensity [mm/h]	11.5	19	56	32	32	32
Time to concentration of SSF (lag time from start of sprinkling to start runoff) [min]	120	104	43	74	74	74
Accumulated amount of sprinkling until start of SSF [mm]	23	33	40	41	41	41
Tracer application by sprinkling						
Time of tracer input, Dirac spike [min since start of sprinkling]	238	–	109	50	105	152
Time of first arrival [min since start of sprinkling]	251	–	116	130	137	158
Time of max. concentration [min since start of sprinkling]	257	–	128	135	–	–
Travel time of tracer, input until first arrival [min]	7	–	8	80	22	6
Degree of saturation for lower hillslope segment (point measurements at 40 cm depth, piezometers) at moment of tracer application	full	–	full	little	less	full
Tracer line source at piezometers						
Time of tracer input [min since start of sprinkling]	240	–	110	–	–	–

Line source salt tracer experiments at a distance of 8 m from the trench were carried out, when piezometers indicated saturated conditions (10-15 cm) above the bedrock interface. The tracer front velocity was 658 mm min^{-1}. For the same conditions tracer front velocity for the 4 m tracer line amounted to 375 mm min^{-1}.

We also calculated volume flux densities according to Eq. (2) which also resulted in a three-dimensional vector. This was needed to get the vector sum q_{tot}, which ranges between 0.9 and 61.6 mm min^{-1} (Table 2.1). The mean value of q_{tot} is 13.4 mm min^{-1}.

2.4.3 Water balance calculations

The water balance in Table 2.4 summarizes that the input for the three sprinkling experiments varied between 97.5 and 199 mm. Overland flow was 2.2 mm for the small sprinkling intensity and reached 53.4 mm at the highest intensity. In contrast SSF decreased with increasing sprinkling intensity. We quantified losses between 22.5 and 62 mm.

Table 2.4. *Waterbalance for sprinkling experiments.*

	03/11/2004	12/11/2004	27/05/2005
sprinkling intensity [mm h^{-1}]	11.5	19	56
Input [mm]	151	97.5	199
Overland flow [mm]	2.2	3.5	53.4
SSF [mm]	54	28	19.8
Soil storage [mm]	33.2	43.5	66
Losses [mm]	62	22.5	59.8

01

02

03

04

05

2.5 Discussion

The vectors are reproducible in repeated experiments, which is in accord with Germann and Zimmermann (2005a). The direction of the vectors also matches well with the data of the previous study. The velocities of both experiments show the same magnitude, although soils are different. The bending of vectors, due to the considerable amount of soil moisture from the run 1 or 2 days before, which Germann and Zimmermann (2005a) showed, could not be observed in these data. This is because repeatable sprinkling events here were far apart from each other in time.

2.5.1 Discussion of temporal patterns

Here, we emphasize the discussion of temporal hillslope response, concentration times and the link to velocities calculated by the triplets. Looking at the lateral velocity of the wetting front (determined as h-component at waves-guides L1 – L6 and at triplets close to bedrock interface) and the travel times obtained by tracer data during steady state conditions we conclude: The lateral velocities (along h-axis) of first line source tracer arrival onto the bedrock are between 140 and 80 times higher than for the vector of wetting front. The difference is obvious as conditions shift from unsaturated to saturated for this shallow layer onto the bedrock while discharge at the trench face occurred. Note further, that we took tracer samples directly at the outlet of the soil pipes.

Our observations of temporal patterns in the unsaturated zone are different from rapid pore pressure responses and the direct control of timing and magnitude of peak discharge (Torres et al., 1998).

2.5.2 Uncertainties and limitations involved in the approach

A major concern in the application of this approach at the Lutertal field site is the dominating runoff generation mechanism. The lateral SSF is delivered by preferential flow in soil pipes occurring at the trench face. For the z-direction we mentioned existing vertical macropores within the sandy loam B-horizon. Thus vertical infiltration, is a combination of preferential pathways and homogenous matrix infiltration. It is likely that water bypassed the wave-guides with their lengths l of 15 cm. In this exercise we showed that 21 out of 123 passages of wetting fronts wetting were excluded and concerned some kind of preferential flow pattern. Up to now, the length of the TDR wave guide has not been changed. We will work on that task in upcoming investigations in order to sufficiently trace preferential flowpaths.

The results presented concern the moment of initial infiltration and the first wetting of soil. They provide evidence for „bending of flow" from a vertical to a lateral component, which was seen in Table 2.2, last row. But an obvious lateral vector, aligned on the h-axis is not

supported by the data. We may further question: a.) Why was there no significant change of h-components as the upslope contributing area (catchment area) increased and b.) why was there a minor dominance in x- or h-direction for deep triplets, although SSF occurred? To answer these questions we must highlight the fact that lateral flow is delayed with respect to infiltration. And second, after the infiltration front passed by, the system shifted to saturated conditions. For this point the TDR technique in general does not allow extraction of any further information on the volume of flux passing by. This is a major restriction of the vector method.

In order to compare average volume flux density q by the TDR wave-guides with discharge data from the trench, we assessed the representative elementary cross-sectional area (RECA). A discussion on that was introduced by Germann and Zimmermann (2005a) who determined the bottom area of the truncated tetrahedron to 0.02 m^2. The sampling volume of TDR wave-guides is widely modelled by numerical approaches (Ferré et al., 1998; Ferré et al., 2001) which may help to get a cross sectional area corresponding to the volume flux density of the triplet. In a first assumption the projection of the TDR rods might be used. Comparisons between q at the triplets and a calculated flux density at the trench face (16x0.45 m^2) for steady state SSF stress the time scales of both measures.

2.5.3 Further steps

Concluding the last sections we see a need to verify the approach presented here and quantitatively link it to discharge data. One useful option to elucidate this is a flow transport model. This would allow comparing the velocity information at triplets and the SSF gauging with the modeled numbers of both measures. On the other hand, the data provided in this work focuses on the wetting front. For this, kinematic wave approximations for subsurface flow in hillslopes are simple but efficient solutions. Here, we see an useful link to the work of Cabral et al. (1992) who showed in their Figure 2 the dimensional analysis of unsaturated flow and its x, z, and volume flux-vectors.

Further, to gain understanding of postponed lateral flow and recorded bending of flow, we must extend the approach and integrate data from the decreasing limb of soil moisture. For the steady state experiments performed, the shape of the recession limb did not allow us to extract more information because of the long tailing of θ.

01
02
03
04
05

2.6 Conclusions

We could find the following answers to our questions:

i)   Vertical infiltration and its propagating fronts do not move truly vertically, as we have shown in this exercise. None of the vectors was an exclusive z-component. Soil heterogeneity causes deviation up to an angle of 67° from the z-axis.

ii)   The approach presented allowed us to determine the spatial direction of the advancing wetting front. This is restricted to the first passage of the wetting front! Thus, up to now the approach is insufficient to fully demonstrate the "bending of flow" because there is a time delay between infiltration and the lateral components. However, several deep triplets provide evidence for lateral components as discussed above.

iii)   For the Lutertal field site we gained knowledge that lateral saturated tracer movements on top of the bedrock are 25-140 times faster than lateral unsaturated zone velocities of the wetting front. The vector velocities ranged in from 0.1 to 89 mm min^{-1}. Time to concentration was sprinkling rate dependent and ranged between 43 and 120 min for the site. No significant relation was found between concentration time and lateral velocity or the vector sum v_{tot}.

iv)   This method is restricted to non-complex substrate (skeleton or portion of big stones) to install TDR wave-guides. A plane bedrock topography with its similarity to the simple surface topography is of further help. This method is restricted to the first wetting front arriving while sprinkling or a rain storm occurs. The uncertainty of this method, e.g. dominance of preferential pathways during runoff, questions the transferability of l=15 cm wave-guide information towards a hillslope of 100 m^2. Quantitative comparisons between measured outflow at the trench and volume flux at the triplet are not possible to date. We believe that there is useful information included, but there is a need to extend the approach.

References

Anderson, M.G. and Burt, T.P.: The role of topography in controlling throughflow generation. Earth Surface Processes and Landforms, 3, 331-344, 1978.

Beven, K. and Germann, P.: Macropores and waterflow in soils. Water Resour. Res., 18, 1311-1325, 1982.

Buttle, J.M. and McDonald, D.J.: Coupled vertical and lateral preferential flow on a forested slope. Water Resour . Res., 38, WR000773, 2002.

Cabral, M.C., Garrote, L., Bras, R.L., and Entekhabi, D.: A kinematic model of infiltration and runoff generation in layered and sloped soils. Advances Wat. Res., 15, 311-324. 1992.

Ferré, P.A., Knight, J.H., Rudolph, D.L., and Kachanoski., R.G.: The sample areas of conventional and alternative time domain reflectometry probes. Water Resour. Res., 34, WR02093, 1998.

Ferré, P.A., Nissen, H.H., Moldrup, P., and Knight, J.H.: The sample area of time domain reflectometry probes in proximity to sharp dielectric permittivity boundaries, p. 195–209. In Dowding, C.H. (ed.): 2nd Proc. Int. Symp. and Workshop on Time Domain Reflectometry for Innovative Geotechnical Applications. Available at http://www.iti.northwestern.edu/tdr/tdr2001/proceedings/Final/TDR2001.pdf (verified 15/07/2005). Infrastructure Technology Institute, Northwestern University, Evanston, IL, 2001.

Germann, P.F., Jäggi, E., and Niggli, T.: Rate, kinetic energy and momentum of preferential flow estimated from in situ water content measurements. European Journal of Soil Science, 53, 607-617. 2002.

Germann, P.F. and Zimmermann, M.: Directions of preferential flow in a hillslope soil. Quasi-steady flow. Hydrological Processes, 19, 887–899, 2005a.

Germann, P.F. and Zimmermann, M.: Water balance approach to the in situ estimation of volume flux densities using slanded TDR wave guides. Soil Science, 170(1):3-12, 2005b.

Gregory, P.J., Roland, P., Eastham, J., and Micin, S.: Use of time domain reflectometry (TDR) to measure the water content of sandy soils. Aust. J. Soil Res., 33, 265–276, 1995.

Greminger, P.: Physikalisch-ökologische Standortuntersuchung über den Wasserhaushalt im offenen Sickersystem Boden unter Vegetation am Hang. Eidg. Anstalt forstl. Versuchswes., Mitt. 60, 151-301, 1984.

Harr, R.D.: Water flux in soil and subsoil on a steep forested slope. J. Hydrol., 33, 37-58, 1977.

Koyama, K. and Okumura, T.: Process of pipeflow runoff with twice increase in discharge for a rainstorm. Trans. Jpn. Geomorphol. Union, 23, 561-584, 2002.

Kruskal, W.H. and Wallis, W.A.: Use of ranks in one-criterion variance analysis. J. American Statistical Association, 47 (260), 583–621, 1952.

Robinson, D. A., Jones, S. B., Wraith, J. M., Or, D., and Friedman, S.P.: A Review of Advances in Dielectric and Electrical Conductivity Measurement in Soils Using Time Domain Reflectometry. Vadose Zone J., 2, 444-475, 2003.

Roth, K., Schulin, R., Flühler, H., and Attinger, W.: Calibration of time domain reflectometry for water content measurements using a composite dielectric approach. Water Resour. Res., 26, WR01238, 1990.

Rothe, A., Weis, W., Kreutzer, K., Matthies, D., Hess, U., and Ansorge, B.: Changes in soil structure caused by the installation of time domain reflectometry probes and their influence on the measurement of soil moisture. Water Resour. Res., 22, WR0474, 1997.

Sherlock, M.D., Chappell, N.A., and McDonnell, J.J.: Effects of experimental uncertainty on the calculation of hillslope flow paths. Hydrological Processes, 14, 2457-2471, 2000.

Sidle, R.C., Noguchi, S., Tsuboyama, Y., and Laursen, K.: A conceptual model of preferential flow systems in forested hillslopes: evidence of self-organization. Hydrological Processes, 15, 1675–692, 2001.

Sidle, R.C., Tsuboyama, Y., Noguchi, S., Hosoda, I., Fujieda, M., and Shimizu, T.: Storm flow generation in a steep forested headwater: a linked hydrogeomorphic paradigm. Hydrological Processes, 14, 369-384, 2000.

Torres, R., Dietrich, W.E., Montgomery, D.R., Anderson, S.P., and Loague, K.: Unsaturated zone processes and the hydrologic response of a steep unchanneled catchment. Water Resour. Res., 23, WR01140, 1998.

02

Uchida, T., Tromp-van Meerveld, I., and McDonnell, J.J.: The role of lateral pipe flow in hillslope runoff response: an intercomparison of non-linear hillslope response. J. Hydrol., 311, 117-133, 2005.

Weyman, D.R.: Measurements of the downslope flow of water in a soil. J. Hydrol., 20, 267-288, 1973.

Wheater, H.D., Langan, S.J., Miller, J.D., and Ferrier, R.C.: The determination of hydrological flow paths and associated hydrochemistry in forested catchments in central Scotland. IAHS Pub. No. 167, Proc. Vancouver Symposium, 1987.

Appendix

Sprinkling intensity measured by seven randomly, spatially distributed point measurements on the hillslope. Mean and standard deviation of the data are provided in the lower right corner. Data concern the experiment on 03/11/2004.

Sampler	Sprinkling intensity [mm h^{-1}] for 1 h of sprinkling while entire experiment											
1	10	5	3	13	10	13	15	17	18	11	12	8
2	11	9	9	13	10	13	13	10	11	13	9	8
3	11	10	14	12	9	12	9	8	9	0	7	9
4	14	16	18	18	15	24	24	23	35	24	17	12
5	10	11	10	13	10	10	10	10	12	11	9	4
6	10	8	11	13	9	10	9	9	12	9	5	9
7	10	8	10	10	8	8	10	9	11	11	8	13
										mean	11.5	
										stddev	4.6	

Chapter 03

The causes for anisotropy measured on a uniform hillslope layer

Matthias Retter[1], Alon Rimmer[2], Peter F. Germann[1]

[1]   Department of Geography, University of Bern, Hallerstr. 12, 3012 Bern, Switzerland
[2]   Israel Oceanographic and Limnological Research, Kinneret Limnological
         Laboratory, Migdal 14950, Israel

01

02

03

04

05

Abstract

This paper investigates downslope vadose flow on a hillslope. Speed and direction of wetting front propagation was obtained by an the TDR triplets method that indicated anisotropy within the soil. Therefore, the following characteristics were tested as controls on anisotropy: 1. small scale soil structure; 2. layering of the soil profile; 3. boundary conditions of flow. To determine small scale soil characteristics, small scale core samples were analysed for saturated hydraulic conductivity in the vertical and horizontal direction; however, no small scale anisotropy was found. Further layering effects were tested using initial soil moisture content and soil structure characterization. The soil contained no evident layering within the soil profile. Initial soil moisture did not contribute to anisotropy. Anisotropy was most likely caused by boundary conditions of flow due to increased moisture content at the soil-bedrock interface that increased the hydraulic conductivity across the soil. The change curved the streamlines downslope, as measured by the TDR triplets. The work also addresses questions of scales of hydraulic conductivity, soil moisture and flux measurements. The experimental setup could have significant implications for studies on anisotropy in the field and help to better understand bending stream lines and downslope flow initiation.

3.1 Introduction

Most landscapes, natural or cultivated, are nonlevel. As water infiltrates vertically into nonlevel soils, it often changes direction to lateral flow. Particularly for hillslopes, soil profile observations are not easily associated with the phenomena of bending stream lines from vertical to downslope flow direction. So far, field observations of infiltration have hardly resolved flow directions in unsaturated soils.

Increasing interest has been directed to hydraulic properties in sloping landscapes. Casanova et al. (2000) studied the influence of aspect and slope on hydraulic conductivity, measured by a tension infiltrometer. A destructive hillslope infiltrometer was introduced by Mendoza and Steenhuis (2002), while Brooks (2004) measured lateral saturated hydraulic conductivity using a hillslope-scale experiment. A further experimental study (Bodhinayake et al., 2004) found that both, tension and double-ring infiltrometers are suitable for the characterization of soil hydraulic properties in landscapes with slopes up to 20%. Recent efforts also improved hydrological modelling of flow in sloping soil layers. Hjerdt et al. (2004) developed a downslope index that allows quantification of downslope influences on local drainage. Chen and Young (2006) adapted the Green-Ampt equation to slope effects, and Akylas et al. (2006) presented an analytical solution to planar flow in sloping layers as a linearized extended Boussinesq equation. Nevertheless, problems arise due to the fact that modelling attempts lack support by diverse field observations.

A new method to measure the speed and direction of wetting front propagation in sloping soils was introduced by Germann and Zimmermann (2005). The experimental approach was

based on TDR wave-guide measurements. Three wave-guides were mounted along the sides of a hypothetical tetrahedron, with its peak pointing down. Such a "triplet" recorded the three-dimensional propagation of the wetting front, which resulted in the vector of wetting front velocity and direction. Using coordinate transformation, vertical and horizontal flow initiation components were derived. Retter et al. (2006) applied this method to a 100 m² hillslope section of shallow soil above an impermeable layer of bedrock. During prescribed sprinkling experiments the resulting vectors were recorded for ten triplets in various depths. They found that vertical flow direction dominated wetting front vectors of velocity close to the soil surface, whereas downslope direction dominated wetting front vectors close to the bedrock.

In this work, we relate measured vectors of flow reported by Retter et al. (2006) to aspects of hydraulic conductivity and anisotropy of shallow unsaturated soil layers. These considerations enhance the understanding of anisotropy and its field scale implementation. Our explanation is mainly a qualitative attempt to explain the anisotropy of the soil layer at the hillslope study site. The quantitative analysis (Appendix, page 58f) was limited to a simple 2D steady state model of unsaturated flow conditions within a hillslope layer, which explain the extended definition of anisotropy.

3.2 Theory of Anisotropy

The hydraulic conductivity, K, of a porous media, defined by Darcy's (1856) Law, is called non-uniform if there is a change of K within the domain of porous media, and is anisotropic if K is a function of the direction. An equivalent definition of anisotropic K is a point within the domain where the vector of the driving force (hydraulic gradient $\nabla\phi$) and the vector of flux $\mathbf{q}$ are not in the same direction. While K is scalar for an isotropic soil, the hydraulic conductivity of an anisotropic soil depends on the flow direction, and Darcy's Law for 2D flow is then expressed as

$$\mathbf{q} = -\mathbf{K}\nabla\phi \qquad\qquad (1)$$

$$\mathbf{K} = \begin{bmatrix} K_{xx} & K_{xz} \\ K_{zx} & K_{zz} \end{bmatrix} \quad ; \quad \mathbf{q} \equiv \begin{bmatrix} q_x \\ q_z \end{bmatrix} = -\begin{bmatrix} K_{xx}\dfrac{\partial\phi}{\partial x} & K_{xz}\dfrac{\partial\phi}{\partial z} \\ K_{zx}\dfrac{\partial\phi}{\partial x} & K_{zz}\dfrac{\partial\phi}{\partial z} \end{bmatrix}$$

Here $\mathbf{q}$ is a 2D flux vector, $\mathbf{K}$ is the hydraulic conductivity symmetrical tensor and ϕ is the hydraulic head. For our discussion, two definitions are proposed:

A. Small scale anisotropy (U) which is often referred to as macroscopic anisotropy (Glass et al., 2005; Khaleel et al., 2002), is the anisotropy which can be defined in a scale less then several centimetres, and can be measured on samples of this size.

B. Average anisotropy ($\overline{U}$): Anisotropy defined in large scale porous media which cannot be measured on samples of the size mentioned above, or anisotropy measured on a non uniform medium.

In a soil layer with a finite thickness, there are three causes for average anisotropy:

B₁. Small scale anisotropy: The hydraulic conductivity is strongly connected to the distributions of pore size and shape of pores in the soil, and thus with soil structure. Any slight directional difference in the arrangement of the soil particles and soil aggregates, resulting from compaction or differential settlement, may render the soil anisotropic with respect to its hydraulic conductivity (Bear 1979, pg. 31). The structural formation effects both swelling and shrinking processes of soils, and the direction-dependent behavior of hydraulic conductivity (Dörner, 2005). Mualem and Dagan (1976) showed that K depends on the hydraulic radius of the pores, which is not necessarily identical in all directions, thus causing small scale anisotropy. Zaslavsky and Sinai (1981) mentioned forest soils and certain grass covered areas, where the accumulated organic matter may have a marked orientation parallel to the soil surface, that form anisotropy. Small scale measurements of K in a soil profile in the vertical and horizontal directions separately, were conducted by various authors (e.g., Dabney and Selim, 1987; Bathke and Cassel, 1991; Ball and Robertson, 1994; Zhang, 1996; Beckwith et al., 2003). In addition to the two main directions, studies were also conducted for diagonal [45°] direction (e.g. Dörner and Horn, 2006), or for radial and vertical hydraulic conductivities (Basak, 1972). In some cases it was found that K is higher in one direction than in the other one due to the flaky shape and orientation of individual particles with respect to the main axes.

B₂. Layer composed of sub-layers which differ in their hydraulic conductivity: A common theoretical analysis represent anisotropic soils as a medium of parallel layers (Miyazaki, 2006, pg. 106). In such a medium consisting of k layers each of a thickness D_i and a uniform saturated hydraulic conductivity K_i, the coefficient of average anisotropy $\overline{U_{xz}}$ is defined by

$$\overline{U_{xz}} \equiv \frac{\overline{K_x}}{\overline{K_z}} = \frac{1}{L^2} \sum_{i=1}^{k} K_i D_i \sum_{i=1}^{k} \frac{D_i}{K_i} \qquad (2)$$

where $\overline{K_x}$ and $\overline{K_z}$ are the average K in the direction lateral and perpendicular to the direction of soil layer, respectively, and L is the thickness of the layer. It can be shown that $\overline{K_x} \geq \overline{K_z}$. When the averaging process is performed on a relatively large scale consisting of different types of soil layers, the soil profile as a whole behaves as an anisotropic medium, and the average hydraulic conductivity coefficient is represented by a 2D tensor (Eq. 1). Mualem (1984) used a continuous probability density function in a layered soil to evaluate the anisotropy coefficient based on saturated hydraulic conductivity K_{sat}. His conclusion was that $\overline{U_{xz}}$ of a saturated soil is determined mainly by the K_u/K_0 ratio, where K_u and K_0 are maximal and minimal K_{sat} in the layer, respectively, rather than by the actual numerical values of the conductivities.

B$_3$. Average anisotropy in layered unsaturated soil caused by boundary conditions of flow: The surface soil layer often consists of small-scale variations in the hydraulic conductivity particularly in the direction perpendicular to the soil surface. With given top and bottom boundaries, this layer will display average anisotropy on a large scale, especially under unsaturated flow conditions. Local minor changes in the hydraulic conductivity can increase or decrease with depth as a result of changes in the flow regime and saturation degree, resulting in the curving of stream lines, which on average may appear as the effect of anisotropy. This phenomenon was studied both by analytical solutions of flow problems in a slanted uniform soil layer (Zaslavsky, 1970; Zaslavsky and Sinai, 1981; Whipky and Kirkby, 1978, pg. 128; Philip, 1991; Wallach and Zaslavsky, 1991; Cabral et al., 1992; Boger, 1998), and numerical solutions (Zaslavsky and Sinai, 1981; Wallach and Zaslavsky, 1991; Jackson, 1992). It has also been experimentally demonstrated by the movement of a tracer in sand soil (McCord and Stephens, 1987).

An average anisotropy in layered unsaturated soil caused by boundary conditions of flow can be exemplified by analyses of steady lateral unsaturated flow on a hillslope. If the thickness of the soil layer from the impervious base to the soil surface is much smaller than its length, and the slope has a uniform angle, we may use a simple analytical solution of the apparent steady state condition (Appendix, page 58; see also Garber and Zaslavsky, 1977), to calculate the soil moisture and lateral flux under a steady state flow assumption for an infinite slope, while the entire profile is unsaturated. To that end we use rotated cartesian space coordinates (s*, n*) where s* is parallel to the soil surface and n* is perpendicular to it (Figure 3.2a), and n*=0 at the interface between the impervious base and the soil above. The K distribution along the n* axis is then given by:

$$K(n) = \frac{K_0^*}{K_{sat}} \exp(-An) \tag{3}$$

$$n = n^*/L; \quad 0 \geq n \geq 1; \quad K = K^*/K_{sat}; \quad A = aL\cos(\alpha) \; ; \; 0 < K_0^* < K_{sat}$$

where K_{sat} and K_0^* are the saturated hydraulic conductivity and the unsaturated hydraulic conductivity at the base of the layer (n*=0), respectively; n is the nondimensional axis; L the thickness of the layer; and the constant a (m^{-1}) is the sorptive number in Gardner's (1958) equation (Appendix). The average anisotropy factor in this case is defined similar to Eq. (2):

$$\overline{U_{sn}} \equiv \frac{\overline{K_s}}{\overline{K_n}} = \int_{n=0}^{1} K \, dn \int_{n=0}^{1} \frac{dn}{K} \tag{4}$$

Such anisotropy is also described by Miyazaki (2006; pg. 113f), who demonstrated how vertical streamlines are diverted downslope in the transition between flow in the upper relatively dry soil to more wet layers below.

In general, the anisotropy factor is a function of both the saturation degree, and the anisotropy parameter, that characterizes the ratio of the local conductivities parallel and normal to the bedding plane (Grebnev and Skal, 2006). According to Mualem (1984), the anisotropy of unsaturated soils was found to change both with K_u/K_0 ratio (see above), and with the degree of saturation. Moreover, in a layered soil profile there might be hysteresis originating from the inter-relationship between the different layers, in addition to the intrinsic hysteresis of each layer (Zaslavsky and Sinai, 1981; Assouline and Or, 2006).

In the following we use the term "apparent anisotropy" for observed flux measurements that indicate a changing of flow direction in the vadose zone, typically associated with anisotropic conditions. Apparent anisotropy may occur as a result of 1. Small scale soil structure; 2. layering of the soil profile; 3. boundary conditions of flow; and 4. the history of the flow process.

3.3 Methodology

3.3.1 Study site and soil structure

The study was conducted on a $8.33 \times 12 = 100$ m² hillslope with an angle $\alpha = 13.5°$ and soil depth between 35 cm and 45 cm (Figure 3.1). During the past 30 years the site has been under grassland. The soil is classified as a Cambisol according to FAO-Unesco (1994). Only subtle changes were observed between the soil horizons, whereas a sharp change of bulk density arose at the transition to the bedrock (Figure 3.1 and Table 3.1). Within the soil, we observed macropores. At the trench face, directly above the bedrock, macropores of small diameters between 3 and 8 mm occurred (Figure 3.1). Rooting depth of the grass was down to about 10 cm soil depth. Laboratory analyses for particle sizes were carried out on dry and sieved (< 2mm) samples. For grain size measurements, carbonates were removed by treatment with HCl, and organic matter was oxidized with 30% H_2O_2. In addition, micro-aggregates smaller 63 μm were dispersed with Na_2CO_3. The sand fractions (63-2000 μm) were separated by wet sieving and the silt (2-63 μm) and clay (< 2 μm) fractions were quantified using a Micromeritics SediGraph 5100. Percentages of coarse fragments were visually estimated using templates (Finnern et al., 1994) and originate from Kienzler and Naef (2007).
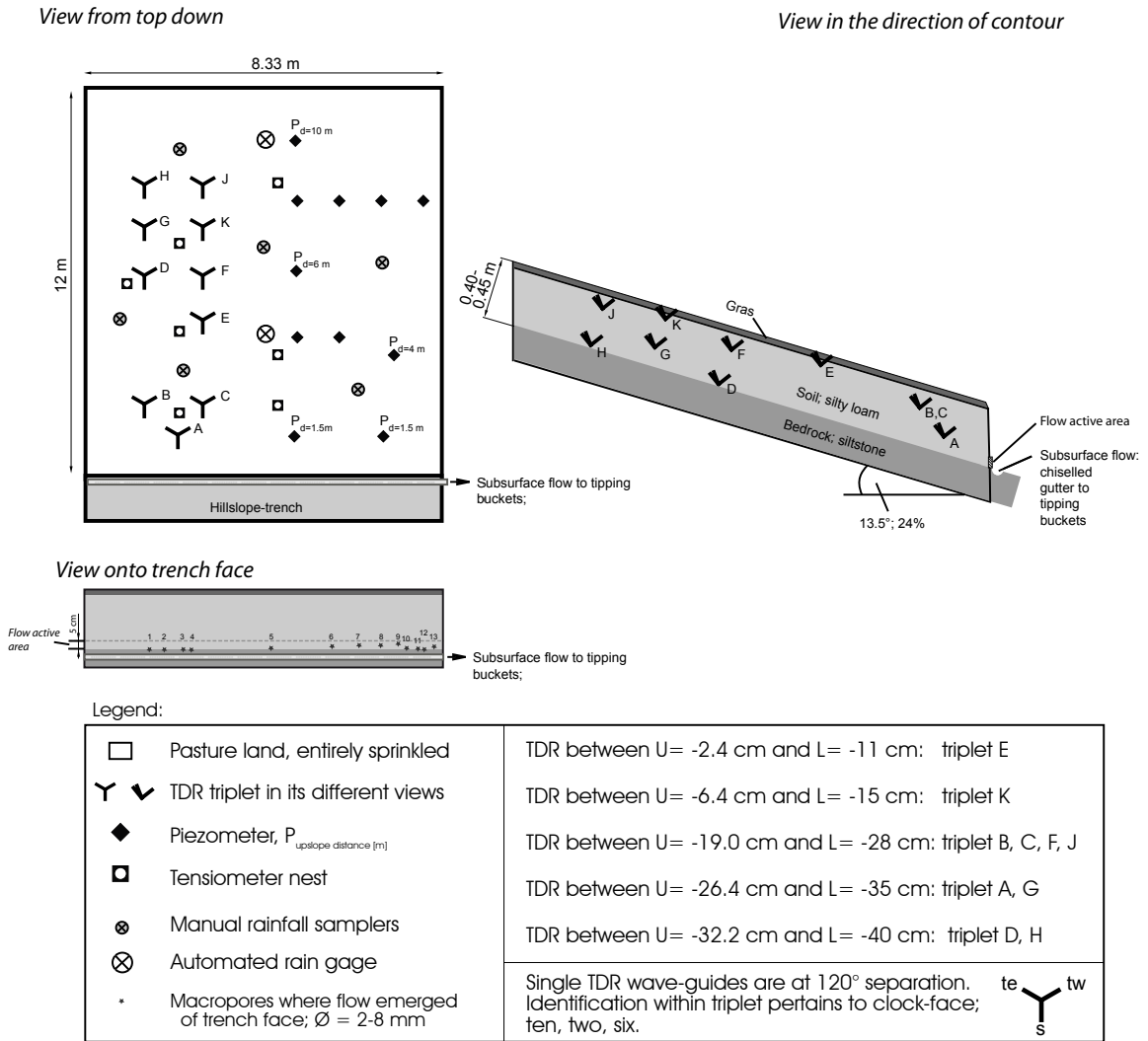
Figure 3.1. Instrumentation of the Lutertal study site.

Table 3.1. Soil characteristics at the study site.

Sample depth	No. of samples $(K_{sat,Z}, K_{sat,x})$	$K_{sat,Z}$					Particle size distribution			Coarse fragments	Porosity	pH
		Median	Mean	Max	Min	STD	Sand [%]	Silt [%]	Clay [%]	[%]	[%]	
[cm]	[–]			$[10^{-5}\,\mathrm{m\,s^{-1}}]$								
11	10, 9	0.31	0.84	3.1	0.02	1.1	24	53	23	<1	51	5
28	11, 12	0.21	0.67	2.9	0.01	0.98	24	53	23	<1	51	6
35	7, 5	0.14	0.23	0.8	0.01	0.26	26	51	23	2–5	56	6
50	2, 2	–	0.00045	0.00057	0.00032	–	–	–	–	–	10	7

3.3.2 Experimental procedure

Three experiments (Exp1 to Exp3) were conducted after the soil was drained for several (up to six) days between November 2005 and May 2006. We studied wetting propagation and subsurface flow formation under mean sprinkling intensities of 11.6, 19.1, and 50.4 mm h^{-1}. For Exp1 and Exp2 with its lower sprinkling intensities, we used two garden sprinklers (Gardena Aquazoom). For Exp3, sprinkling was conducted by 15 nozzles arranged in three lines. Two automatic rainfall gauges, six distributed small rainfall samplers and a water meter allowed for precise determination of the input and its uniformity (see appendix of Retter et al., 2006). Duration of sprinkling was 700, 305, and 209 minutes accordingly for Exp1 to Exp3 (Kienzler and Naef, 2007; Retter, 2007).

3.3.3 Soil characteristics measurements

Two weeks after Exp3, soil samples were taken at the study site in soil depths of 11, 28, and 35 cm. Samples were taken in the x-direction (n=26) and z-direction (n=28) using metallic rings (diameter 5.5 cm, height 4 cm) as stated in Table 3.1. Sampling procedure for undisturbed core samples was according to Dirksen (1999, p. 18ff). Samples were analysed in the lab to determine the saturated hydraulic conductivity K_{sat} (Dirksen, 1999). After the soil cores were saturated, a Mariotte device supplied water to the upper soil surface of the core at a constant hydraulic head. Measurements of flux density were repeated four to ten times.

During the field experiments changes in volumetric soil moisture θ were continuously monitored with 10 triplets of TDR wave-guides, that were evenly distributed (Figure 3.1). A TDR wave-guide consisted of two 0.15 m long, 5 mm in diameter, parallel stainless steel rods, 30 mm apart. The triplets' structure contained three TDR wave-guides which are orthogonally aligned to each other (Figure 3.2). This special setup was used to measure 3D vectors of wetting front velocity and direction (Retter et al., 2006). The triplets were installed in depth between 11 cm (close to soil surface) and 40 cm (~at the boundary of soil-bedrock). TDR instrument noise was 0.002 m^3 m^{-3} and the measurement interval was set to 90 s in order to more closely record the breakthrough of the wetting front. For further details on the TDR equipment see Retter (2007).

During each experiment twelve tensiometers recorded the matric potential ψ at four different soil depths. They were arranged in three nests at distances of 2 m ("lower"), 4 m ("middle") and 8 m ("upper") upslope from the trench face (Figure 3.1).
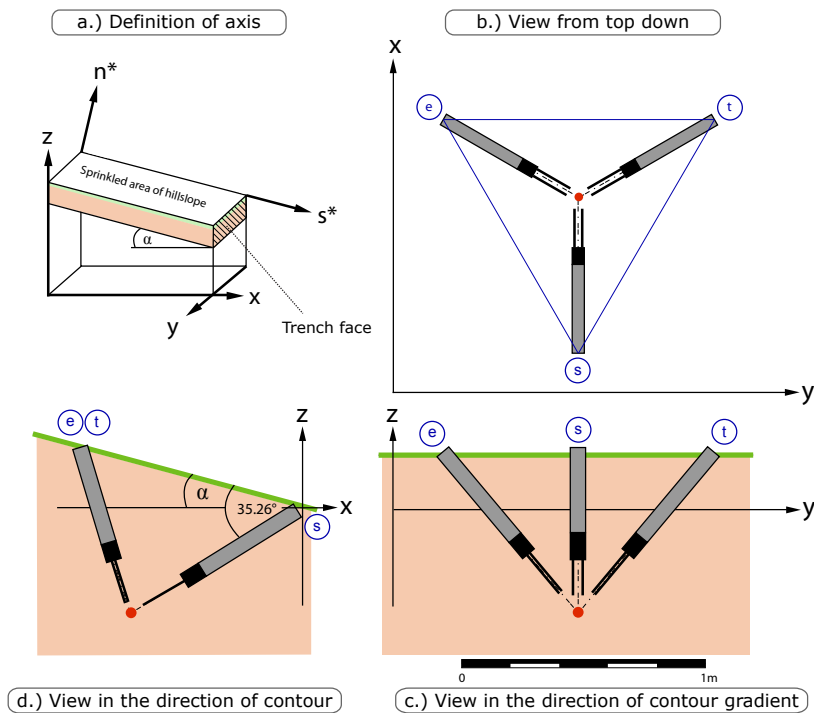
Figure 3.2. Definition of axis, and scheme of mounting a triplet of TDR wave-guides at the hillslope study site by its different views. Electrode length of probes (black) was 15 cm. (Adopted from Retter et al., 2006).

Five piezometers were situated in 1.5, 4, 6, and 10 m upslope the trench (-s* direction) as shown in Figure 3.1. The piezometers reached between 0.7 and 1.2 m deep and were screened over the lower 30 cm. Pressure sensors recorded piezometric head every five minutes.

Subsurface flow was collected by a flow gutter in the trench at the downslope end of the hillslope plot. It was then recorded by tipping buckets. After start of sprinkling a video camcorder monitored the trench face for the initial response of subsurface flow.

3.4 Results of field observations

3.4.1 Hydraulic conductivity

According to the analysis of soil samples in the lab, $K_{sat,z}$ in 11 cm depth varied between 2.1×10^{-7} and 3.1×10^{-5} m s^{-1}, $K_{sat,z}$ for 28 cm varied between 1.4×10^{-7} and 2.9×10^{-5} m s^{-1}, while samples of 35 cm depth ranged between 1.4×10^{-7} and 7.6×10^{-6} m s^{-1} (Figure 3.3). The equivalent means for the three soil depths resulted in $8.4 \times 10^{-6} \pm 1.1 \times 10^{-5}$ m s^{-1}, $6.7 \times 10^{-6} \pm 9.8 \times 10^{-6}$ m s^{-1}, and $2.3 \times 10^{-6} \pm 2.6 \times 10^{-6}$ m s^{-1} (Table 3.1). No correlation of K_{sat} with soil depth was found. These findings, supported by visual determinations at the soil profile, and by measurements of bulk density (Table 3.1), also indicated that no obvious layering occurred. Moreover, the directional sets of K_{sat} were analysed by a statistical z-test. It showed with significance of 0.005 that the maximal $K_{sat,x}$ was equal to the maximal of $K_{sat,z}$ for depths of 28 and 35 cm, and similar findings applied for the minimal values.
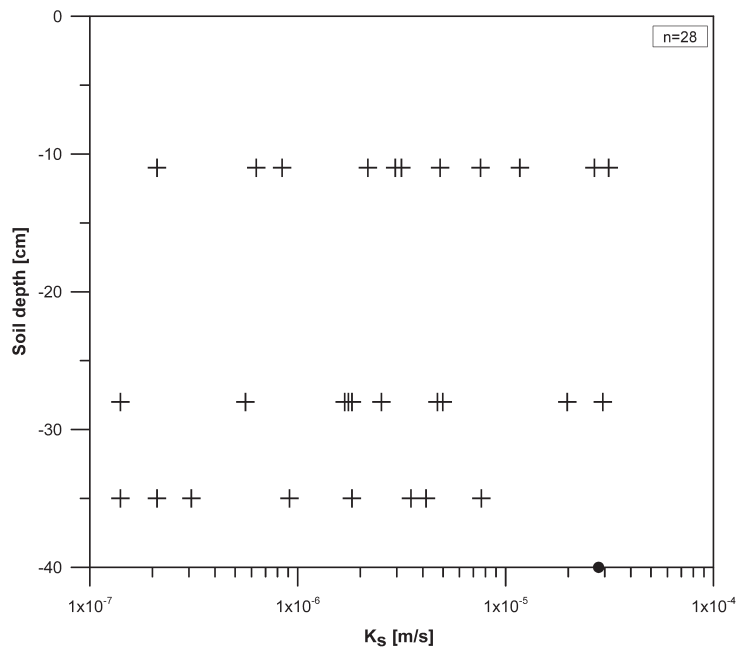
Figure 3.3. Saturated hydraulic conductivity $K_{sat,z}$ versus soil depth. The soil samples were taken in vertical direction. The hydraulic conductivity of the underlying siltstone, below 42 cm, resulted between $3.2\pm0.02x10^{-9}$ and $5.7\pm0.02x10^{-9}$ m s^{-1}. For purposes of comparison, the point on the abscissa represents the calculated mean hillslope K.

3.4.2 Soil moisture and wetting front propagation

TDR measurements indicated that initial conditions of volumetric soil moisture content within the hillslope did not show a clear depth dependency (Figure 3.4).
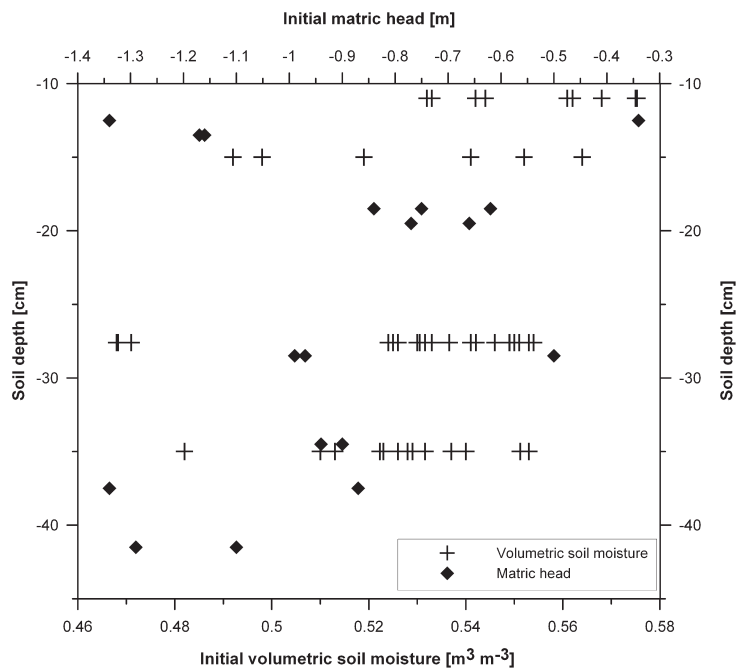

Figure 3.4: Initial volumetric soil moisture (obtained by TDR wave-guides) and initial matric head (recorded by tensiometers) for different points in depth. Data of matric head originates from Kienzler and Naef (2007).

The distributions of arrival times of wetting front, as monitored both by the TDR and tensiometers during the sprinkling experiments, were similar to each other, and correlated well with soil depth (Figure 3.5).
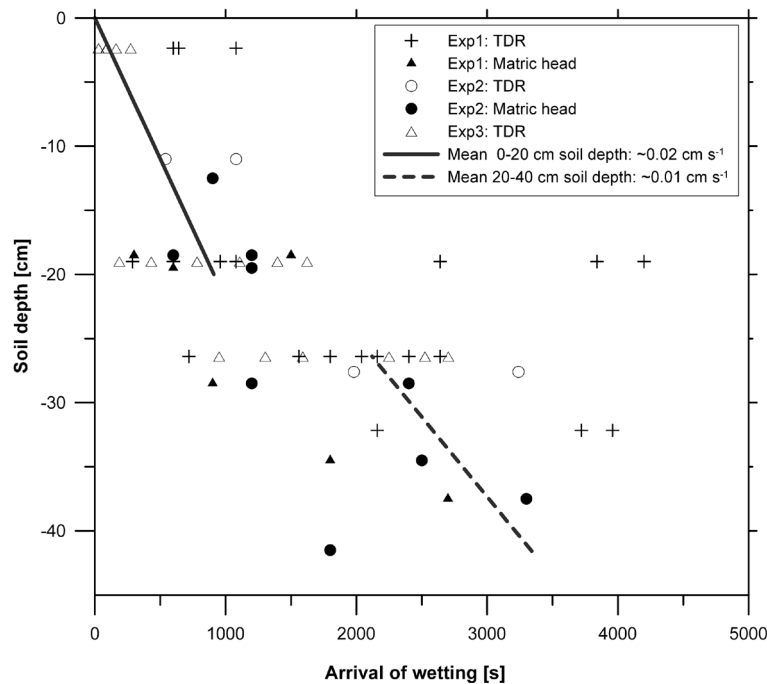
Figure 3.5. Arrival of wetting front at different soil depths as monitored by TDR wave-guides and tensiometers during Exp1 to Exp3. Lines represent the calculated "average" arrival times per depth. Data of matric head originates from Kienzler and Naef (2007).

The average vertical velocity (z) in the upper 20 cm was ~0.02 cm s^{-1}. It was faster than the average velocity for the depth of 20-40 cm which was ~0.01 cm s^{-1}. The downslope flow component at locations close to the bedrock (28 and 35 cm depth) was larger than in 11 cm depth (Figure 3.6). The ratio of the wetting velocities in horizontal (x) over vertical wetting velocities (z) varied between 1.8, 3.6, and 2.2, and was dependent on the different soil depths. Full records of θ(t,z) series during Exp1 to Exp3 are shown by Kienzler and Naef (2007) respectively Retter (2007).

3.4.3 Soil moisture saturation

Piezometers situated in 1.5, 4, 6, and 10 m upslope the trench (s* direction) showed the irregular piezometric head (Figure 3.7a-c). A saturated water table above the bedrock (~40 cm depth) was merely built up in piezometers of the lower half of the hillslope (1.5 and 4 m upslope from the trench), while the upslope piezometers (6 and 10 m from the trench), did not record water table formation (Figure 3.7a-c). Patterns were repeated for different experiments and sprinkling intensities. Different reactions of two piezometers in 1.5 m distance indicated patches of different localised saturation during the first two hours. This was also supported by TDR and tensiometer measurements which responded faster to

changes. Matric potential data showed highly saturated conditions with ψ up to 0 m. In one case positive pressure up to +0.1 m, where the probe was situated close the bedrock, was recorded but is not shown in the average change of tensiometer readings (Figure 3.7d-e).

General orientation

At soil depth of 11 and 15 cm

$$\overline{U_{V_x V_z}} = \frac{\overline{V_x}}{\overline{V_z}} = 1.8$$

At soil depth of 28 cm

$$\overline{U_{V_x V_z}} = \frac{\overline{V_x}}{\overline{V_z}} = 3.6$$

At soil depth of 35 cm

$$\overline{U_{V_x V_z}} = \frac{\overline{V_x}}{\overline{V_z}} = 2.2$$

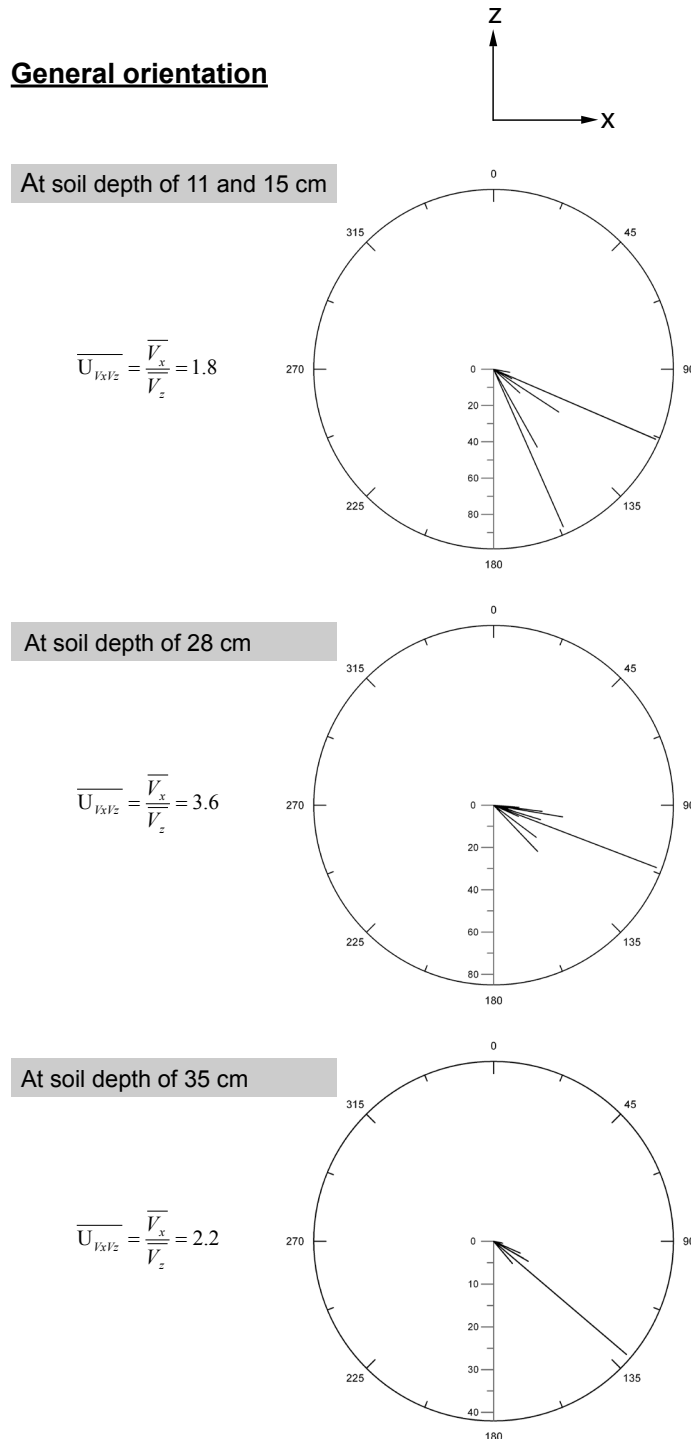*Figure 3.6. Direction of flow (°) in various soil depths at the field site. The originally three dimensional vector was restricted to the two dimensions (horizontal and vertical). The length of the vector corresponds to the velocity of wetting propagation [mm min⁻¹]. The slope angle, α, at the site was 13.5°. Data concern Exp 1 to Exp 3 and origin from Retter et al. (2006).*

a.)

b.)

c.)

d.)

e.)

f.)

Time since start of sprinkling [h]
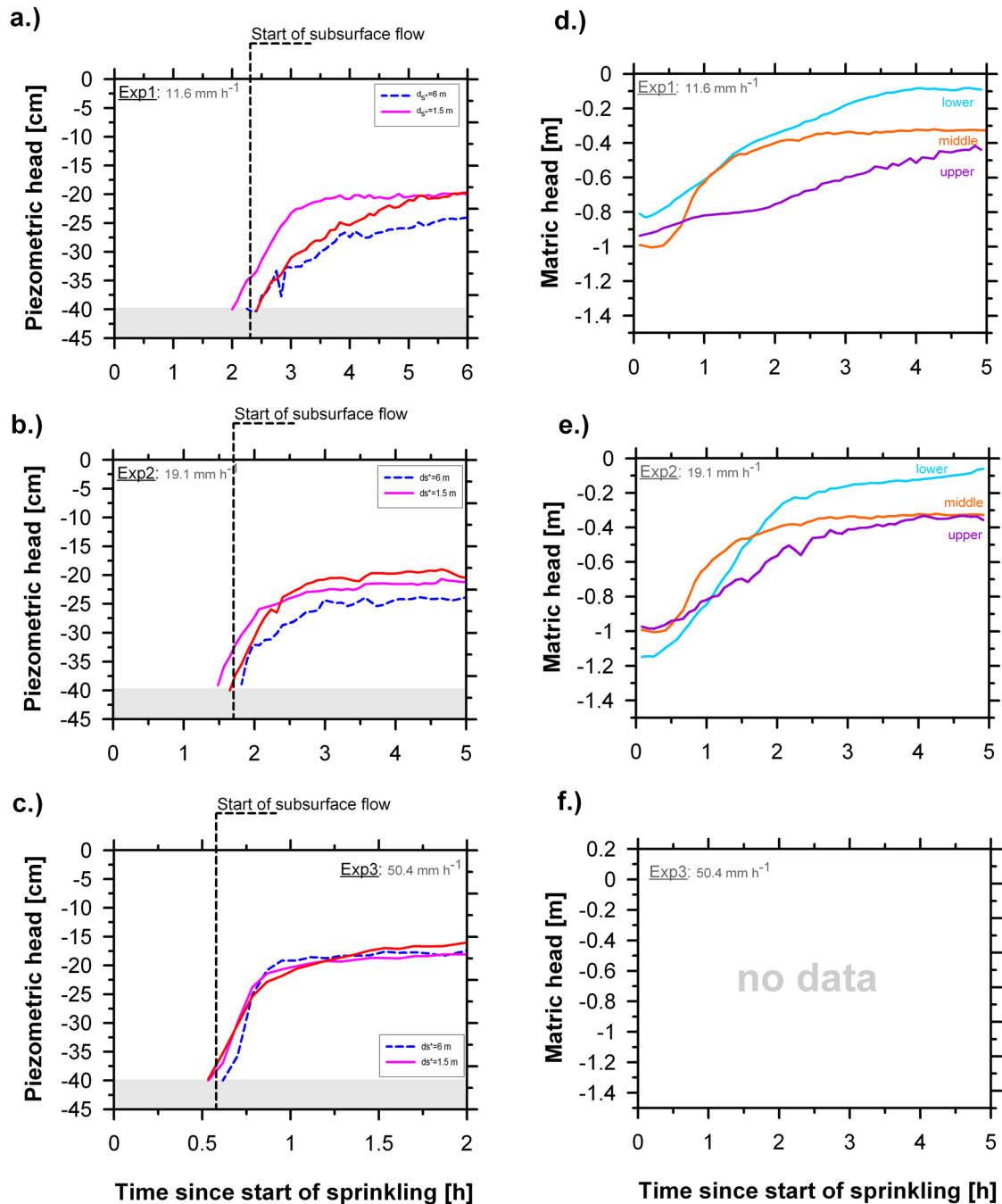
Figure 3.7. Overview of piezometeric head during the three sprinkling experiments (a.-c). Grey shaded areas indicate average depth of bedrock. Location of piezometers is given by the distance in s* direction. Further (d.-e.), series of average soil matric head at the three tensiometer nests (upper, middle, and lower). Data originate from Kienzler and Naef (2007) respectively Retter (2007).

3.4.4 Subsurface flow

Start of subsurface flow, as observed at the trench face, corresponded with appearance of water table in piezometers of 1.5 m distance from the trench. Flow increased until it reached steady state of 0.14, 0.21, and 0.16 l s^{-1} in response to the three input rates respectively. Note that the three input rates differed up to factor 4 (Retter, 2007). Assuming totally impermeable bedrock and lined sidewise borders of the experimental plot, the subsurface

outflow at the trench face (cross-sectional area: 8.33x0.4 m²) equalled 4.2×10^{-5} m s^{-1}, 6.2×10^{-5} m s^{-1}, and 4.7×10^{-5} m s^{-1}, and resulted in a mean of 5×10^{-5} m s^{-1} in s* direction. Furthermore, the entire subsurface flow originated from a 5-cm layer above the bedrock whereas no major subsurface flow was observed in the upper region of the trench profile. A mean hillslope K_{sat} was calculated by the Darcy's Law (reduced cross-sectional area of 8.33x0.05 m²; mean flow= 5×10^{-5} m s^{-1}; α=13.5°) and resulted in 2.8×10^{-5} m s^{-1} (also in s* direction). It is marked for comparison in Figure 3.3.

3.5 Discussion of field observations

The measurements of soil moisture and especially wetting front propagation indicated clearly that on average, the soil layer performed as if it were anisotropic. In the following section we look for the causes of this apparent anisotropy.

First, we look for small scale anisotropy (see B_1 in the theory section). The saturated hydraulic conductivity, K_{sat}, is a challenging soil hydraulic property to spatially characterize because it changes by orders of magnitude over short distances (Figure 3.3). Despite our effort to also look for non-simple relationships like $\log_{10}$-K distribution with depth (Beckwidth et al., 2003), no significant spatial variations were found. Therefore, we concluded that K_{sat} at the experimental site did not produce small scale anisotropy.

Moreover, measurements of initial soil moisture content (Figure 3.4), did not show a clear depth dependency, and the same applied to measurements of porosity (Table 3.1) and visual determinations of the soil profile. The option of layered soil, composed of sub-layers, which on average appear anisotropic (B_2), was therefore rejected as well.

According to Zaslavsky and Sinai (1981) and Miyazaki (2006) the development of a horizontal flow component ($q_x>0$) in the downslope direction, from the vertical infiltration flux at the soil surface is a measure of average anisotropy, and point towards increased hydraulic conductivity with depth. It is therefore suggested here that the anisotropy of the experimental soil layer was of the third type (B_3) - average anisotropy in layered unsaturated soil, caused by lower conditions of flow - as explained in the following.

In Eq. (3) K_{sat}, the saturated hydraulic conductivity of the soil layer (~1×10^{-5}) and K_0^* is the unsaturated hydraulic conductivity at the base of the impermeable layer (n*=0). Following the explanations of Miyazaki (2006), if K_0^* is small then the absolute changes of K upward are small, and vertical streamlines from the soil surface will only slightly bend downslope. However, if $K_0^* \approx K_{sat}$ (nearly saturated) and K at the rest of the profile decreases upward continuously, the changes of K upward might be by far larger, and vertical downward streamlines from the soil surface will bent downslope (see for example the analytical solution of Boger, 1998 for steady state flow on a uniform hillslope layer). This is the actual meaning of average anisotropy caused by boundary conditions.

In our experiments vertical soil moisture content before the sprinkling was nearly uniform (although with large local variations, Figure 3.4). Therefore the measurements of flow direction in the upper triplets (11 cm depth) were governed by the downward component. During the experiments wetting was progressing downward in various velocities (Figure 3.8a). For soil close to bedrock the available pore volume was small because pores were already filled up, which enhanced the saturation and the water table built up on top of the impermeable layer. Saturation was established obviously near the trench, downslope the experimental plot (see piezometer readings in Figure 3.5). As less water volume was needed, saturation occurred very soon after the first wetting. This was also proven by effective soil moisture calculations (increase between θ_{ini} and saturation). From the time of formation of saturation on top of the impermeable layer, the measurements of the triplets were superimposed by the downward movement of the wetting front and by accumulation of saturation upward (Figure 3.8b). Moreover, the increased moisture content, specifically in the soil depth 35-40 cm, caused K to increase (e.g., Stephens and Heermann, 1988; Grebnev and Skal, 2006; see also the Appendix) and this new K(n) distribution with depth imposed curving of streamlines and apparent anisotropic behavior (Mualem, 1984; Miyazaki, 2006). This anisotropic behavior was observed as an increased ratio of wetting velocities in horizontal (x) over vertical direction (z) (Figure 3.6).
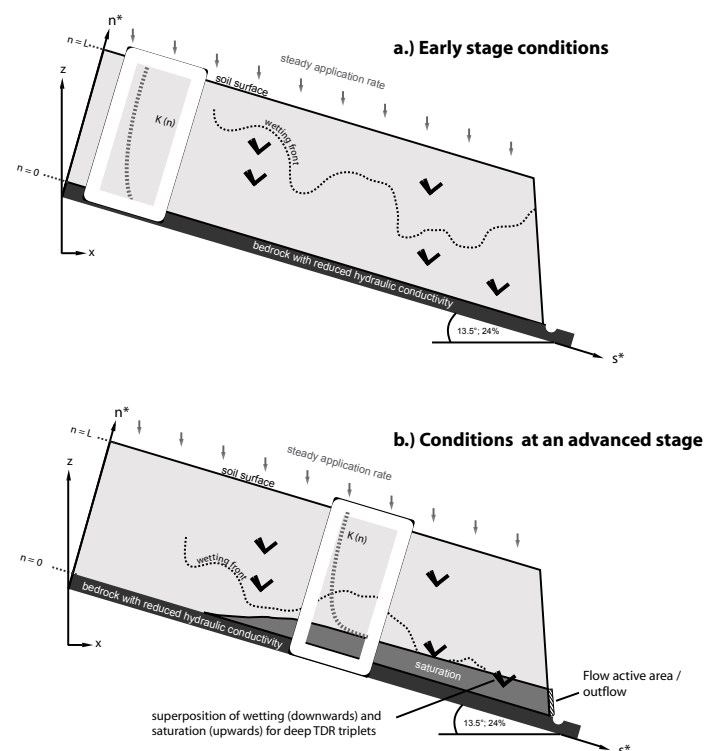
Figure 3.8. Conceptual understanding of wetting front progress and vector determination for initial conditions when wetting front was situated in the upper soil depth (a.) and conditions of later stage (b.) when the wetting front arrived deeper to the soil and superposition with saturation took place. Accentuated graph K(n) of initial conditions results from modelling of Eq. A3b whereas K(n) of advanced stage results from field observations (see discussion).

Causes for anisotropy

Anisotropic behavior of the soil depth 35-40 cm is also supported by lateral flow phenomena at the bedrock interface. As a consequence of saturation subsurface flow at the trench emerged firstly out of two (and with time up to 13) little macropores (Retter, 2007). The macropores' development and formation throughout time is another soil characteristic which is usually not taken into account in small scale measurements, and thus increase the effect of apparent anisotropical behavior of the soil.

Support is also provided by the modelling results of steady state flow within a sloping layer (Appendix; Boger, 1998). The analytical solution showed that an increase of soil moisture content along the n* coordinate from the soil surface to the bedrock layer (Figure 3.8b) may cause an increase of K*(n) by an order of magnitude from the soil surface towards the bedrock, and thus impose terms of anisotropy of the soil layer. A calculation (Eq. A10) of the the average anisotropy factor of the initial conditions resulted in 2.9 ± 0.2 for data of our study site, which is similar to the factors obtained by the vectors in Figure 3.6.

The final section addresses uncertainties that should be accounted for when relating small scale measurements to field scale phenomena. The wide range of experimental measurements in this case allows us to compare between the local small scale measurements and the wider scale results that were detected for the entire 100 m^2 hillslope.

One example is the measured wetting front vectors. The anisotropy derived from the vector determination in 28 cm soil depth was larger than those in 35 cm (Figure 3.6) while according to the discussion and theoretical interpretation the anisotropy within the soil layer should be larger with the depth of the soil. We assume that these results indicate uncertainties imposed by the method of vector determination (Germann and Zimmermann, 2005; Retter et al., 2005). The method includes two assumptions that do not necessarily reflect real conditions at every point in the study site. For a correct measurement, first, wetting front should propagate from the upper half space into the TDR volume of the triplet; and second, wetting front propagation should be stable. As shown in our measurements in some cases there was probably a wetting procedure from the bottom up (Figure 3.7), and the overall propagation of the wetting front was not stable (Figure 3.5).

We further challenged problems of scale, as the Representative Elementary Volume (REV) was differed for each of the measurements. The REV size ranged between 95 cm^3 (K_{sat} measurements to determine small scale anisotropy), to about 3000 cm^3 (REV of flow vectors measurements), and to the scale of ~400 m^3 representing the entire hillslope (measurements of flow to the trench, and the formation of a saturated region). Scaling problems require that small core volumes of soil often fail to cover the properties of the large scale REV (Vepraskas and Williams, 1995; Davis et al., 1999; Sherlock et al., 2000). In the present study, the measured spatial distribution of small scale saturated hydraulic conductivity was not sufficient to conclude the direction of flows, since the phenomena of curving streamlines downslope was determined within the much larger scale of the entire hillslope. Moreover, the mean hillslope K (Figure 3.3) is between one and two orders of

magnitude larger than most of the small scale K_{sat} measurements, but such a result was previously observed by other researchers (Nilsson et al., 2001; Brooks, 2004).

It is therefore suggested that often small scale measurements are not good representations of large scale process, and we should always combine them with general and wide scale observations.

3.6 Conclusions

In this contribution, we discussed field measurements of a new technique that allowed us to observe downslope flow initiation and apparent anisotropy. We further examined and tested the soils' properties that caused this phenomena.

The measurements of K_{sat} in core samples of separate direction did not show small scale anisotropy, did they prove a significant layering within the soil profile. Measured initial soil moisture prior to sprinkling experiments showed that the initial conditions of flow process could not cause significant anisotropy. However, measurements during the sprinkling experiments revealed the process by which the soil became saturated, and detected water table formation on top of the bedrock. Vectors of flow in soil depth of 28 and 35 cm indicated increased hydraulic conductivity in direction parallel to the slope. It was suggested that this was the cause of the apparent anisotropy that we observed during the experimental process (type B_3 in theory section). Support for these findings was found in previous studies, and was also seen in the observed lateral flow through macropores at the bedrock interface. A simple model showed that under steady state flow within an inclined soil layer, there was an increase of $K^*(n)$ towards bedrock, which appears on average as anisotropy of the soil layer.

01

02

03

04

05

References

Akylas, E., A.D. Koussis, and A. Yannacopoulos. 2006. Analytical solution of transient flow in a sloping soil layer with recharge. Hydrological Sciences Journal, IAHS, 51(4):626-641.

Assouline, S., and D. Or. 2006. Anisotropy factor of saturated and unsaturated soils . Water Resour. Res. 42:W12403.

Ball, B.C., and E.A.G. Tobertson. 1994. Effects of soil-water hysteresis and the direction of sampling on aeration and pore function in relation to soil compaction and tillage. Soil and tillage research,32(1):52-60.

Bathke, G.R., and D.K. Cassel. 1991. Anisotropic variation of profile characteristics and saturated hydraulic conductivity in an ultisol landscape. Soil Sci. Soc. Am. J.l 55(2):333-339.

Basak, P. 1972. Soil structure and its effects on hydraulic sonductivity. Soil Science 114(6):417-422.

Bear, J. 1979. Hydraulics of Groundwater. McGraw-Hill, New York, 569p.

Boger, M. 1998. Solutions of unsaturated seepage problem by power-series method, ASCE J. Hydrol. Eng., 3, 182-192,

Beckwith, C.W., A.J. Baird, and A.L. Heathwaite. 2003. Anisotropy and depth-related heterogeneity of hydraulic conductivity in a bog peat. I: laboratory measurements. Hydrol. Process. 17:89-101.

Bodhinayake, W., B. Cheng Si, and K. Noborio. 2004. Determination of Hydraulic Properties in Sloping Landscapes from Tension and Double-Ring Infiltrometers. Vadose Zone J. 3:964-970.

Brooks E.S. 2004. A hillslope-scale experiment to measure lateral saturated hydraulic conductivity. Water Resour. Res. 40:W04208.

Cabral, M.C., L. Garrote, R.L. Bras, and D. Entekhabi. 1992. A kinematic model of infiltration and runoff generation in layered and sloped soils. Advances Wat. Res.15:311-324.

Casanova, M., I. Messing, and A. Joel. 2000. Influence of aspect and slope gradient on hydraulic conductivity measured by tension infiltrometer. Hydrol. Process. 14:155-164.

Chen, L., and M.H. Young. 2006. Green-Ampt infiltration model for sloping surfaces. Water Resour. Res. 42:W07420.

Dabney, S.M., and H.M. Selim. 1987. Anisotropy of a fragipan soil: Vertical vs. Horizontal Hydraulic Conductivity. Soil Sci. Soc. Am. J. 51(1):3-6.

Darcy, H. 1856. Les fontaines publiques de la ville de Dijon. (Transl.: The public fountains of the city of Dijon). Paris, Dalmont.

Davis, S.H., R.A. Vertessy, and R.P. Silberstein. 1999.: The sensitivity of a catchment model to soil hydraulic properties obtained by using different measurement techniques. Hydrol. Processes 13:566-577.

Dirksen, C. 1999. Soil physics measurements. GeoEcology, Catena, Reiskirchen, 154p.

Dörner, J., and R, Horn. 2006. Anisotropy of pore functions in structured Stagnic Luvisols in the Weichselian moraine region in N Germany. J. Plant Nutr. Soil Sci. 169:213–220.

Dörner, J.M. 2005. Anisotropie von Bodenstrukturen und Porenfunktionen in Böden und deren Auswirkungen auf Transportprozesse im gesättigten und ungesättigten Zustand. Ph.D. thesis, Schriftenreihe des Instituts f. Pflanzenernährung u. Bodenkunde 68, Christian-Albrecht-University, Kiel, Germany, 182p.

FAO-Unesco. 1994. Soil map of the world. ISRIC, Wageningen.

Finnern, H., W. Grottenthaler, D. Kühn, W. Pälchen, W.G. Schraps, and H. Sponagel. 1996. Bodenkundliche Kartieranleitung. Bundesanstalt f. Geowissenschaften u. Rohstoffe Bundesrepublik Deutschland, Hannover, 392p.

Garber, M., and D. Zaslavsky. 1977. Flow in a soil layer underlined by an impermeable membrane. Soil Sci. 123:1-9.

Gardner, W.R. 1958. Some steady state solutions of the unsaturated moisture flow equation with applications to evaporation from a water table. Soil Sci. 85:228-232.

Germann, P.F., and M. Zimmermann. 2005. Directions of preferential flow in a hillslope soil. Quasi-steady flow. Hydrol. Processes 19:887–899.

Germann, P.F., A. Helbling, and T. Vadilonga. 2007. Rivulet approach to rates of preferential infiltration. Vadose Zone J.: in print.

Grebnev, I., and A.S. Skal. 2006. Percolation Approach to the Anisotropy Factor in an Unsaturated Porous Medium. Transport Porous Media 63:91–98.

Glass, R.J., J.R. Brainard, and T.-C.J. Yeh. 2005. Infiltration in Unsaturated Layered Fluvial Deposits at Rio Bravo: Macroscopic Anisotropy and Heterogeneous Transport. Vadose Zone J. 4:22–31.

Hjerdt, K.N., J.J. McDonnell, J. Seibert, and A. Rodhe. 2004. A new topographic index to quantify downslope controls on local drainage. Water Resour. Res. 40:W05602.

Hewlett, J.D, and A.R. Hibbert. 1963. Moisture and energy conditions within a sloping soil mass during drainage, J. Geophys. Res. 68(4):1081-1087.

Jackson, C.R. 1992. Hillslope Infiltration and Lateral Downslope Unsaturated flow. Water Resour. Res. 28:WR00664.

Khaleel, R., T.-C.J Yeh, and Z. Lu. 2002. Upscaled flow and transport properties for heterogeneous unsaturated media. Water Resour. Res. 38(5):WR000072.

Kienzler, P. and F. Naef (2007): Use of vertical and lateral flow characteristics to infer mechanisms of subsurface storm flow formation on a grassland hillslope. Manuscript in preparation.

Lauren, J.G., R.J. Wagenet, J. Bouma, and J.H.M. Wosten. 1988. Variability of saturated hydraulic conductivity in a glossaquic haludalf with macropores. Soil Sci. 145:563-573.

McCord, J.T., and D.B. Stephens. 1987. Lateral moisture movement on sandy hillslope in the apparent absence of an impeding layer. Hydrol. Processes 1(3):225-228.

Mendoza, G., and S.T. Steenhuis. 2002. Determination of hydraulic behavior of hillsides with a hill slope infiltrometer. Soil Sci. Soc. Am. J. 66:1501–1504.

Miyazaki, T. 2006. Water flow in soils. 2nd edition. Taylor & Francis, London, 418p.

Mualem, Y., and J. Bear. 1978. Steady phreatic flow over a sloping semipervious Layer. Water Resour. Res. 14:403-408.

Mualem, Y. 1984. Anisotropy of unsaturated soils. Soil Sci. Soc. Am. J. 48:505-509.

Mualem, Y., and G. Dagan. 1976. Methods of predicting the hydraulic conductivity of unsaturated soils. Research report to the BSF, Technion, Haifa, Israel.

Nilsson, B., R.C. Sidle, K.E. Klint, C.E. Bøggild, and K. Broholm. 2001.Mass transport and scale-dependent hydraulic tests in a heterogeneous glacial till–sandy aquifer system. J. of Hydrology 243:162–179.

Philip, J.R. 1991. Hillslope Infiltration: Planar Slopes. Water. Res. Research 27:109-117.

Retter, M (2007): Use of vertical and lateral flow volocities to characterise subsurface storm flow formation on a grassland hillslope. Manuscript in preparation.

Retter, M., P. Kienzler, and P.F. Germann. 2006. Vectors of subsurface stormflow in a layered hillslope during runoff initiation. Hydrology Earth Sci. Systems 10:309-320.

Sherlock, M.D., N.A. Chappell, and J.J. McDonnell. 2000. Effects of experimental uncertainty on the calculation of hillslope flow paths. Hydrol. Processes 14:2754-2471.

Stephens, D., und S. Heermann. 1988. Dependence of Anisotropy on Saturation in Stratified Sand. Water Resour. Res. 24:770-778.

Vepraskas, M.J., and J.P. Williams. 1995. Hydraulic conductivity of saprolite as a function of sample dimensions and measurement technique. Soil Sci. Soc. Am. J. 48:864-870.

Wallach, R., and D. Zaslavsky. 1991. Lateral flow in a layered profile of an infinite uniform slope. Water Res. Research 27,1809-1818.

Whipky, R.Z., and Kirkby, M.J. 1978: Flow within the soil. In: Kirkby, M.J. (editor), Hillslope Hydrology, John Wiley, NewYork, 121-144.

Zhang, H.Q. 1996. Anisotropic variation of saturated hydraulic conductivity of a variously grazed salt marsh soil. Zeitschrift f. Pflanzenernährung u. Bodenkunde 159(2):129-135.

Zaslavsky, D., and G. Sinai. 1981. Surface Hydrology: Flow in sloping layered soil, J. Hydraulic Division 107:53-63.

Zaslavsky, D. 1970. Some aspects of Watershed Hydrology. Spec. Rep. USDA ARS 41-157. Washington D.C., 95 p.

Appendix: Analytical model for anisotropy

We will examine the option that soil moisture and hydraulic conductivity distribution on a hill slope may allow average anisotropic conditions.

Consider an infinite soil layer on a hill slope, with an impervious base, which forms a soil layer with thickness L and an angle α with the horizon (Figure 3.1). In the following analysis we examine the soil moisture content and hydraulic conductivity in the slanted soil layer. We use a mathematical solution to calculate the soil properties and lateral flux under a steady state flow assumption for an infinite slope, and without infiltration, while the entire profile remains unsaturated (see also Garber and Zaslavsky, 1977). To that end we use a rotated cartesian space coordinates (s*, n*) where s* is parallel to the soil surface and n* is perpendicular to it, with n*=0 at the interface between the impervious base and the soil above (Figure 3.1 and 2a).

$$s^* = x\cos\alpha - z\sin\alpha \qquad x = s^*\cos\alpha + n^*\sin\alpha$$
$$n^* = x\sin\alpha + z\cos\alpha \qquad z = -s^*\sin\alpha + n^*\cos\alpha \tag{A1}$$

During steady state, there will be lateral flow in the s* direction, and no flow in the n* direction. It can therefore be assumed that the total head distribution ($\phi(n^*)=\psi(n^*)+z(n^*)$) is hydrostatic. Therefore:

$$K^*\left(\frac{\partial\psi}{\partial n^*} + \cos\alpha\right) = 0 \tag{A3}$$

where K* is the unsaturated hydraulic conductivity (m s^{-1}).

The constitutional equations which describe the connections between the hydraulic conductivity K*, the dimensionless moisture content S_e (equivalent to degree of saturation), the soil water content θ and the matric (or capillary) head are:

(a.) $K^* = K_{sat}\exp[a\hat{\psi}] \quad ; \quad \hat{\psi} = (\psi - \psi_c)$

(b.) $K^* = K_{sat}[S_e]^b \quad ; \quad Se = \dfrac{\theta - \theta_r}{\theta_s - \theta_r}$ $\tag{A3}$

(c.) $\theta = (\theta_s - \theta_r)\exp\left[\dfrac{a}{b}(\psi - \psi_c)\right] + \theta_r$

In Eq. (A3a) of Gardner (1958) the constant a (m^{-1}) is the sorptive number, ψ_c the air entry pressure (m) and K_{sat}, the saturated hydraulic conductivity (m s^{-1}). In Eq. (A3b) θ_s and θ_r stands for the saturated and residual moisture content, respectively (obtained by θ(t)-series of vector determination), and a constant b which was considered in the range of 3-4 according to several authors (Mualem and Dagan, 1976). Combining Eqs. (A3a) and (A3b) gives the moisture retention curve, ψ(θ) relationship, in Eq. (A3c).

Using Eq. (A3a), Eq. (A2) can be written in a linear form with a non-dimensional variables:

$$\frac{\partial K}{\partial n} + KA = 0$$

(A4)

where $n = n*/L$; $0 \geq n \geq 1$; $K = K*/K_{sat}$; $A = aL\cos(\alpha)$

The analytical solution of Eq. (A4) is the K distribution along the n axis. This solution is:

$$K(n) = \frac{K_0^*}{K_{sat}} \exp(-An) \; ; \; 0 > K_0^* > K_{sat}$$

(A5)

where K_0^* is the hydraulic conductivity at the base of the layer (n*=0). The distribution of the dimensionless moisture content S_e along the n axis at the same state is:

$$S_e(n) = \left(\frac{K_0^*}{K_{sat}}\right)^{1/b} \exp\left(-\frac{A}{b}n\right)$$

(A6)

The matric potential and total head are given by:

$$\hat{\psi} = \frac{\ln\left[S_e(n*)^b\right]}{b}$$

(A7)

and

$$\phi = \hat{\psi} + \psi_c + z*$$

(A8)

respectively, while the lateral flux q(n*) is given from Darcy Law:

$$q(n) = -K^*(n)\left(\frac{\partial \hat{\psi}}{\partial s^*} - \sin\alpha\right)$$

(A9)

Note that since $\partial\hat{\psi}/\partial s^* = 0$ the flux for each n* is determined by $q(n*) = K^* \sin\alpha$, and changes according to the K*(n) distribution (Eq. A6). The average anisotropy factor is defined by:

$$\overline{U_{sn}} \equiv \frac{\overline{K_s}}{K_n} = \int_{n=0}^{1} K dn \int_{n=0}^{1} \frac{dn}{K}$$

(A10)

where the integral includes the soil layer from the impervious base to the soil surface. Such anisotropy is also described by Miyazaki (2006; pg. 113f). Interested readers in the full development of this theory are directed to Garber and Zaslavsky (1977).

Chapter 04

Use of vertical and lateral flow velocities to characterise subsurface stormflow formation on a grassland hillslope

04

Matthias Retter[1]

[1]   Department of Geography, University of Bern, Hallerstr. 12, 3012 Bern, Switzerland

Manuscript in preparation

Abstract

Artificial sprinkling that included tracer experiments and detailed readings of soil moisture changes allowed to characterise subsurface vertical and lateral flows within a hillslope where subsurface stormflow response of individual soil pipes showed large variation. Kienzler and Naef (2007) explained this variation by the different degree of connectivity of vertical macropores and lateral pipes at the site. Now, a closer look on flow velocities is provided. In vertical direction there was no difference between local and profile flow velocites. Subsequent lateral velocities were higher. Both flows occurred in preferential flow paths of different length. However, these flow paths did not transfer the water directly and immediately from the soil surface to the trench face, but were initiated and intersected from patches of localised saturation within the soil matrix. During infiltration water is retained by patches, while flow is retarded and limited. The extent of such localised saturation was observed highly variable on a small scale. Correspondingly, individual preferential flow paths can vary with regard to flow response, flow velocity and flow rate. One could therefore also describe the essential variation of subsurface flow by the different retardation of flow, which has more direct implications for numerical modeling of subsurface flow.

4.1 Introduction

In studies of runoff generation at hillslopes, increasing interest has been directed towards subsurface storm flow (SSF), which can be an important contributor to stream flow in many headwater basins (Jones and Connelly, 2002; Weiler et al., 2006). SSF has been observed to occur via lateral preferential flow paths of variety of forms, e.g. "soil pipes" or "highly permeable layers", which occur in particular on steep hillslopes above impermeable bedrock or other impeding layers (e.g. McDonnell, 1990; Peters et al., 1995; Koyama and Okumura, 2002). Such flow paths can be formed either by biological activity or by subrosion at the soil-bedrock interface (Terajima et al., 2000). Depending on the particular forming process, they show large variation in diameter, shape, length and network form (Jones, 1987; Noguchi et al., 1999; Terajima et al., 2000).

SSF flow rates are limited by the vertical infiltration rate, which changes if water moves with high flow velocities in vertical macropores (Beven and Germann, 1982). Macropore flow rates and flow velocities vary substantially depending on macropore geometry and type of flow initiation. Weiler and Naef (2003) observed that macropore flow can be initiated either from the soil surface or from a saturated subsurface soil layer. They concluded that the particular initiation process and the interaction between macropores and the surrounding soil matrix govern the flow rate distribution in macropores.

SSF intensity varies widely in different catchments and even over short distances. While studies have been highly ambivalent in identifying and agreeing on the most relevant factors responsible for the intensity of SSF, conzeptualisation of SSF formation has become more detailed. However, the processes within the black-box nature of a hillslopes vary widely.

For example, Kienzler and Naef (2007) studied SSF formation at the present hillslope and explained the substantially different responses of SSF by the degree of direct or indirect feeding of SSF. When precipitation feeds directly into preferential flow paths, SSF responds quickly. In contrast, SSF response is delayed and weak when it is fed indirectly via large saturated zones of the soil. However, due to the heterogeneity and the black box nature of a hillslope, some conzeptual models lack clear evidence, which could be provided by direct measurements.

Anderson et al. (1997) analysed subsurface flow especially in lateral direction by instrumentation arrays allong rows across the micro-catchment. Buttle and McDonald (2002) pointed to the coupling of vertical and lateral flow. Both studies focused on integrated flow characteristics in the two dominant directions. The present study follows these ideas and analyses characteristics of vertical and lateral flows on the basis of combined sprinkling, tracer experiments, and detailed soil moisture measurements. Special attention is dedicated to flow velocities, that serve as integrated information along the heterogeneous space. The findings may therefore help in characterising SSF dependent on vertical and lateral properties.

4.2 Study site

The small catchment of the creek "Luter" (4.0 km^2) is situated on the Swiss Plateau south of Zofingen (Canton Lucerne). In this catchment, a site was selected where substantial subsurface flow was expected, according to a decision scheme which required input of hydrological properties of the surface and each major horizon of the soil (Scherrer and Naef, 2003). The site has an inclination of 24% (13.5°) and faces south. Elevation is 690 m asl, about 200 m above the valley floor. During the past 30 years the site was used as grassland. Accordingly, vegetation consists of native grasses and species typical for rich pastures like *Ranunculus acris* and *Dactylis glomerata*. The plants were cut down to 10 cm prior to the experiments. Mean annual temperature at a nearby meteorological station was 8.2°C between 1961 and 1990 (Wynau, MeteoSwiss) and mean annual precipitation was 1013 mm. Soil depth at the site varies between 38 cm and 45 cm. Only subtle changes are observed in this cambisol between the soil horizons, whereas a sharp change of bulk density and macropore density occurs at the transition to bedrock (Table 4.1). Up to 5 cm above the bedrock surface, small lateral soil pipes with diameters between 3 and 8 mm occur (Figure 4.1c). Within the soil profile, vertical macropores were observed with diameters between 1 and 10 mm, probably created by earthworms (*Lumbricus terrestris*). Macropore density was identified by visual count on plots of 0.25 m^2 at different depths. The particle size distribution was determined with the pipette method. Bulk density and percentage of coarse fragments were estimated according to Finnern et al. (1994). Saturated hydraulic conductivity K_{sat} was determined using the method of FAL (1996) with 54 soil samples (sample volume = 95 cm^3). It resulted between 0.025 and 0.096 mm s^{-1} (Table 4.1) and was discussed in a detailed manner in Retter et al. (2007). The bedrock consists of dense molasse siltstone of the „Oeningien"

period. A siltstone cube was detached by a saw and the hydraulic permeability resulted between $3.2\pm0.02\times10^{-9}$ and $5.7\pm0.02\times10^{-9}$ m s^{-1} (I. Hincapié, University of Bern, personal communication). A photo of the study site can be found in Retter et al. (2006).

Table 4.1. **Soil characteristics of cambisol at the „Lutertal" study site, developed from siltstone bedrock (Oeningien Molasse, C-horizon).**

Depth	Horizon	Mean vertical K_{sat}	Grain size distribution			Coarse Fragments	Bulk density	Macropore density	pH
[cm]		[mm s^{-1}]	Sand [%]	Silt [%]	Clay [%]	[%]	[g cm^{-3}]	[m^{-2}]	
0–10	A	0.083	24	53	23	<1	1.3	184	5
10–25	B	0.096	24	53	23	<1	1.3	248	6
25–40	B/Cv	0.025	26	51	23	2–5	1.8	132	6
>42	C	4.5×10^{-6}					2.38	0	7

4.3 Methods

4.3.1 Experimental setup

Sprinkling experiments were performed on a 100 m^2 plot with different sprinkling intensities (Table 4.2). The system for high sprinkling intensities provided about 50 mm h^{-1} and achieved uniform sprinkling with 15 nozzles arranged in three lines (details in Scherrer et al. 2006). For lower intensities (mean of 11.6 and 19.3 mm h^{-1}), two garden sprinklers (Gardena Aquazoom) were used. Two automatic rainfall gauges, six distributed small rainfall samplers and a water meter allowed for precise determination of the input and its uniformity. Prior to experiments a wind protection was installed around the site. Total SSF was measured above the bedrock at the lower end of the hillslope site in an 8.3 m long trench (oriented along the contour) with a 100 ml tipping bucket gauge. Surface overland runoff was measured separately with a 45° Thompson weir. Twelve tensiometers recorded matric head every five minutes at four different depths, which were evenly distributed along the profile. They were arranged in three nests at distances of 2 m, 4 m and 8 m upslope from the trench face (Figure 4.1a). Five pressure sensors recorded piezometric head every five minutes. All probes were sealed with bentonite at the surface to prevent vertical bypass flow along the tubes. Water content changes in the soil were monitored with 30 TDR wave-guides at different depths. One TDR wave-guide consisted of two 0.15 m long, parallel stainless steel rods (Figure 4.2). TDR wave-guides were installed in ten "triplets" with an angle of 21.8° against horizontal. Thus, in each "triplet", three wave-guides (te, tw, s) were orthogonally aligned close to each other with a distance of about 2 cm at depth L. The depth L of the wave-guides ranged between 11 and 40 cm. For technical details on the TDR equipment see Retter et al. (2006). The experimental design located TDR probes apart from the line source experiments because of opposite interference.
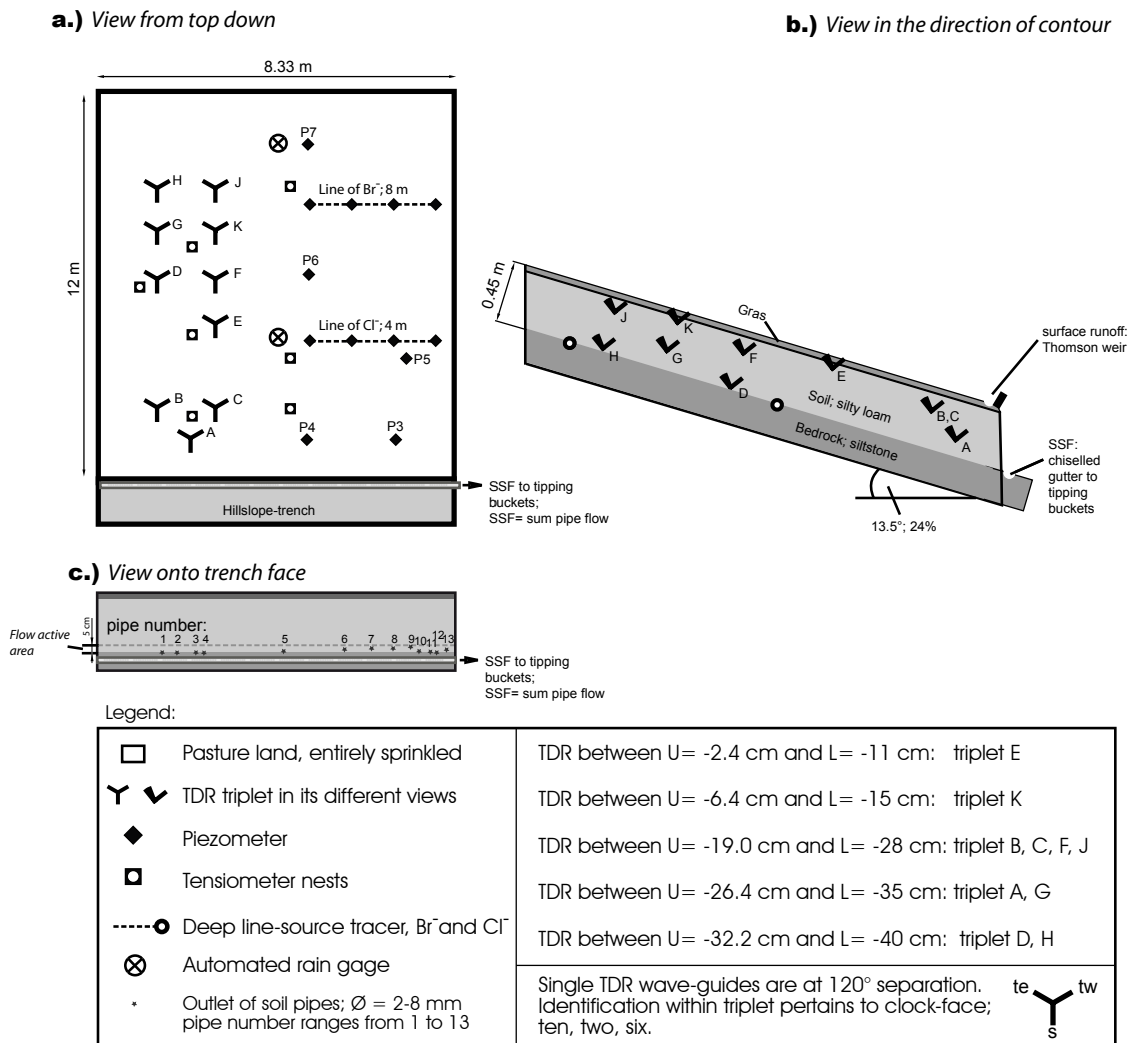
a.) *View from top down*

8.33 m

12 m

P7

H   J
G   K
D   F
E
B   C
A

Line of Br⁻; 8 m

P6

Line of Cl⁻; 4 m
P5

P4   P3

0.45 m

Hillslope-trench

→ SSF to tipping buckets;
SSF= sum pipe flow

b.) *View in the direction of contour*

Gras

J   K
H   G   F
E
D   Soil; silty loam   B,C
A
Bedrock; siltstone

13.5°; 24%

surface runoff:
Thomson weir

SSF:
chiselled
gutter to
tipping
buckets

c.) *View onto trench face*

Flow active
area

5 cm

pipe number:
1 2   3 4   5   6   7   8 9 10 11 12 13

→ SSF to tipping
buckets;
SSF= sum pipe flow

Legend:

▢	Pasture land, entirely sprinkled	TDR between U= -2.4 cm and L= -11 cm: triplet E
Y	TDR triplet in its different views	TDR between U= -6.4 cm and L= -15 cm: triplet K
◆	Piezometer	TDR between U= -19.0 cm and L= -28 cm: triplet B, C, F, J
▣	Tensiometer nests	TDR between U= -26.4 cm and L= -35 cm: triplet A, G
----○	Deep line-source tracer, Br⁻and Cl⁻	TDR between U= -32.2 cm and L= -40 cm: triplet D, H
⊗	Automated rain gage	Single TDR wave-guides are at 120° separation.
*	Outlet of soil pipes; Ø = 2-8 mm pipe number ranges from 1 to 13	Identification within triplet pertains to clock-face; ten, two, six.

Figure 4.1. *Instrumentation of the Lutertal study site.*

Similar to Weiler et al. (1999), Collins et al. (2000), and Buttle and McDonald (2002), artificially labelled sprinkling water was used to separate event and pre-event water during the sprinkling experiments. The fluorescent dye naphthionate was chosen for this purpose. Overland flow, outflow from individual soil pipes and entire subsurface flow (sum of flow from all soil pipes) were sampled directly at the trench face using 100 ml brown glass bottles. Samples were taken as often as possible, at least one every 10 minutes. Event water fraction was outflow concentration divided by input concentration.

Table 4.2. *General information on sprinkling experiments.*

Experiment	Date	Sprinkling intensity (average) [mm h^{-1}]	Duration of sprinkling [min]	Tracer experiments
Exp1	3 Nov 2004	11.6	700 + break of 15 + 88	yes
Exp2	12 Nov 2004	19.3	305	no
Exp3	27 May 2005	50.8	209 + break of 80 +27	yes
1 m^2 subplot	various	30, 50, and 80	various	no

4.3.2 Determination of flow characteristics

Response of TDR wave-guides was analysed for volumetric soil moisture θ [m^3 m^{-3}], start of soil moisture increase t_{ini}, and slope of this increase m_{loc}. When interpreted as arrival of wetting at the TDR wave-guide, t_{ini} can be used to calculate the vertical flow velocity, $v_{profile}$ during infiltration. A similar approach was presented by Germann and Hensel (2006). The velocity is calculated as follows:

$$v_{profile} = \frac{U}{t_{ini}} \qquad (1)$$

The resulting velocity is seen as a macroscopic scale measure, that contrast to precise measures of the process scale. It has to be interpreted with caution as the method neglects initial losses during wetting and the occurrence of different flow types. Also the method neclects mobilized of pre-event water that is stored in the matrix which may contribute to flow velocity (Kienzler and Naef, 2007). Additionally, the true flow distance and t_{ini} cannot be defined precisely. Nevertheless, it is a helpful measure to chacarterise the hilllslope black box system. One determined t_{ini} with respect to the exceeded standard deviation of $\theta(t)$-observations prior to sprinkling and used the minimal flow distance between the soil surface and the uppermost point of the wave-guide (U) for the calculation (Figure 4.2).

The increase between the initial volumetric soil moisture, θ_{ini}, and the maximum volumetric soil moisture, θ_{max}, with respect to the time interval t_{ini} to $t_{\theta max}$ is outlined for two selected $\theta(t)$-time series in Figure 4.2. Other wave-guides responded less pronounced and exhibited larger fluctuations. The slope of this increase

$$m_{loc} = \frac{\Delta\theta}{\Delta t} \qquad (2)$$

is caused by the water flux into the survey volume of a wave-guide. While it is not possible to define precisely this survey volume, it is possible to treat single measurements as a representation and thus, the range of m_{loc} can be interpreted as water flux variability into the soil during infiltration.
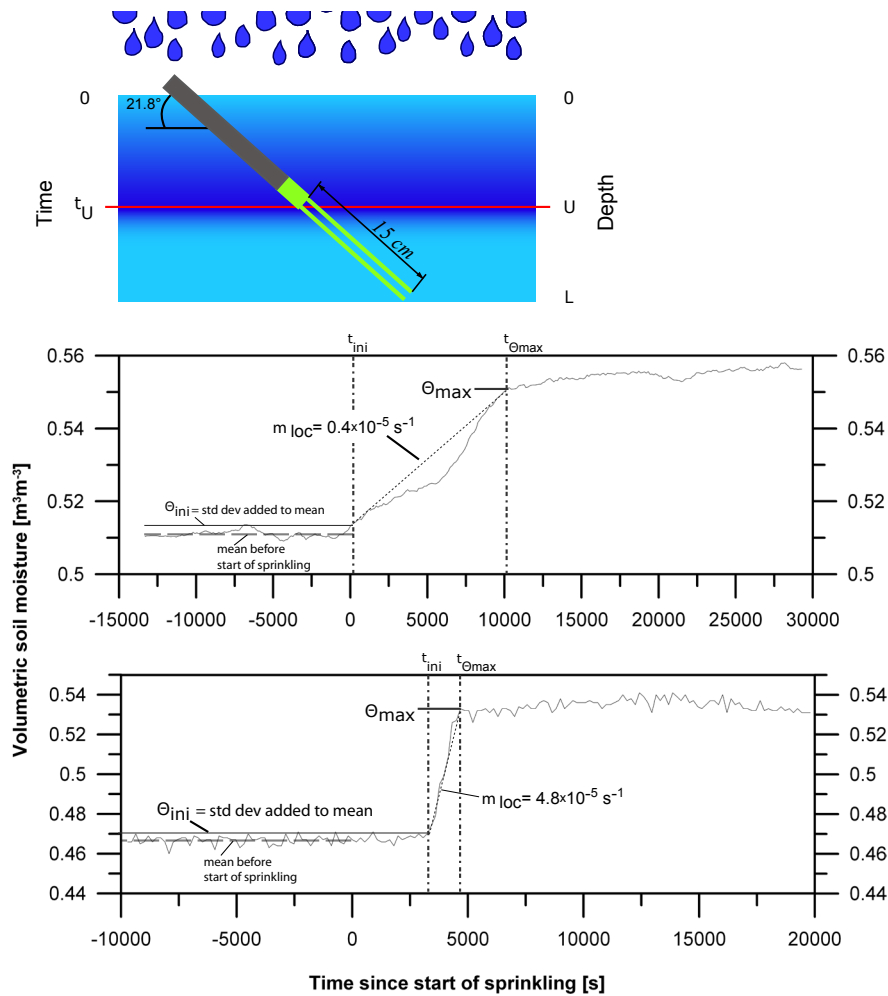
Figure 4.2. Schematic representation of oblique installed TDR wave-guide as well as selected time series of volumetric soil moisture. With respect to the slope of θ(t)-data (Eq. 1), upper time series represents an example of smooth increasing θ(t) between t_U and t_{max} and lower time series represents a sharp increase of θ(t). Definitions on volumetric soil moisture include the initial $θ_{ini}$ and final maximal $θ_{max}$. Measurements are taken at resolution of 90 s.

using m_{loc} it is further possible to calculate the local velocity of wetting propagation v_{loc} during the interval t_U to t_L :

$$v_{loc} = \frac{l}{t_L - t_U} = m_{loc} \cdot \frac{l}{w_{max_i}}$$
(3)

where $w_{max} = θ_{max} - θ_{ini}$ [m³ m⁻³], l is the length of wave-guides positioned between U and L, t_U and t_L are the arrival times of the wetting at U and L.

To estimate lateral subsurface flow velocities, different artificial tracers were injected instantaneously as subsurface line sources when SSF at the trench reached steady state. Parallel line sources were located at distances of 4 m (chloride) and of 8 m (bromide) upslope

of the trench. There, the tracers were injected into four piezometers above the bedrock between 30 cm to 40 cm depth (Figure 4.1a). Samples were taken as mentioned above. Tracer breakthrough curves from each soil pipe were analysed to determine flow velocity and tracer recovery. Maximum velocity, v_{max}, was calculated using the time of first tracer arrival t_{max}. Accordingly, peak velocity was calculated using time of peak tracer concentration t_{peak}. Mean lateral velocity, v_{avg}, was estimated according to time of 50% of tracer mass recovery (t_{avg}).

In addition to the line source tracers, the fluorescent dye pyranine was applied instantaneously on the surface over all of the sprinkled area during steady state conditions. As it is not possible to calculate well-defined flow velocities from the surface source, only the time of first tracer arrival, t_{max}, peak time t_{peak}, and time of 50% of tracer mass recovery t_{avg} of the surface tracer breakthrough curves are given in Table 4.3 and Table 4.4.

4.4 Results

4.4.1 SSF formation

During Exp1, lateral SSF started about 2.5 hours after start of sprinkling out of small soil pipes situated directly above the bedrock at the trench face. With time soil moisture content increased at the upper parts of the trench face (visual prove) but not flow emerged from these upper parts of the trench face. Gradually additional pipes were activated at the lower parts. Individual pipes showed time lags between 2.5 and 7 hours. In response to the mean sprinkling intensity of 11.6 mm h^{-1}, SSF reached a steady state of 5 mm h^{-1} after 5.5 hours; overland flow started after 4 hours and did not exceed 0.7 mm h^{-1} (Figure 4.3a). During Exp2 and Exp3 with higher mean sprinkling intensities of 19.3 mm h^{-1} and 50.8 mm h^{-1}, SSF reached again 5 mm h^{-1} and overland flow went up to 2 mm h^{-1} and 20 mm h^{-1}, respectively (Figure 4.3b). Again, SSF was only observed as outflow from the same soil pipes, which were activated with substantial time differences. Figure 4.3g+h as well as Tables III and IV show the substantial variations of pre-event water amounts emanating from individual pipes. During the low-intensity sprinkling Exp1, the outflow from one pipe (e.g. pipe 2) contained over 80% of pre-event water, whereas others contained only 25% (e.g. pipe 4, pipe 8). During Exp3 with higher sprinkling intensity, pre-event water concentrations were in general lower, but varied again substantially between different pipes. Several time series showed a progressive change during the first interval of sprinkling while others remained more or less constant.
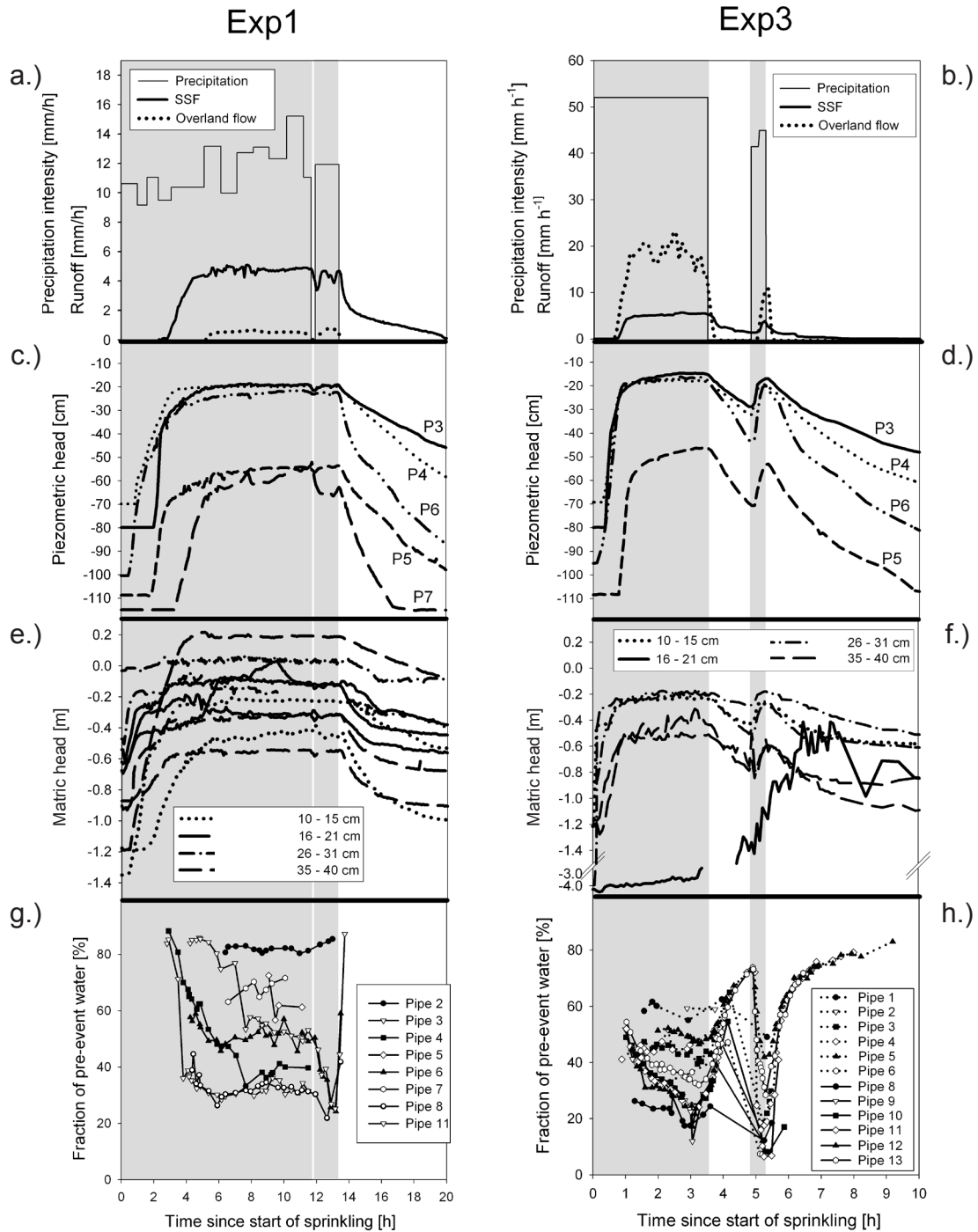
Figure 4.3. *Overview of hydrometrical results and pre-event water fractions during Exp1 and Exp3. Grey shaded areas indicate sprinkling periods. Data provided by Peter Kienzler.*

For both experiments matric head in different depths and at different locations showed slightly different initial conditions between Exp1 and Exp3. Further, measurement indicated irregular distributed patches of higher saturation degree in the soil (Figure 4.3e+f). Matric head indicated highly saturated conditions with ψ up to 0 m, respectively positive pressure up to +0.1 m in one case, where the probe was situated close the bedrock (depth 35-40 cm).

Piezometric head quickly responded to sprinkling (Figure 4.3c+d). The different offsets of

piezometric head in originated from different installation depths (max possible drill hole into bedrock). The water tables were irregular as P3 and P4 in the lower part of the site showed (both similar distance to trench). A closer look on the development of water tables is provided in Figure 4.4. Subsurface flow started just as piezometric heads of P3 and P4 reached the bedrock surface. Then, piezometric heads levelled off between 20 cm and 25 cm below surface. Upper piezometers (P5 and P7) had a more delayed response and piezometric heads did not reach the bedrock surface.
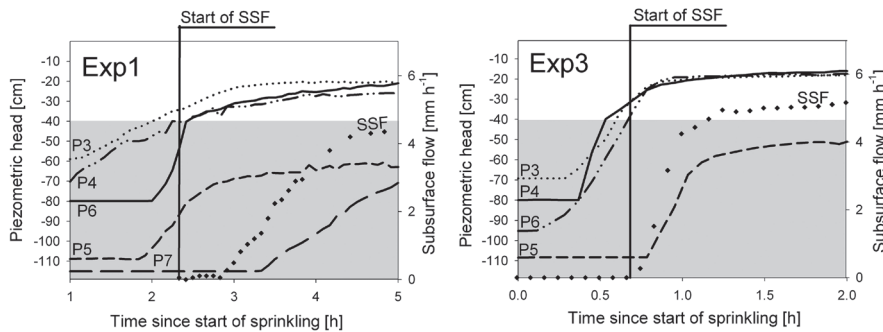

Figure 4.4 *Piezometric heads during Exp1 and Exp3 compared to SSF formation. Locations of piezometers are given in Figure 4.1a. Grey shaded areas indicate bedrock. Data kindly provided by Peter Kienzler and Felix Naef, ETH Zürich).*

Table 4.5 summarizes the previously shown characteristics during the experiments and gives water balance estimates. Soil water storage is calculated from average matric head and refers to the point in time when SSF stopped. The term percolation into bedrock was the remainder term of the balance.

Table 4.5. *Water balance during the different sprinkling experiments. Data kindly provided by P. Kienzler and F. Naef, ETh Zürich.*

ID	Precipitation intensity [mm h^{-1}]	Precipitation sum [mm]	Subsurface runoff; SSF [mm]	Overland runoff [mm]	Total runoff [mm]	Soil water storage [mm]	Percolation into bedrock [mm]
Exp1	11.6	152	53	5	58	33	62
Exp2	19.3	98	28	4	32	44	22
Exp3	50.4	198	20	52	72	66	60

4.4.2 Characteristics of vertical flow

Soil moisture during initiation before the sprinkling varied between the experiments. Although there was variation and differences were small, the initial soil moisture for Exp1 was higher than for Exp3 (Figure 4.5). Response to sprinkling at different TDR wave-guides varied widely with regard to soil moisture increase, start of soil moisture increase and slope of increase, even at closely aligned wave-guides within one triplet. This is shown in Figure 4.5 for the selected triplets E and B, where even a partially stepwise increase occurred. The response of other triplets was more similar to each other and less pronounced.
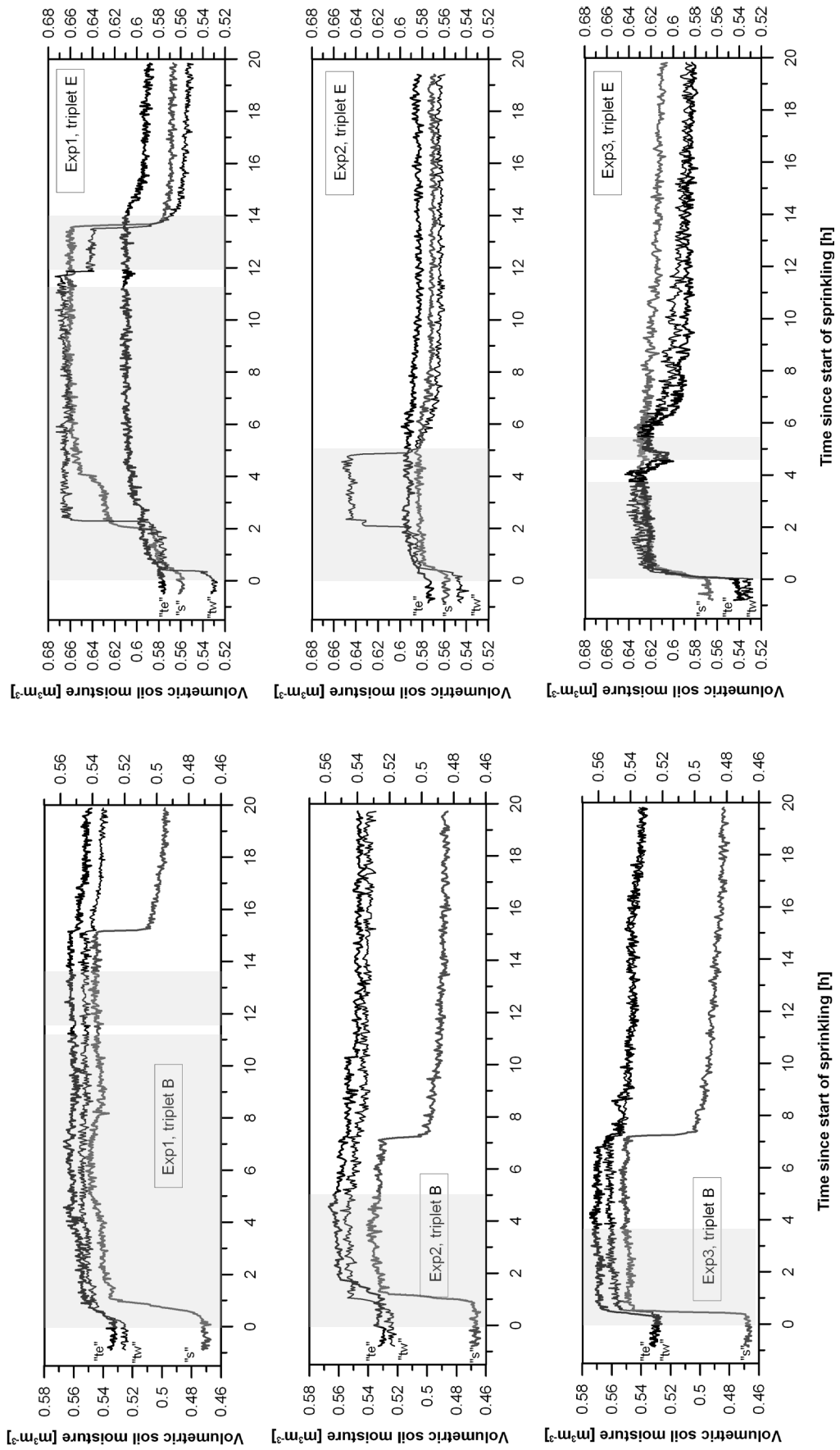
Figure 4.5. *Selected time series of θ(t) of triplets B and E during Exp1, Exp2 and Exp3. Grey shaded areas indicate sprinkling periods.*

Soil moisture increased up to 0.11. The slope of soil moisture increase, m_{loc}, varied between 0.2×10^{-5} s^{-1} and 29×10^{-5} s^{-1}. Decrease of volumetric soil moisture during drainage was correlated with soil moisture increase during infiltration (Figure 4.6). Wave-guides with substantial increase of soil moisture and high m_{loc} were associated with low initial soil water content. In contrast, wave-guides showing small and smooth increase started at relatively high initial soil moisture content.
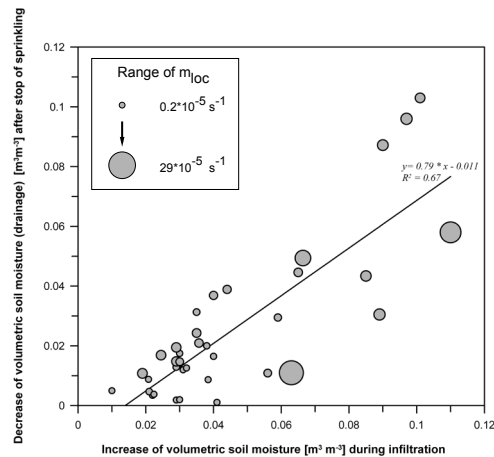

Figure 4.6. *Corresponding increase and decrease of volumetric soil moisture due to start and end of sprinkling. Decrease refers to the difference between maximal soil moisture (θ_{max}) and soil moisture 18 h after end of sprinkling.*

The large variations of start of soil moisture increase, t_{ini}, are depicted in Figure 4.7. For instance, at the 19 cm depth, soil moisture started to increase between 288 s and 4200 s during Exp1.
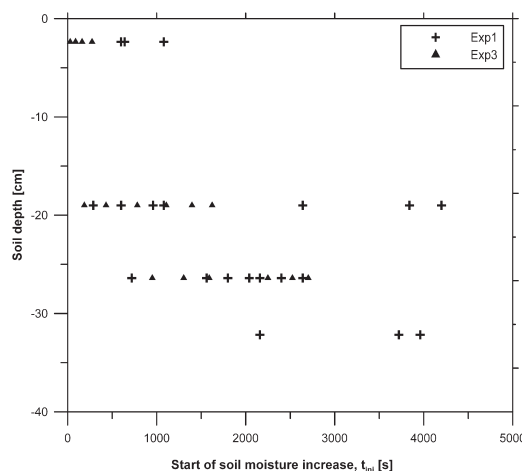

Figure 4.7. *Start of soil moisture increase at TDR wave-guides in different depths.*

In comparison, t_{ini} were slightly decreased during Exp3, indicating faster wet-up response, although there was large variation with depth. As calculated from t_{ini}, vertical flow velocity during infiltration, $v_{profile}$, ranged between 0.003 and 1.01 mm s^{-1}, with a median of

0.12 mm s^{-1} (Figure 4.8a). Here, $v_{profile}$ was not correlated with soil depth and also no significant correlation was found between $v_{profile}$ and m_{loc}. A Kolmogorov-Smirnov test showed that $v_{profile}$ and v_{loc} (Figure 4.8b) are consistent with a log normal distribution. Given P=0.005, $v_{profile}$ and v_{loc} are considered to show similar distributions.

04
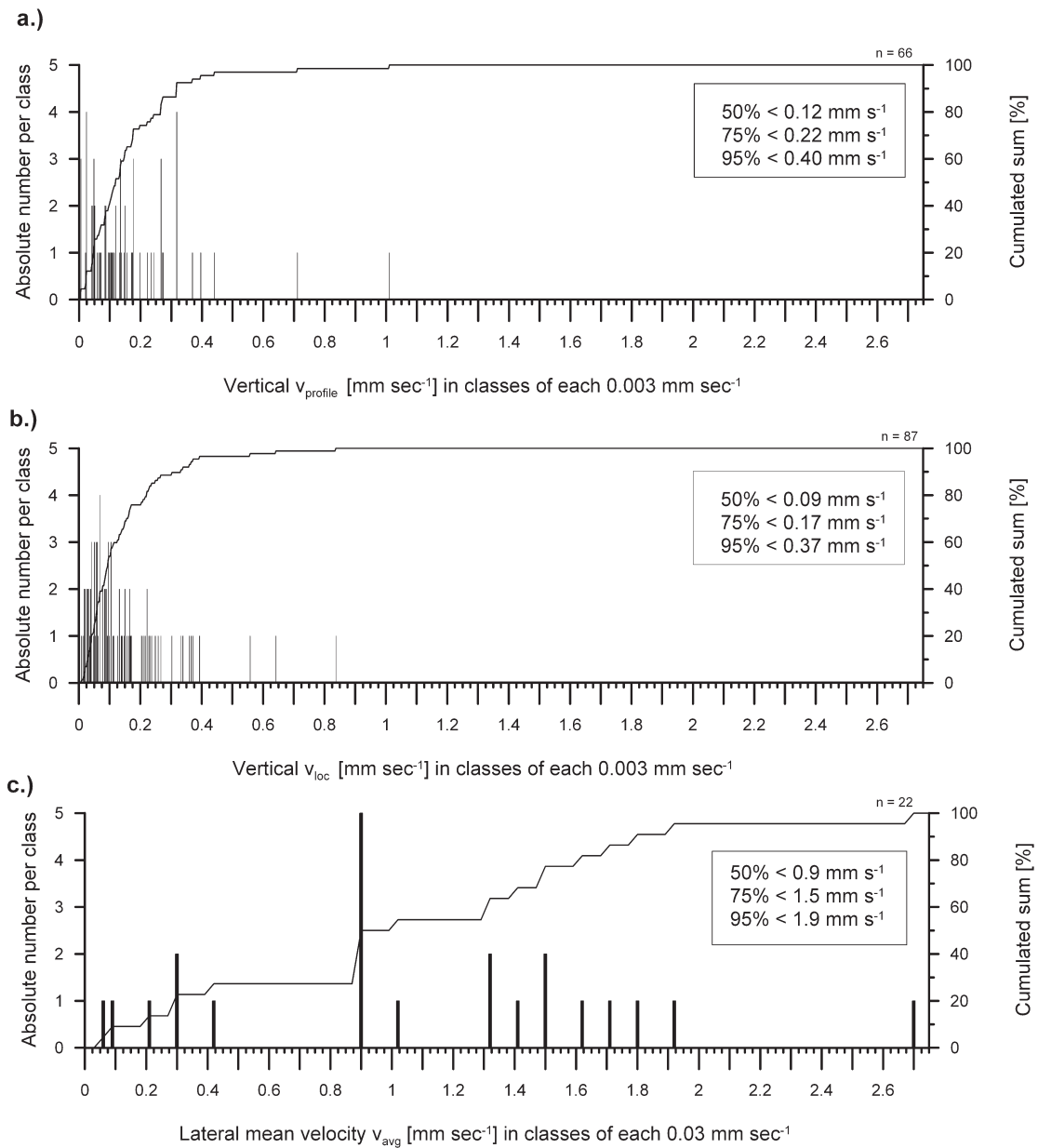
Figure 4.8. Histograms of a.) $v_{profile}$, b.) v_{loc} , and c.) mean lateral v_{avg}. Histogram of $v_{profile}$ includes TDR response from all soil depths during all 3 experiments. Mean lateral velocities include line source tracer studies from Exp1 and Exp3. Maximal lateral velocities exceed the range of abscissa.

Characteristics of individual soil moisture changes were qualitatively reproduced during follow-up experiments. For instance, at triplet B (Figure 4.5) the TDR wave-guide „s" showed prominent increase and also decrease compared to the other wave-guides within the same triplet.

4.4.3 Characteristics of lateral flow

Mean lateral flow velocities, v_{avg}, from the two line sources, ranged between 0.06 and 2.7 mm s^{-1} with a median of 0.9 mm s^{-1} (Figure 4.8c). The corresponding maximal lateral flow velocities in different soil pipes ranged between 3.6 and 17 mm s^{-1} and exceed the range of the diagram by far. Maximal velocities are therefore shown in Table 4.3 and Table 4.4. Both line sources are 4 m and 8 m distance to the trench were instantaneously injected which allows for comparisions. During low-intensity sprinkling (Exp1) substantially higher flow velocities and recovery rates occurred for the 4 m line when compared to the 8 m line. During the high-intensity sprinkling Exp3, there was nearly no difference between the two line sources.

Table 4.3. *Analysis of tracer breakthrough curves in different soil pipes and total SSF during Exp1. Lag time to start of flow is the time between start of sprinkling and start of flow from individual soil pipe. Data kindly provided by P. Kienzler and F. Naef, ETH Zürich.*

Pipe number	2	3	4	5	6	7	8	11	SSF
General characteristics									
Location at trench face [cm]	657	612	596	410	270	204	157	75	0
Average pre-event water concentration [%]	82	32	38	68	51	66	32	59	57
Lag time to start of flow [min]	385	170	175	395	255	395	262	255	170
4 m line source									
v_{max} [mm/s]					8.3		8.3	8.3	8.3
v_{peak} [mm/s]					4.4		3.0	0.8	3.0
v_{avg} [mm/s]					0.9		1.8	0.2	0.6
Tracer recovery [%]									18
Peak concentration [mg/l]					729		1281	95	92
8 m line source									
v_{max} [mm/s]					6.1		5.1	3.6	6.1
v_{peak} [mm/s]					0.3		0.6	0.3	0.3
v_{avg} [mm/s]					0.3		0.3	0.1	0.2
Tracer recovery [%]									6
Peak concentration [mg/l]					12		12	12	7
Surface source									
t_{max} [min]		10	10		15		8	15	3
t_{peak} [min]		11	20		22		14	21	12
t_{avg} [min]		30	31		162		56	480	30
Tracer recovery [%]									0.05
Peak concentration [μg/l]		19.0	3.8		3.2		6.1	0.4	4.3

Flow response and tracer breakthrough varied widely in individual soil pipes as shown for the two most differently responding soil pipes during Exp3. In comparison to pipe 6, pipe 8 showed higher flow velocities and higher peak tracer concentrations for the line source experiments (Figure 4.9a+c). Higher peak tracer concentrations were also found for surface source (Figure 4.9b). Moreover, flow contained less pre-event water (Figure 4.9d).

Table 4.4. *Analysis of tracer breakthrough curves in different soil pipes and total SSF during Exp3. Lag time to start of flow is the time between start of sprinkling and start of flow from individual soil pipe. Lag time to stop of flow is the time between stop of sprinkling and stop of flow. Data kindly provided by P. Kienzler and F. Naef, ETH Zürich.*

| Pipe number	1	2	3	4	5	6	7	8	9	10	11	12	13	SSF
General characteristics														
Location at trench face [cm]	688	657	612	596	410	270	204	157	116	97	75	59	34	0
Average pre-event water concentration [%]	60	60	45	46	36	51	33	23	31	35	34	30	39	45
Lag time to start of flow [min]	95	174	87	154	120	159	61	75	61	62	63	73	63	61
Lag time to stop of flow [min]	32	16	43	205	40	263	–	8	13	40	29	19	99	263
Outflow at t=185 min [l/min]	0.3	0.1	0.8	1.5	0.3	3.0	0.5	0.5	0.6	0.3	0.8	0.4	1.0	10.0
4 m line source														
v_{max} [mm/s]						10		10		17	13	13	13	8
v_{peak} [mm/s]						4		10		3	3	5	3	8
v_{avg} [mm/s]						0.9		2.7		0.9	1.5	1.4	1.5	1.7
Tracer recovery [%]														17
Peak concentration [mg/l]						9		16		16	16	20	27	24
8 m line source														
v_{max} [mm/s]						9		5		13	13	10	10	8
v_{peak} [mm/s]						4		5		3	3	3	3	3
v_{avg} [mm/s]						1.0		1.9		0.8	1.3	1.3	0.9	1.3
Tracer recovery [%]														7
Peak concentration [mg/l]						11		31		25	51	72	49	24
Surface source														
t_{max} [min]	11	3	13	13	13	19	9	26	8	8	11	11	14	
t_{peak} [min]	53	11	21	13	13	24	14	36	15	18	16	18	14	
t_{avg} [min]	43	23	26	43	21	32	21	40	22	22	21	22	21	
Tracer recovery [%]														0.9
Peak concentration [μg/l]	49	58	46	50	38	52	81	17	84	71	75	58	83	
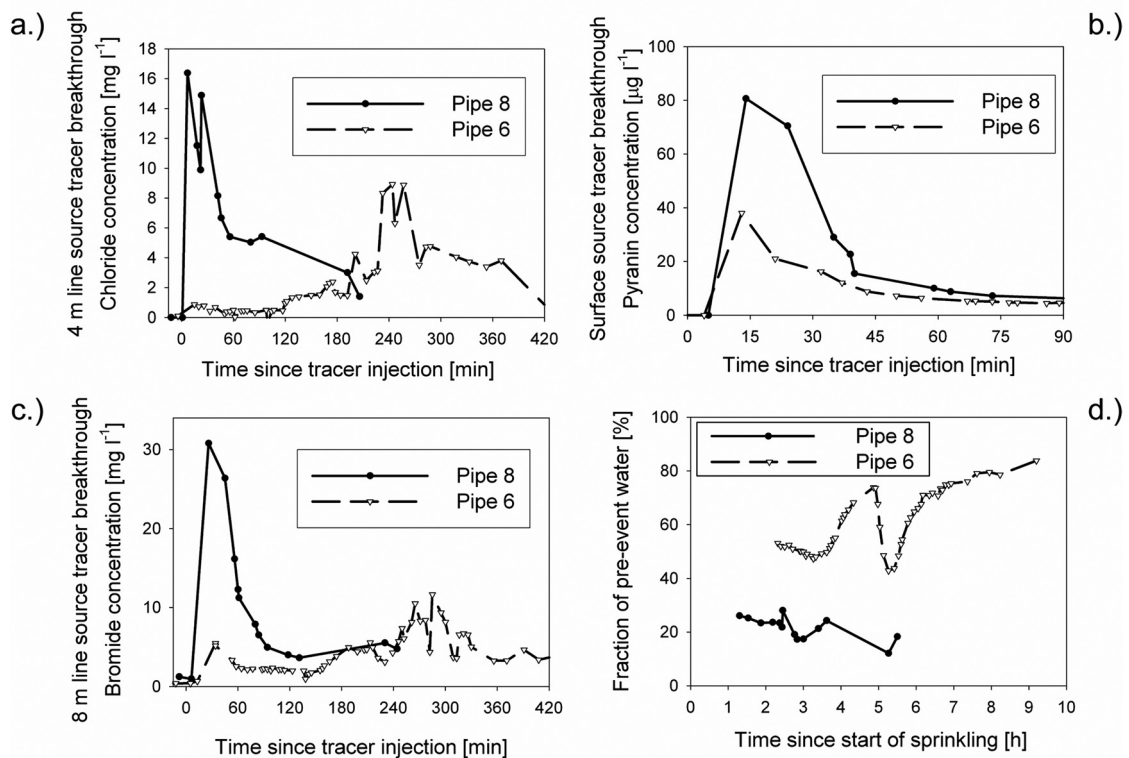
Figure 4.9. *Comparison of tracer breakthrough curves during Exp3 in two extremely differently responding individual soil pipes. Data kindly provided by P. Kienzler and F. Naef, ETH Zürich.*

The peaks and medians of the surface source breakthrough curves show similar temporal delay as the 4 m line source. However, tracer recovery was substantially lower for the surface source: During Exp1 the relation of 4 m-line recovery: 8 m-line-recovery: surface source recovery resulted in 340:120:1. During Exp3 this relation resulted in 10:8:1. Displaying the tracer tailing in double-logarithmic scale, two distinct sections to the surface breakthrough curve (Figure 4.10) were found. First, there is a rapid concentration decrease followed by a break in slope and a lower slope section. In contrast, the line sources show a slower and uniform (single slope) tracer tailing. Note that the tracers were injected during steady state conditions (Exp3) and unconsciously some time ahead of steady state conditions (Exp1).
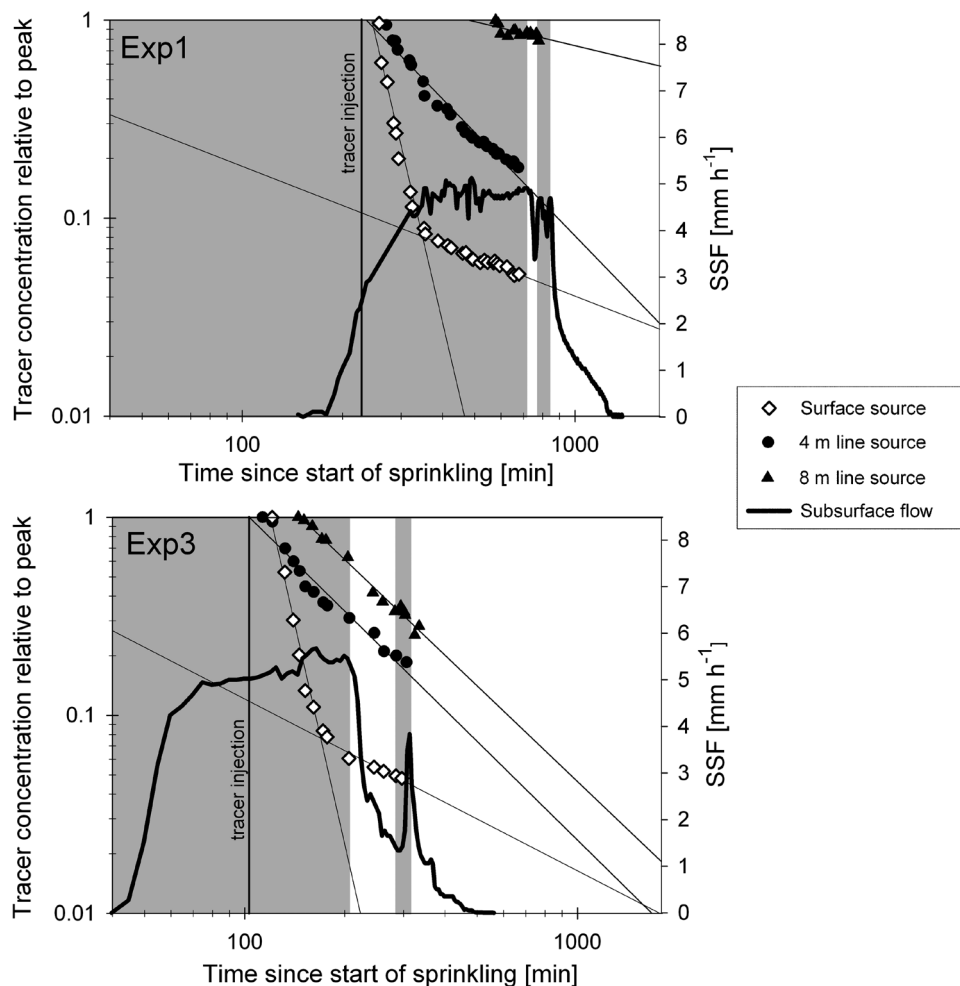

Figure 4.10. *Tailing of tracer concentrations in total SSF displayed in double logarithmic scales. Tracers were injected instantaneously into two line sources in 4 m and 8 m distance to the trench and over all the sprinkled area. Time series start at t_{peak} and are restricted to a time window in order to not account for effects of reduced discharge on concentrations towards end of experiment. Note also the different time of tracer injection. Data kindly provided by P. Kienzler and F. Naef, ETH Zürich.*

4.5 Discussion

Beforehand estimates of the water balance comprehensively summarised the sprinkling experiments. However, percolation into the bedrock was higher than expected by the hydraulic permeability of the bedrock ($\sim4.5\text{x}10^{-9}$ m s^{-1}). It is further likely that water also escaped through the sidewise cross section of the plot (12x0.4 m^2), because the soil body was not isolated using plastic sheeting (see e.g. Brooks et al., 2004).

4.5.1 Vertical flow during infiltration

Start of soil moisture increase, total increase of soil moisture and slope of increase varied substantially at closely aligned TDR wave-guides even within a few centimetres. This indicates an irregular pattern of different types of vertical flow rather than a continuous wetting front coherent in space. Flury et al. (1994) and Weiler and Naef (2003) made similar observations when they stained flow paths during infiltration. They concluded that irregular infiltration and patchy saturation is typical for almost all soils due to spatially limited high water fluxes in preferential flow paths. For the study at hand this suggests that TDR wave-guides with high and rapid increase of soil moisture were directly influenced by preferential flow or even contained preferential flow paths within their survey volume.

This is consistent with the observation of relatively low initial soil moisture at wave-guides with a pronounced increase. The survey volume of these wave-guides supposed to have great effective porosity and then filled up with infiltrating water. By contrast, wave-guides with a smaller effective porosity within their survey volume showed higher initial soil moisture and a less pronounced increase.

The correlation of soil moisture decrease with increase provides a further indication that different responses were caused by stable structures in the soil. Sharp and substantial soil moisture decrease after sprinkling is interpreted as drainage that is strongly influenced by preferential flow.

Patterns of soil moisture increase and decrease were repeated in the course of follow-up experiments. Our observations indicate infiltration flows were stable over extended periods of time. This corresponds to other studies on root-derived macropores (Beven and Germann, 1982), preferential flow fingers (Glass et al., 1989), flow paths in soil columns (Buchter et al., 1995), and the enrichment of radionuclides in preferential flow paths (Bundt, 2000). Pronounced soil moisture increase occurred with temporal delay and was partially stepwise (Figure 4.5). This can be interpreted as delayed subsurface initiation of preferential flow flow from localised saturation within the soil (Weiler, 2001; Weiler and Naef, 2003). Also, Kienzler and Naef (2007) suggested a pictorial conceptual model. Water infiltrated into the soil matrix and vertical preferential flow was initiated from such localized areas of higher saturation degree. But one could also interpret the phenomena as impeded flow that can

be described by momentum dissipation of an advancing moisture shock wave in rivulets (Germann et al., 2007).

These considerations allow to discriminate wave-guides that were exposed to preferential flow and wave-guides not necessarily exposed to preferential flow. For this purpose, a simple estimation of the maximum slope of soil moisture increase for the mean saturated hydraulic conductivity (10-20 mm h^{-1}) can be made. Under this assumtion preferential flow influence occurs for m_{loc} greater than 0.6×10^{-5} s^{-1}. On this assumption, 13% of all TDR wave-guides at Lutertal have been influenced by preferential flow during the sprinkling experiments (P. Kienzler, ETH Zürich, personal communication). Visual proof of θ(t)-series from closely aligned TDR wave-guides resulted that 21 of 123 series indicated preferential flow which results in 17% (Retter et al., 2006).

The observed vertical velocities are key to characterize vertical flow. The lower edge of the velocity distribution in Figure 4.8a is 0.003 mm s^{-1}. This number matches well with an estimation of matrix flow velocity (0.001 to 0.005 mm s^{-1}; Table 4.6, upper part) for the study site grain size distribution and bulk density (P. Kienzler, ETH Zürich, personal communication). Overall, Germann and Hensel (2006) concluded a similar range to our range of $v_{profile}$ for gravity dominated wetting front velocities $v_{profile}$ (also calculated from initial moisture increase) from sprinkling on 25 different sites, belonging to seven soil suborders. They summarized that the entire velocity range is situated between matrix flow velocities and preferential flow. In the present interpretation the upper range of $v_{profile}$ is therefore caused by preferential flow. Generally, the range of $v_{profile}$ of this study (0.003-1.01 mm s^{-1}) corresponds to preferential flow measurements in a soil core (McIntosh et al., 1999) and vertical wetting front velocities that were approximated by Torres (1998) using Stephens's (1996) calculation. Also Kung et al. (2005) similarly reported velocities of wetting and tracer fronts in soils of about 1 m in 15 min (1 mm s^{-1}). Other studies reported $v_{profile}$, although differenly termed as effective wetting front velocities, that were between 0.00218 and 0.00248 mm s^{-1} (Young et al., 1999). Young et al. (1999) further concluded, that their $v_{profile}$ and v_{loc} were statistically the same, a fact that was also observed in this study. Consistently, vertical infiltration at the study site is more coherent than previously expected. Further, the frequency distribution of vertical velocities show a filtered range that indicates a retardation of flow with different velocities (Figure 4.8a+b). This retardation is a consequence of the interaction of flow with the matrix and the extent of saturation along the vertical flow paths.

Table 4.6. *Selected studies on vertical and lateral flow velocities in soil. Table was encouraged by P. Kienzler, ETH Zürich.*

Subject of study/ remarks	Maximal velocity [cm s^{-1}]	Mean velocity [cm s^{-1}]	Flow distance [m]	Saturated/steady state conditions?	Reference
Vertical flow velocities					
Macropore flow/diameter 6 mm	50			no	Peterson and Dixon (1971)
Macropore flow/diameter 6 mm	0.6–33			no	Bouma et al. (1982)
Macropore flow/diameter 8 mm/4 mm	68/60			yes	Weiler (2001)
Water flow and tracer study in soil core (Ø=30 cm)	0.002–0.08		0.38	no	McIntosh et al. (1999)
Arrival of wetting at TDR probes	0.02–0.55	0.04	<1.15	no	Germann and Hensel (2006)
Approximation of wetting front velocity		0.028		no	Torres (1998) using Stephen (1996)
Wetting and tracer fronts		~ 0.1		no	Kung et al. (2005)
Effective wetting front velocities (= v$_{profile}$)	0.000218 - 0.000248			no	Young (1999)
Local wetting front velocities (= v$_{loc}$)	0.000203 - 0.000436			no	Young (1999)
Arrival of wetting at TDR probes	0.0003–0.11	0.009	0.02–0.4	no	this study
Matrix flow estimation		0.0001–0.0005			this study
Lateral flow velocities					
Observation of water flow	0.42	0.3	1	no	Mosley (1982)
Tracer study, Cambisol/Gleysol	0.61/0.35	0.03/0.06	10	yes	Mikovari et al. (1993)
Tracer study	0.34	0.012	2	no	Tsuboyama et al. (1994)
Tracer study	2	0.6	19	yes	Anderson et al. (1997)
Tracer study, grassland/forest		0.6/0.15	8	yes	Weiler et al. (1998)
Tracer study	0.24–0.38			no	Noguchi et al. (1999)
Tracer study	0.31/0.35		35/40	yes	Nyberg et al. (1999)
Tracer study	3	0.6	115	yes	Kienzler and Naef (2007)
Tracer study	1.3/1.7	0.2/0.3	4/8	yes	this study

4.5.2 Lateral flow characteristics

The comparison of tracer breakthrough from the two line sources provides information on the length and continuity of lateral preferential flow paths. During Exp1, the higher flow velocities and tracer recovery of the 4 m line compared to the 8 m line indicate that lateral flow paths were relatively short and not directly connected to each other. By contrast, in the course of Exp3 the differences between the two line sources were less pronounced and lateral flow was more continuous. Hence, there is a difference in connection between Exp1 (low infiltration rate) and Exp3 (high infiltration rate) (P. Kienzler, ETH Zürich, personal communication).

By comparing tracer breakthrough curves of the line sources and of the surface source it is possible to evaluate how vertical and lateral flows are linked to each other. In both experiments, tracer breakthrough curves of the surface source showed similar temporal delay to the 4 m line source and offered a rapid tailing. This suggests that the surface source tracer was transported through the soil by quick bypass flow. However, as total tracer recovery of the surface source was extremely low during Exp1 (0.05%), quick bypass flow transported only a small portion of the total discharge. This indicates that vertical flow did not directly merge with lateral flow. In contrast, during Exp3 the tracer recovery from the surface source

was higher (0.9%), which indicates a better connection between vertical flow and lateral flow (P. Kienzler, ETH Zürich, personal communication).

What is now the difference between these two experiments? Besides rainfall intensity it is the variable moisture conditions that correspond to time of tracer injection. Only the tracer injection in Exp3 was conducted under steady state conditions, whereas in Exp1 the tracers were injected "too early", when water table and steady state flow rate were not yet fully developed (Figure 4.10). Flow from the first soil pipes only started after a water table built up above the bedrock. Results from piezometers and tensiometers indicate that this water table was irregular and patchy. These observations point to the conceptual model that lateral pipe flow was initiated from patches of higher saturation degree in the soil above the bedrock. McDonnell (1990) suggested that localized zones of saturation caused tracer lateral movement to depth. Similarly, Kienzler and Naef (2007) infered that coupling of vertical flow with lateral flow and coupling of lateral flow with each other took place via such localised zones of higher saturation degree. Kienzler and Naef (2007) further summarized that it is the spatial extent of these zones that determines sensitively the intensity of SSF. Uchida et al. (2004) described this behaviour by the expansion of the hydrologically active area that overlays the bedrock. Once steady state conditions were achieved, preferential flow paths were connected to each other and flow velocities as well as tracer recovery were higher.

Tracer injection in Exp3 revealed maximal and mean lateral flow velocities that were in a similar range to measurements of other studies (Table 4.6, lower part). For example both flow velocities (and thus also the ratio) within an unchanneled valley in the Oregon Coast Range at Coos Bay were very close (Anderson et al., 1997). However, tracer breakthrough and corresponding flow velocity varied substantially in individual pipes (Figure 4.8c). Kienzler and Naef (2007) infered that the highest flow velocities therefore indicate lateral pipe flow that was almost continuous or well connected. By contrast, small flow velocities from other pipes (Table 4.3 and IV) point to discontinuous preferential flow which is interpreted by short soil pipes that were indirectly connected by saturated patches (Kienzler and Naef, 2007). This conceptual model for preferential flow incorporates a threshold behaviour similarly to the "fill and spill hypothesis" (Tromp-van Meerveld et al. 2006b). However, more recent concepts on preferential flow note that complete saturation is not a rigorous necessity to allow connected preferential flow. A corresponding threshold that indicates when preferential flow may pass or pause at a particular stage is a property of the soil matrix. Germann et al. (2007) that it might be the soil moisture at the cessation of drainage. Although this was found for vertical flow, great similarity is seen to the retardation of lateral flow that is discussed here.

4.5.3 Flow characteristics and SSF formation

Although Exp1 to Exp3 had different initial conditions and were conducted with different sprinkling intensities, the observed SSF rates were similar and were limited to a maximum steady state of about 5 mm h^{-1}. Total soil storage directly prior to the onset of SSF in the first soil pipe varied little during the three experiments, between 32 and 38 mm. However, the different soil pipes showed large variation with regard to start of flow and pre-event water concentration. Pipes with extended lag time to onset of flow had higher pre-event water concentrations than pipes where flow started quickly (Kienzler and Naef, 2007). Table 4.3 demonstrates this for Exp1 (lag times of 385, 395, and 395 min correspond to 82, 68, and 66% pre-event water concentrations) and likewise in Table 4.4. Kienzler and Naef (2007) concluded from the present data that fast responding pipes were fed directly from precipitation, whereas delayed responding pipes did not have a direct connection and were fed indirectly from saturated patches in the soil. According to them, SSF response can be explained using the two extremes of this conzeptual model.

This contribution focuses on directly measured vertical and lateral flow characteristics. Pipe flow formation at the study site can be described on the basis of the idea of two flow domains. Vertical as well as lateral flow occurred in preferential flow paths. **Vertical velocities during infiltration [0.003 - 1.01 mm s^{-1}] were smaller than lateral flow velocities [mean: 0.06 - 2.7 mm s^{-1}; max: 3.6 -17 mm s^{-1}]. However, these flow paths did not transfer the** water directly and immediately from the soil surface to the trench face, but were initiated and intersected from patches of localised saturation within the soil. This phenomena was especially observed in soil depths of 35-40 cm in the lower half of the hillslope, but also within the soil profile (see matric head).

Retardation of flow occurred at several different spots during flow formation, where preferential flow stopped and was re-initiated not until localised saturation of the soil matrix built up. Once steady-state flow was established, single preferential flow paths were linked with each other via patches of localised saturation. Flow took place mainly in a preferential way, but was intersected by flow through smaller pores in the partially saturated soil matrix. Increasing soil moisture content at the upper parts of the trench face supported these interpretation, although highly saturated during end of sprinkling not flow emerged from the matrix. The extent of localised saturation was not only responsible for delay until start of flow and concentration of pre-event water in flow, but was also responsible for deceleration of flow from the soil surface to the trench face and for limitation of flow rate. Integrated flow velocities capture these threshold phenomena well. The range and the frequency distribution are therefore essential to describe the SSF emanating from soil pipes. To the authors opinion, such data that are necessary to adress the critical value that allows preferential flow to proceed. In turn, modelling the effects of lateral soil pipes will be pushed forward (Weiler et al., 2003).

4.6 Conclusions

Detailed soil moisture measurements and tracer injections during sprinkling experiments made it possible to analyse vertical and lateral flow characteristics on a test hillslope, where substantial subsurface storm flow in the form of pipe flow occurred. The findings of this study support the conclusion of other studies that vertical as well as lateral unsaturated flow in the soil can be described on the basis of two flow domains. Vertical velocities were similar for local and integrated measurements. Preferential flow paths do not transfer the water directly and immediately from the soil surface to the stream, but are retarded and interrupted by the soil matrix. Thus, during flow formation, patches of localised saturation develop, from where preferential flow can be re-initiated. Water is therefore retained at such patches, and their extent determines how quick flow response emerges. Once, steady-state flow is established, preferential flow paths can be connected directly with each other or can be connected indirectly via such patches of localised saturation. This is a tendency to self-organize into larger preferential flow systems as sites become wetter, that was dubbed earlier by Sidle et al. (2001). The extent of such localised saturation can be highly variable on a small scale. Correspondingly, individual preferential flow paths can vary substantially with regard to flow velocity. The here shown considerations provide essential temporal information on the formation of pipe flow and may help to improve numerical models.

References

Anderson SP, Dietrich WA, Montgomery DR, Torres R, Conrad ME, Loague K. 1997. Subsurface flow paths in a steep, unchanneled catchment. Water Resources Research 33 (12), 2637 – 2653.

Beven K, Germann P. 1982. Macropores and water flow in soils. Water Resources Research 18 (5), 1311-1325.

Bouma M, Belmans, CFM, Dekker LW. 1982. Water infiltration and redistribution in a silt loam subsoil with vertical worm channels. Soil Science Society of America Journal 46, 917-921.

Brooks E.S. 2004. A hillslope-scale experiment to measure lateral saturated hydraulic conductivity. Water Resources Research 40, W04208.

Buchter B, Hinz C, Flury M, Flühler H. 1995. Heterogeneous flow and solute transport in an unsaturated stony soil monolith. Soil Sci. Sot. Am. J. 59, 14-21.

Bundt M. 2000. Highways through the soil: properties of preferential flow paths and transport of reactive compounds. Dissertation, ETH Zürich, http://e-collection.ethbib.ethz.ch/show?type=diss&nr=13825.

Buttle JM, McDonald DJ. 2002. Coupled vertical and lateral flow on a forested slope. Water Resources Research 38 (5), doi: 10.1029/2001WR000773.

Collins R, Jenkins A, Harrow M. 2000. The contribution of old and new water to a storm hydrograph determined by tracer addition to a whole catchment. Hydrological Processes 14, 701-711.

Dixon RM, Peterson AE. 1971. Water infiltration control: A channel system concept. Soil Science Society of America Journal 36, 968 - 973.

Faeh AO. 1997. Understanding the processes of discharge formation under extreme precipitation. A study based on the numerical simulation of hillslope experiments. Mitteilungen der VAW 150.

Faeh AO, Scherrer S, Naef F. 1997. A combined field and numerical approach to investigate flow processes in natural macroporous soils under extreme precipitation. Hydrology and Earth System Sciences 4, 787–800.

FAL; RAC; FAW. 1996. Schweizerische Referenzmethoden der Eidg. Landwirt-schaftlichen Forschungsanstalten. [Swiss reference methods of federal agricultural Service] 2, Bodenuntersuchung zur Standortcharakterisierung. EDMZ.

Feyen H, Wunderli H, Wydler H, Papritz A.1999. A tracer experiment to study flow paths of water in a forest soil. Journal of Hydrology 225, 155-167.

Finnern H, Grottenthaler W, Kühn D, Pälchen W, Schraps WG, Sponagel H. 1996. Bodenkundliche Kartieranleitung. Bundesanstalt für Geowissenschaften und Rohstoffe Bundesrepublik Deutschland, Hannover, 392 pp.

Flury M, Flühler H, Jury WA, Leuenberger J. 1994. Susceptibility of soils to preferential flow of water: A field study. Water Resources Research 30(7), 1945-1954.

Germann, P.F., Helbling, A., and T. Vadilonga (2007) Rivulet approach to the in-situ characterisation of flow in a highly saturated soil. Vadose Zone Journal, in press.

Germann PF, Hensel D. 2006. Poiseuille flow geometry inferred from velocities of wetting in soils. Vadose Zone Journal 5, 867 - 876.

Germann PF, Di Pietro L. 1999. Scales and dimensions of momentum dissipation during preferential flow in soils. Water Resources Research 35(5), 1443-1454.

Beven K, Germann P. 1982. Macropores and water flow in soils. Water Resources Research 18, 1311-1325.

Glass RJ, Steenhuis TS, Parlange J-Y. 1989. Mechanism for finger persistence in homogeneous, unsaturated, porous media: Theory and verification. Soil Sci. 148, 60-70.

Jones JAA, Connelly LJ. 2002. A semi-distributed simulation model for natural pipeflow. Journal of Hydrology 262, 28-49.

Jones JAA. 1987. The effects of soil piping on contributing area and erosion pattern. Earth Surface Processes Landforms 12, 229– 248.

Kienzler P, Naef F. 2007. Subsurface storm flow formation at different hillslopes and implications for the „old water paradox". Hydrological Processes, accepted.

Koyama K, Okumura T. 2002. Process of pipeflow runoff with twice increase in discharge for a

04

rainstorm. Trans. Jpn. Geomorphol. Union 23, 561– 584.

Kung KJS, Hanke M, Helling CS, Kladivko EJ, Gish TJ, Steenhuis TS, Jaynes DB. 2005. Quantifying pore size spectra of macropore-type preferential pathways. Soil Sci. Soc. Am. J. 69, 1196-1208.

McDonnell JJ. 1990. A rationale for old water discharge through macropores in a steep, humid catchment. Water Resources Research 26, 2821– 2832.

Mikovari A, Peter C, Leibundgut C. 1995. Investigation of preferential flow using tracer techniques. IAHS Publication 229, 87-97.

McIntosh J, McDonnell JJ, Peters NE. 1999. Tracer and hydrometric study of preferential flow in large undisturbed soil cores from the Georgia Piedmont, USA. Hydrological Processes 13. 139-155.

Mosley MP. 1982. Subsurface flow velocities through selected forest soils, South Island, New Zealand. Journal of Hydrology 55, 65-92.

Noguchi S, Tsuboyama Y, Sidle R, Hosoda, I. 1999. Morphological Characteristics of Macropores and the Distribution of Preferential Flow Pathways in a forested Slope Segment. Soil Science Society of America Journal 63, 1413 - 1423.

Nyberg L, Rodhe A, Bishop K. 1999. Water transit times and flow from two line injections of ^{3}H and ^{36}Cl in a microcatchment at Gårdsjön, Sweden. Hydrological Processes 13, 1557-1575.

Peters DL, Buttle JM, Taylor CH, LaZerte JM. 1995. Runoff production in a forested, shallow soil, Canadian Shield basin. Water Resources Research 31, 1291– 1304.

Retter, M, Rimmer A, GermannPF. 2007. The causes for anisotropy measured on a uniform hillslope layer. Vadose Zone Journal, manuscript under review.

Retter M, Kienzler P, Germann PF. 2006. Vectors of subsurface stormflow in a layered hillslope during runoff initiation. Hydrology and Earth Science Systems 10, 309-320, SRef-ID: 1607-7938/hess/2006-10-309.

Sidle RC, Noguchi S, Tsuboyama Y, Laursen K. 2001. A conceptual model of preferential flow systems in forested hillslopes: Evidence of self-organization. Hydrological Processes 15(10), 1675-1692, doi: 10.1002/hyp.233.

Scherrer S, Naef F, Faeh AO, Cordery I. 2006. Formation of runoff at the hillslope scale during intense precipitation. Hydrology and Earth Science Systems - Papers in open Discussion, 2523-2558, SRef-ID: 1812-2116/hessd/2006-3-2523.

Scherrer S, Naef F. 2003. A decision scheme to identify dominant flow processes at the plot-scale for the evaluation of contributing areas at the catchments-scale. Hydrological Processes 17(2), 391-401. doi: 10.1002/hyp.1131.

Schudel B, Biaggi D, Dervey T, Kozel R, Müller I, Ross JH, Schindler U. 2002. Einsatz künstlicher Tracer in der Hydrogeologie – Praxishilfe. Berichte des BWG, Serie Geologie 3, Bundesamt für Wasser und Geologie.

Stephens DB. 1996. Vadose Zone Hydrology, CRC Press, Boca Raton, Fla. p. 82.

Tromp-van Meerveld HJ, McDonnell JJ. 2006a. Threshold relations in subsurface flow: 1. A 147 storm analysis of the Panola hillslope. Water Resources Research 42(2), W02410 doi: 10.1029/2004WR003778.

Tromp-van Meerveld HJ, McDonnell JJ. 2006b. Threshold relations in subsurface stormflow: 2. The fill and spill hypothesis. Water Resources Research 42, W02411, doi:10.1029/2004WR003800.

Terajima T, Sakamoto T, Shirai T. 2000. Morphology, structure and flow phases in soil pipes developing in forested hillslopes underlain by a Quaternary sand-gravel formation, Hokkaido, northern main island in Japan. Hydrological Processes 14, 713-726. doi: 10.1002/(SICI)1099-1085(200003).

Torres R, Dietrich WE, Montgomery DR, Anderson SP, Loague K. 1998. Unsaturated zone processes and the hydrologic response of a steep unchanneled catchment. Water Resources Research 23, WR01140.

Tsuboyama Y, Sidle RC, Noguchi S, Hosoda I. 1994. Flow and solute transport through the soil matrix and macropores of a hillslope segment. Water Resources Research 30(4), 879-890.

Uchida T, Tromp-van Meerveld I, McDonnell JJ. 2005. The role of lateral pipe flow in hillslope runoff response: an intercomparison of non-linear hillslope response. Journal of Hydrology

311, 117-133, doi: 10.1016/j.jhydrol.2005.01.012.

Uchida T, Asano Y, Mizuyama T, McDonnell JJ. 2004. Role of upslope soil pore pressure on lateral subsurface storm flow dynamics. Water Resources Research 40, W12401, doi: 10.1029/2003WR002139

Weiler M, McDonnell JJ, Tromp-van Meerveld I, Uchida T. 2006. Subsurface Stormflow. in: Anderson, MG. and McDonnell JJ. (eds.): Encyclopedia of Hydrological Sciences, Volume 3, Part 10. Wiley and Sons.

Weiler M, Naef F. 2003. An experimental tracer study of the role of macropores in infiltration in grassland soils. Hydrological Processes 17, 477–493. doi: 10.1002/hyp.1136.

Weiler M, Uchida T, McDonnell J. 2003. Connectivity due to preferential flow controls water flow and solute transport at the hillslope scale. Proceedings of MODSIM 2003. Townsville, Australia.

Weiler M. 2001. Mechanisms controlling macropore flow during infiltration - dye tracer experiments and simulations. Dissertation, ETH Zürich, http://e-collection.ethbib.ethz.ch/show?type=diss&nr=14237

Weiler M, Naef F, Leibundgut C. 1998. Study of runoff generation on hillslopes using tracer experiments and a physically based numerical hillslope model. IAHS Publications 248, 353-360.

Young MH, Wierenga PJ, Warrick AW, Hofman LL, Musil SA. 1999. Variability of wetting front velocities during a field scale infiltration experiment. Water Resources Research 35(10), 3079-3087.

04

01

02

03

04

05

Chapter 05

Synthesis

5.1 Conclusion on subsurface flow formation

The present study concerns recent advances in understanding the processes by which flow occurs gained by experimental studies at the plot and hillslope scale. The aim of this thesis is to respond to questions associated with vertical preferential flow and rapid lateral flow. Major attention is dedicated to the shift from vertical flow (commonly termed "infiltration") to lateral flow, which actually forms the transition from soil hydrology to hillslope hydrology. To improve the hydrological understanding of a trenched hillslope study site with thin soil (100 m^2), an innovative instrumentation was introduced that allowed the determination of in-situ flow vectors during sprinkling experiments. The approach was applied to the hillslope scale for the very first time and consists of three obliquely installed TDR wave-guides that provide the velocity of the wetting front and its direction of travel. A triplet of wave-guides mounted along the sides of an hypothetical tetrahedron, with its peak pointing down, produces a three-dimensional vector of the wetting front. The method is based on the passing of wetting fronts. In our experiments vertical soil moisture content before sprinkling was nearly uniform, however there were large local variations. During sprinkling wetting progressed downward at various velocities. Flow vectors revealed that vertical infiltration and its propagating fronts did not move truly vertically. Vectors of the wetting fronts were generally gravity dominated and downslope orientated. Downslope direction dominated close to bedrock (35 cm), whereas no preference between vertical and downslope direction was found in vectors close to the surface. Vectors of volume flux density were also calculated for each triplet, but it was difficult to compare the values to those of the calculated flux density at the trench face (chapter 2).

The observed orientation of flow vectors indicated apparent anisotropy within the soil (chapter 3). The observations were explained using a qualitative hydro mechanical approach. Therefore, the following characteristics were tested as controls on anisotropy: (1) small scale soil structure; (2) layering of the soil profile; (3) boundary conditions of flow; (4) initial conditions. To determine small scale soil characteristics, small scale core samples were analysed for saturated hydraulic conductivity in the vertical and horizontal direction. However, no small scale anisotropy was found. Further, initial condition and layering effects were tested using initial soil moisture content and soil structure characterization. The soil was not evidently layered. Measurements during sprinkling revealed the process by which the soil became saturated, and detected water table formation on top of the bedrock. It was concluded that apparent anisotropy was caused by boundary conditions of flow, namely increased moisture content at the soil-bedrock interface that caused changes of hydraulic conductivity across the soil layer. Vectors of flow in 35 cm soil depth indicated increased hydraulic conductivity in direction parallel to the slope. It was suggested that this was the cause of the apparent anisotropy that we observed during the experimental process as an increased ratio of wetting velocities in horizontal over vertical direction (chapter 2). Previous studies support these findings and observed lateral flow through preferential flow at the

bedrock interface. A simple model showed that under steady state flow within an inclined soil layer, there was an increase of K*(n) towards bedrock, which appears on the average as anisotropy of the soil layer. Moreover, the increased moisture content, specifically in the soil depth 35-40 cm, caused K to increase exponentially and the new K-distribution with depth imposed curving of streamlines and apparent anisotropic behaviour. These considerations might have implications for general rainfall-runoff modelling, which are certainly more complex.

Chapter 4 includes characteristics of plot scale vertical and hillslope scale lateral flows for the study site. Such investigations on flow within the two major domains were previously performed, but were less focused on the two flow velocities (Anderson et al., 1997; Buttle and McDonald, 2002). Vertical velocities during infiltration [0.003 - 1.01 mm s^{-1}] were smaller than lateral flow velocities [mean: 0.06 - 2.7 mm s^{-1}; max: [3.6 -17 mm s^{-1}]. However vertical preferential flow did not transfer the water directly and immediately from the soil surface to the investigation trench, which was derived from total recovery of artificially labeled sprinkling water. It was inferred, that preferential flow was disrupted and water was retained in patches of increasing degrees of saturation, which extended differently in space. This retardation of flow was observed by the filtered distributions of flow velocities in vertical and lateral direction (Figure 4.8). Flow rate and flow response of subsurface storm flow of the hillslope system is therefore essentially controlled by the retardation. After overcoming flow retardation during infiltration as was indicated by steady-state conditions, preferential flow continued through such patches of high degrees of saturation. This process was previously described as subsurface initiation either from a saturated or partially saturated area (Weiler and Naef, 2003) and includes a tendency to self-organize into larger preferential flow systems as sites become wetter (Sidle et al., 2001). The locations where bending of flow from vertical to lateral direction occurs are therefore areas of higher saturation degree. Greminger (1984), for instance, found that lateral flow components developed even under incomplete saturation (83%) as derived from 700 tensiometers on a 275 m^2 study site.

The vector approach to subsurface flow contains uncertainties:

- The control volume for assessing the vectors was discussed in chapter 2. The longer the wave-guides, the less sensitive the measurements will get. On the other hand, the longer the wave guides the larger the control volume for assessing the vectors.

- Soil substrates containing rock fragments hinder a proper installation of TDR wave-guides.

- The measurement interval of the TDR system was 90 s. This time resolution depended on the setup of 15 waive-guides. Decreasing the number of waive guides per TDR system allow measurement intervals of down to 30 s. However, the actual time

resolution used (90 s) is sufficient for the vector determination. More crucial to the method is the determination of t_L (see chapter 2 and 4).

- The method is based on the concept of wetting fronts that are coherent within the triplet survey volume (~ 3 dm³). At the Lutertal field site 21 out of 123 passages of wetting fronts showed some kind of preferential flow pattern and thus deviated from the concept.

- For a correct measurement and also for coordinate transformation the wetting front should propagate from the upper half space into the TDR volume of the triplet. As shown in our measurements, in some cases wetting probably advanced from the bottom up.

- The method records best the first wetting front, which usually imposes the higher differences in saturation degrees. Following fronts and particularly when the hillslope system is close to steady state are hardly monitored.

In conclusion, the flow direction, as determined by the vector approach, contains uncertainties. Vertical characteristics recorded by individual TDR wave-guides (chapter 4) rather than a triplet seem more reliable. Moreover, for the aim of integrated flow formation of a hillslope, it is the distribution of integrated wide scale flow velocities in vertical and lateral direction that determine important characteristics of the hydraulic system rather than the detailed point measurements within the heterogeneous flow system.

A refinement of the method depends therefore on the investigation goals and scales of observations, which is outlined below.

5.2 Further potential research

The section presents two subjects for further research. Firstly, it considers the potential of the vector method for small scale investigations in the laboratory. Secondly, future aspects on subsurface flow research at the hillslope scale are addressed.

- Application of the vector approach (2 D) in the laboratory: Unsaturated lateral flow in hillslopes was firstly studied in the early 1970s (Zaslavsky, 1970). Thereafter, many studies gained experimental evidence about this topic such as the series of papers by Zaslavsky and Sinai (1981) which received great attention and were recently classified as benchmark papers in hydrology (Beven, 2006). While this experimental evidence was gathered long ago, it seems there is a renaissance today. Lately, Sinai and Dirksen (2006) presented the lateral movement of flow, studied during a sand box experiment in the 1970s (Figure 5.1a). Also, Miyazaki (2006) visualized the refraction of water flow in layered soil by sandbox experiments of the 1980s (Figure 5.1b), but still concluded that further experimental studies are required to clarify the 2 D behavior. However, experimentation in sandboxes is limited and differs from conditions in the field. Hence, it is not clear if the recent revival of interest in this

method is merely nostalgia or offers truly something new to research. Combining the sandbox setup with the vector approach might be a way forward because it allows the determination of in-situ flow vectors. Herefore, it is easy to confine the method to 2 D. Apparently, the electrode of the small scale investigation length needs to be adjusted to the dimensions off the sandbox. Others addressed questions of anisotropy in the field and lacked more modern measurement techniques which could be used to solve remaining problems (Glass et al., 2005). Reassessment of the sandbox experiments of Sinai and Dirksen (2006) and Miyazaki (2006) has high potential to refine our understanding on refraction of flow and curving of streamlines based on a multiple technical approach (flow vectors, photographs, and dye tracer movements). However, the shift from vertical flow to lateral flow is at present poorly understood.
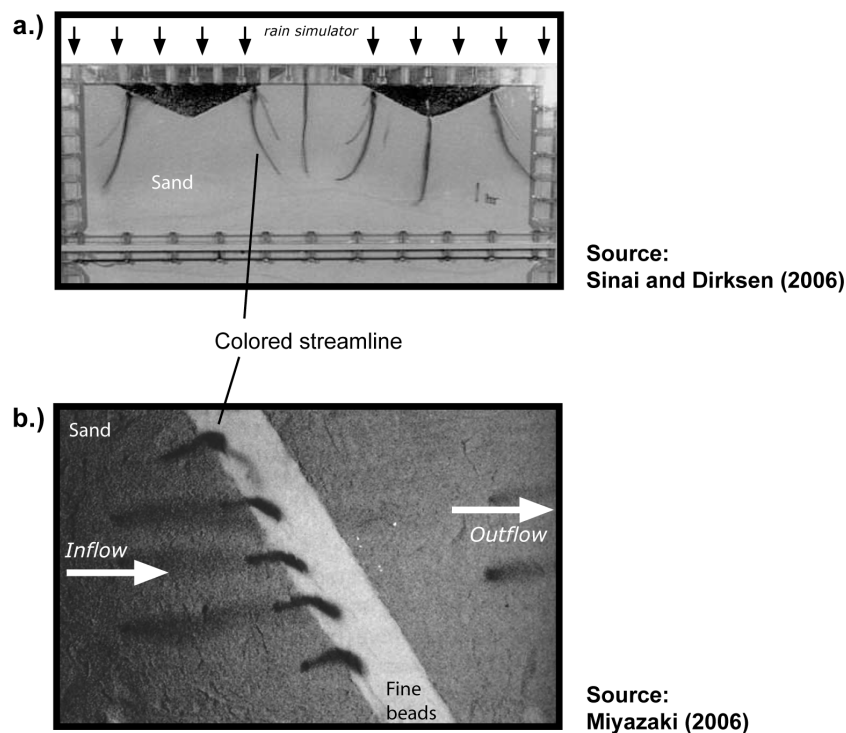
Figure 5.1. *Colored streamlines in unsaturated sand with two V-trenches after one hour of rainfall (a) and in unsaturated sand-fine beads-sand layer (b).*

■ Further research on the formation of subsurface flows at the hillslope scale: Experimental process studies are crucial to a better understanding of subsurface flow formation. More than ever, new opportunities have emerged that increase our awareness of their significance. This directly results in an urgent need to expand and prioritise experimental hydrological research. The current rapid development of new systems (see below) will enable real-time monitoring of hydrological variables in unprecedented detail, allowing for example, real-time forecasting of hydrologic variables such as soil moisture. Amongst these, there are wireless sensor networks,

the use of ground-penetrating radar for identifying subsurface flow (Gish et al., 2002), ground-based gravity measurements to infer large scale hydraulic properties (Ferré et al., 2006). Also, there are new TDR probes consisting of one conducting rod whose volume is larger and more symmetrical than the volume sampled by a two-rod probe of equal size. Further, relationships between local water content and pore water conductivity allowed the development of a profile reconstruction algorithm for electrode lengths up to 96 cm that use the full information content of TDR reflection data (Nussberger, 2005; Schlaeger, 2005). Based on electromagnetic field distribution of the guided wave Nussberger (2005) determined the sensitivity of the probes to scattering objects. The study showed, that a single rod probe is more suitable for non-local measurements of water content with TDR.

These techniques will help to provide representative measurements of subsurface flow formation because the methods have sufficient support volumes to constrain parameter estimates of soil hydraulic properties that are appropriate at large scales. Therefore integrated large scale flow characteristics can be derived that are directly linked to integrated flow formation of a hillslope.

5.3 Outlook: Prediction in ungauged basins (PUB) initiative

The present studies demonstrate enhanced understanding on the connection of vertical and lateral flows and thus on subsurface flow formation. This in turn directs us to a better conceptualization of the hydrological processes in rainfall-runoff models, which improves predictions for similar but ungauged hillslopes. It is therefore a valuable contribution to the PUB initiative. Nevertheless, presently it is about halfway through the PUB decade and upcoming years until 2012 will show the benefits of process understanding in order to reduce uncertainties in the predictions. By the end of the initiative, hydrology will then hopefully be (no more "many things", but) a "very specific thing" for the people of Bern on the banks of the river Aare.

References

Anderson, S.P., W.A. Dietrich, D.R. Montgomery, R. Torres, M.E. Conrad, and K. Loague (1997): Subsurface flow paths in a steep, unchanneled catchment. Water Resources Research 33 (12): 2637–2653.

Beven, K.J. (2006): Streamflow generation processes. Benchmark papers in hydrology, No. 1, IAHS Press, Wallingford, UK, 431p.

Buttle, J.M. and D.J. McDonald (2002): Coupled vertical and lateral flow on a forested slope. Water Resources Research 38 (5), doi: 10.1029/2001WR000773.

Ferré, T.P.A., J. Blainey, A.C. Hinnell, and J.A. Vrugt (2006): Using gravity measurements to infer large scale hydraulic properties. Geophysical Research Abstracts, Vol. 8, 02046, SRef-ID: 1607-7962/gra/EGU06-A-02046

Gish, T.J., P. Dulaney, K.-J.S. Kung, C.S.T. Daughtry, J.A. Doolittle, and P.T. Miller (2002): Evaluating Use of ground-penetrating radar for identifying subsurface flow pathways. Soil Sci. Soc. Am. J. 66: 1620–1629.

Glass, R.J., J.R. Brainard, and T.-C.J. Yeh (2005): Infiltration in unsaturated layered fluvial deposits at Rio Bravo: Macroscopic Anisotropy and Heterogeneous Transport. Vadose Zone Journal 4, 22–31.

Greminger, P (1984): Physikalisch-ökologische Standortsuntersuchung über den Wasserhaushalt im offenen Sickersystem Boden unter Vegetation am Hang. Eidg. Anstalt forstl. Versuchswes., Mitt. 60: 151-301.

Miyazaki, T. (2006): Water flow in soils. 2nd edition. Taylor & Francis, London, 418p.

Nussberger, M. (2005): Soil moisture determination with TDR: Single-rod probes and profile reconstruction algorithms. Dissertation, Federal Institut of Technology, Zürich, Nr. 15965, http://e-collection.ethbib.ethz.ch/show?type=diss&nr=15965

Schlaeger, S. (2005): A fast TDR-inversion technique for the reconstruction of spatial soil moisture content. Hydrology and Earth System Sciences 9, 481–492.

Sidle RC, Noguchi S, Tsuboyama Y, Laursen K. 2001. A conceptual model of preferential flow systems in forested hillslopes: Evidence of self-organization. Hydrological Processes 15(10), 1675-1692, doi: 10.1002/hyp.233.

Sinai, G. and C. Dirksen (2006): Experimental evidence of lateral flow in unsaturated homogeneous isotropic sloping soil due to rainfall. Water Resources Research 42(12), W12402, doi: 10.1029/2005WR004617.

Zaslavsky, D. and G. Sinai (1981): Surface Hydrology: Flow in sloping layered soil, J. of Hydraulic Division 107, HY1, 53-63.

Zaslavsky, D. (1970): Some aspects of watershed hydrology. Spec. Rep. USDA ARS 41-157. Washington, D.C., 95 pp.

05

Words of Thanks

Firstly, I am very grateful to my supervisor and 'Doktorvater' Peter Germann for his valuable personal support, guidance, and help throughout this work. I cannot imagine a better supervisor and boss. A little kindness goes a long way.

I would like to thank Markus Weiler, who introduced me to experimental hillslope hydrology, for his advice during the past years and for taking the co-reference on the final thesis. A trade in hand, finds gold in every land.

The very nice cooperation with Peter Kienzler from the ETH group around Felix Naef was a great benefit. Thanks for the practiced way of sharing ideas and resources in this joint work. Four eyes see more than two.

Highly appreciated is also the cooperation with Alon Rimmer. It was our trip on the paddlesteamer at the lake of Zurich where a manuscript was born. Thank you for fruitful discussions and endurace. Unity is strength.

Exchange with a number of colleagues of the IAHS working group SLICE within the PUB initiative stimulated my research. Jeff McDonnell helped to sharpen a lot of points during my past research. Well begun is half won.

My colleagues Abdallah Alaoui, Marco Carizzoni, Basilio Ferrante, Andreas Helbling, Jana Ilgner, Beatrice Moser, Agnes Petro, Jürg Schenk, Andreas Schellenberger, Hansruedi Wernli, Stefan Wunderle, and Roland Zech kept me on track various times. Give credit where credit is due.

I would like to thank my flatmates Maria Stein and Rezia Ladina Peer. A trouble shared is a trouble halved.

My colleagues Ingrid Hincapié and Jan-Hendrik May were friends in good and in bad days. A friend in need is a friend indeed.

My parents, Friedhild and Martin, receive my deepest gratitude for their dedication and the many years of support during my undergraduate studies that provided the foundation for this work. I also apprechiated the meaningful accompany by my godfather Eberhard Retter (†). A tree must be bent while it is young.

And finally…
Man proposes, God disposes.

Curriculum Vitae

Matthias Retter

06/2004 – 01/2007	Dissertation, Department of Geography, University of Bern
	Supervised by Prof. P. Germann
05/2006 – 11/2006	Essentials of Management Program, University of St. Gallen
12/2003	**Diploma in hydrology, University of Freiburg, Germany**
	Supervised by Prof. Ch. Leibundgut & Prof. S. Uhlenbrook
03/2003 – 07/2003	Diploma thesis at Hillslope and Watershed Hydrology Lab Oregon State University, USA
	Supervised by Prof. Dr. J. McDonnell & Ass. Prof. M. Weiler
10/2001 – 02/2002	National Institute of Water and Atmospheric Research, New Zealand, catchment processes group
	Supervised by Dr. R. Woods
10/1998	Entry to University of Freiburg, Germany
09/1997 – 10/1998	Community service, Nature reserve Altmühlsee
1997	School Leaving Certificate, Technisches Gymnasium Lörrach
1994	Equivalent of GCSE, Realschule Zell i.W.
1978	born in Rheinfelden, Germany